CALIFORNIA INSTITUTE OF TECHNOLOGY

ELECTRON TUBE AND MICROWAVE LABORATORY

FIELD THEORY OF TRAVELING-WAVE TUBES WITH APPLICATION TO THE STUDY OF ATTENUATOR SATURATION EFFECTS

by

William Buchman

Technical Report No. 2

August 1955

A REPORT ON RESEARCH CONDUCTED UNDER

CONTRACT WITH THE OFFICE OF NAVAL RESEARCH

FIELD THEORY OF TRAVELING-WAVE TUBES WITH LOSS: APPLICATION TO THE STUDY OF ATTENUATOR SATURATION EFFECTS

by

William Buchman

CALIFORNIA INSTITUTE OF TECHNOLOGY

Pasadena, California

A Technical Report to the Office of Naval Research

Prepared For

Office of Naval Research Contract

Nonr 220(13)

August 1955

ACKNOWLEDGEMENTS

Without the continual advice and encouragement given by Dr. Lester M. Field, this project could never have been started or completed. Many discussions with Dr. Field and Roy W. Gould have helped shed much light on the attenuator and associated problems. T. E. Feuchtwang did some of the numerical and experimental work associated with the space charge bunching effects in attenuators. Much is owed to J. B. Opfell, W. G. Sly, R. A. Pasternak, and J. S. Rollett of the Chemistry and Chemical Engineering Division and to Jerry Cramb of I.B.M. for teaching the author how to use the computing machinery. Ruth Brown typed the final version of this report, a formidable task.

ABSTRACT

Propagation constants have been calculated for a lossy traveling-wave tube by means of a field theory. These results have been applied to the prediction of an attenuator power loss of the order of 2 or 3 db. compared to attenuatorless operation. It is shown that the gain of the higher order modes is negligible. Admittance matching by means of radial admittance transformation is the underlying method used throughout.

The Pierce-Fletcher theory in common use at this time is examined in some detail to determine its range of validity. It is found to break down when the ratio of beam to helix radius is almost unity and when $p_0 a$ is small. Furthermore, it is shown that complex parameters must replace the real ones, Q, K, and C, if one wants to extend the Pierce notation correctly to lossy tubes. Not doing so leads to discrepancies of approximately 10% in the propagation constants calculated here. There is reason to believe that parameters other than those used here will not result in greater discrepancy.

The effects of space charge bunching on saturation has been treated. Criteria have been set for determining whether bunching is important or not in determining saturation.

CONTENTS

Section I

INTRODUCTION

It has been known for some time that attenuators used to prevent unwanted oscillation in traveling-wave tube amplifiers cause a considerable reduction of the available power output and efficiency in some way that has not yet been well understood. The object of this study is to develop a partial understanding of these attenuator effects by means of a field theory approach similar to that of Chu and Jackson.[R-1]*

Fig. 1.1 is a schematic representation of such a traveling-wave tube.

Heretofore, and for the immediate future, no practical method is known by which a traveling-wave tube may be operated without an attenuator. An attenuator is necessary in order to prevent oscillation of a tube when it is used as an amplifier. If an attenuator were not used, the amplified signal would undergo partial reflection at the output end of the tube because of the imperfect match at the output; it is impossible to obtain a perfect match over a wide band of frequencies corresponding to the useful bandwidth of a traveling-wave tube. The reflected signal will be reflected again when it reaches an imperfect match at the input end of the tube. If the second reflection is larger than the initial signal that set up the twice-reflected wave, a sizable signal could be built up from noise alone, that is, the tube

*(R-1) refers to the first reference, (R-2) to the second, etc.

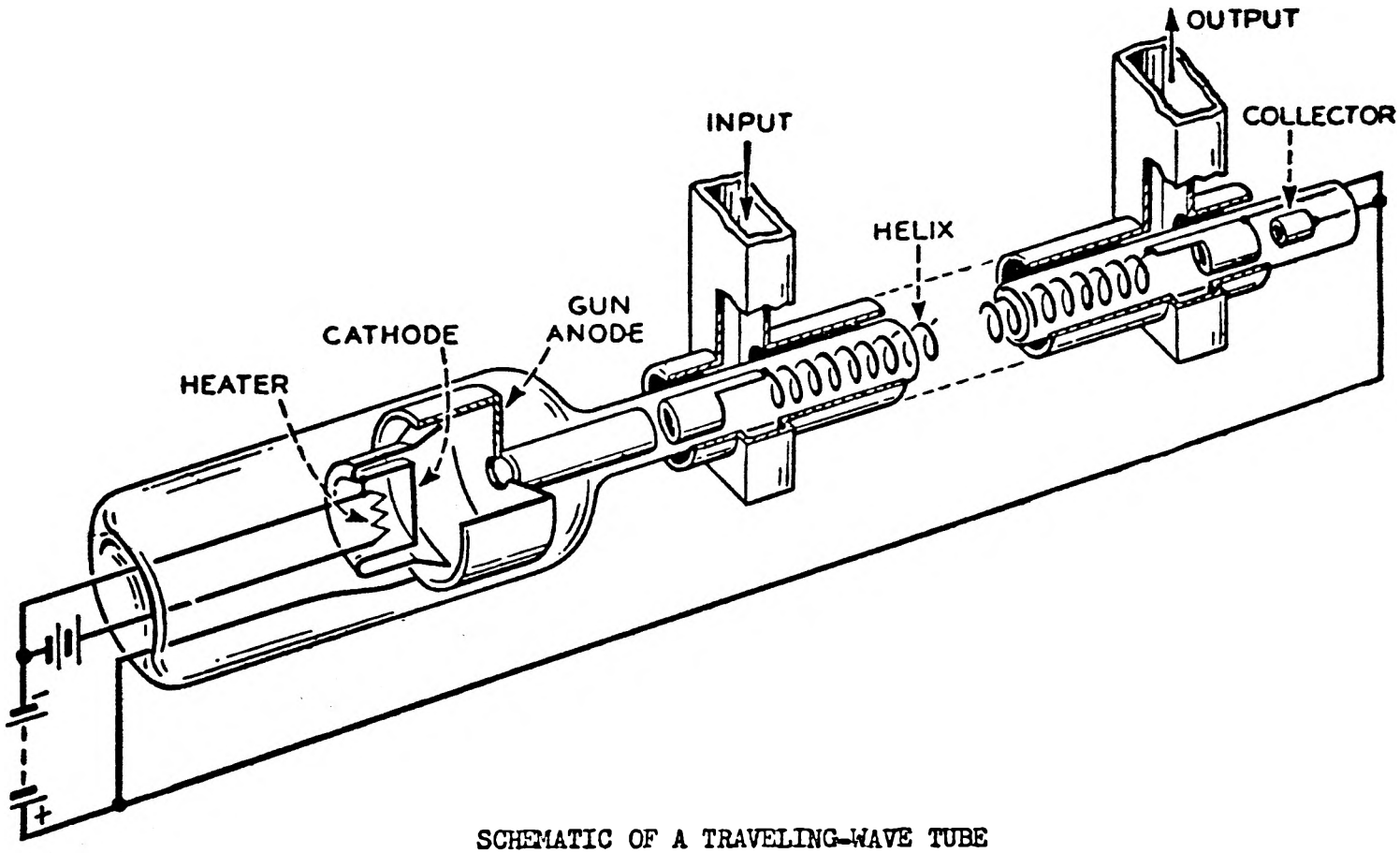

SCHEMATIC OF A TRAVELING-WAVE TUBE

Fig. 1.1

will self oscillate. An attenuator placed somewhere between the input and output of the tube can attenuate the backward reflected wave, a wave which does not interact with the beam, without reducing the forward gain of the tube below a useful value.

At present, there are several methods of introducing attenuation. The only practical method, which does not set up reflections by its introduction, is the application of some attenuating material such as graphite, the density of the application being tapered so as not to set up reflections. The lossy material may be applied in several ways, for example, by spraying or painting aquadag onto the outside of the tube envelope or by supporting the helix on ceramic rods which have been made lossy by the application of graphite.

Several processes have been suggested for the attenuator region which would explain the observed behavior. These will be discussed later in more detail. Here, some of the qualitative aspects of these processes will be noted.

The first process assumes that the attenuator coating is so heavy that for all practical purposes the attenuator region operation can be represented by means of a conducting pipe with an electron beam drifting through it. The incident electron beam is modulated in such a fashion that there is essentially an $I_o(\beta_e r)$ distribution of the alternating current density and velocity throughout the beam. This is brought about from the fact that slow wave cylindrical structures have modified Bessel function variation of E_z in the radial direction.

Inside the drift space, however, the modal distributions correspond to ordinary Bessel functions, $J_o(\tau_n r)$. These distributions are associated with the plasma waves for a beam in a conducting pipe.

It is obvious that the incident growing wave will have to split up among the various modes of the drift tube. Since each of these modes has a different plasma wavelength, there will be a scrambling of the modes with the result that different parts of the beam may have alternating current densities essentially of opposite sign. At any distance from the point of initiation of these modes, the various modes will be at various incommensurable space phases with respect to one another. The net effect will be strong local modulation at some distance from the beginning of the attenuator region, but with a small overall alternating current in the z direction over an entire cross sectional plane compared to the peak current density multiplied by the area of the beam. See Fig. 1.2 .

The higher order modes have longer plasma wavelengths than the lower order modes so that the lower ones are the ones whose signs get changed in traveling the short distances involved with typical attenuator lengths.

The effects of velocity modulation of the beam are such as to emphasize the distortion of the modulation distribution across the beam. The velocity modulation leads to klystron bunching of the electron beam. The bunching length and degree of bunching varies considerably from mode to mode. Again the effect is such as to produce large local modulations of the beam. When the excitation of a new gaining wave in a new lossless region is calculated, the size of the newly excited growing wave turns out to be much smaller than that of an increasing wave with the same degree of <u>local</u> modulation as in the exciting beam. The result is that the beam has lost its

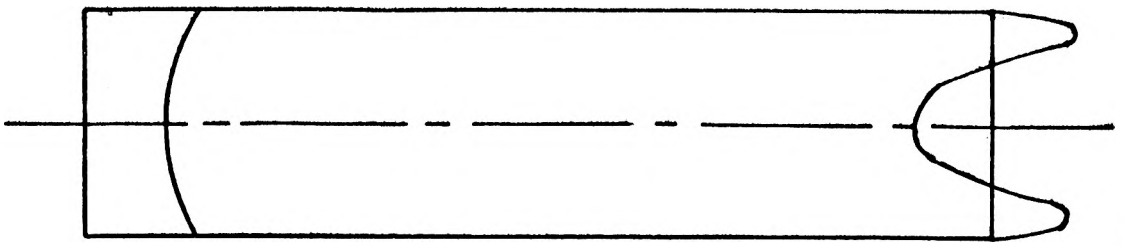

Overall Wave

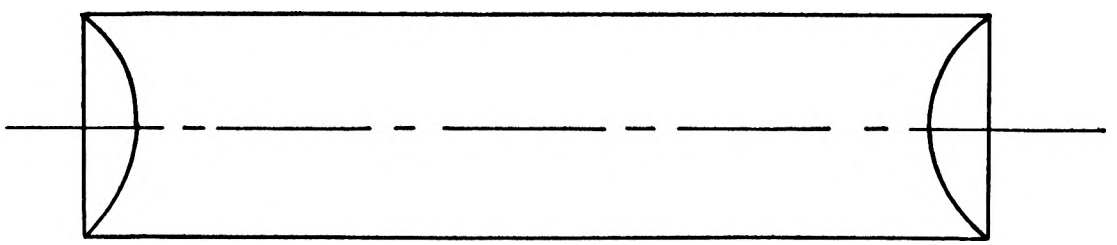

First Mode

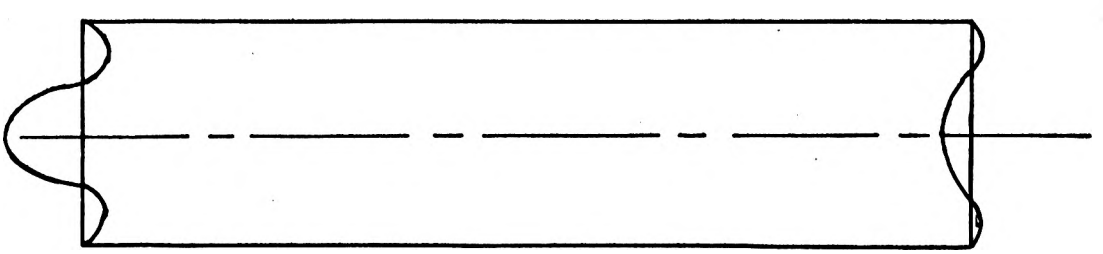

Second Mode

Fig. 1.2

ability to interact with the growing wave because of its full modulation, and furthermore, the size of the increasing wave is still relatively small when the beam finally saturates compared to what it could be if there were no attenuator.

Several low power tubes were built to demonstrate the effects discussed above. The behavior agreed qualitatively with the description above and will be discussed later. There is no surety, however, that the process described above is dominant.

Some numerical calculations based on the hypothesis just described did not and could not explain the experimental results obtained for a high power traveling-wave tube built at the Hughes Aircraft Company(R-2). The only possible explanation was that some gaining process was taking place in the attenuator region. This led to a search for the possibility that admittance wall amplification of some kind was taking place under the attenuator, and that somehow, this amplification was causing much of the trouble encountered.

One can consider the effect of an increasing incident wave upon the attenuating section of a traveling-wave tube. The energy associated with the electric and magnetic fields of the wave is absorbed by the attenuating material. This process begins while the modulation on the beam is still below saturation level. The resistive wall associated with the attenuator permits the beam to continue being bunched. The result is that a "worn out" bunched beam comes out of the attenuator region. This beam has to excite a new increasing wave in the lossless region. It also has to be capable of getting bunched even further in order to be able to supply energy to the new electro-

magnetic wave that is excited. Perhaps a better way of understanding the process is to realize that the electrons are injected into the helix at a speed that is higher than the growing wave velocity. The energy in the growing wave is supplied by slowing the electrons down to the velocity of this wave. If the average velocity of the electrons is reduced in going through an admittance wall amplifier, the amount of subsequent velocity reduction available is reduced. Therefore, less energy will be available to the newly excited growing wave.

Pierce (R-3) has shown by means of his circuit theory, and it has been verified by the present more fundamental field approach, that the current to electric field ratio is larger in a lossy section of a traveling-wave tube than in a lossless section. This means that a lossy attenuator section has, at its end, a greater current associated with each unit of electric field than would be associated with each unit of electric field in a pure growing wave of a lossless section. Since both the current and field are continuous, a finite length of lossless helix is needed beyond the attenuator in order for the growing wave to grow larger than any of the others. This is needed if one wants to have the most field associated with a given amount of current. If saturation sets in before the point at which the current to field ratio is restored, the fields will be low compared to what they would be at saturation for a pure increasing wave. Since the available output power is associated with the stored field energy, the result is that the power output will be below that which would be available without an attenuator.

In order to place all these arguments on a firm theoretical

basis, the approach taken here is to work with the field theory of Chu and Jackson (R-1) and Birdsall and Whinnery (R-4). A combination of these two methods will give the propagation constants of all the modes involved. In addition, one will have to determine the amplitudes of the various modes which get excited at discontinuities in the structure propagation characteristics which vary with distance along the tube. The determination of these amplitudes appears to be a formidable task indeed. Sollfrey (R-5) has presented a method of determining such excitation for a lossless traveling-wave tube. It is very unsuitable for simple computation. It should not be conceptually difficult to extend his method to traveling-wave tubes with loss. Sollfrey shows that a continuum of solutions is also necessary to describe the fields in a traveling-wave tube. He states, but does not show, that the continuum and the higher order space charge modes are unimportant.

Instead of describing qualitatively all the material in the preceding paragraphs in greater detail, it will prove more profitable to examine these aspects in greater quantitative detail.

As a further result of these investigations, some questions have arisen as to the range of validity of the Pierce theory. The Pierce theory depends upon the knowledge of certain parameters which are calculated from the field theory. The relationships permitting such calculation have been established by Fletcher (R-6). It appears, however, that the parameters calculated by Fletcher are insufficient to describe a traveling-wave tube adequately under conditions which

may be of considerable practical interest.

The system under consideration will have an infinite magnetic field along the z axis. This will restrict motion of the electrons to the z direction only. No variation in the azimuthal direction will be considered. The beam will be assumed to be of uniform direct velocity and charge density. Only the linearized equations of motion will be considered. See Fig. 1.3 .

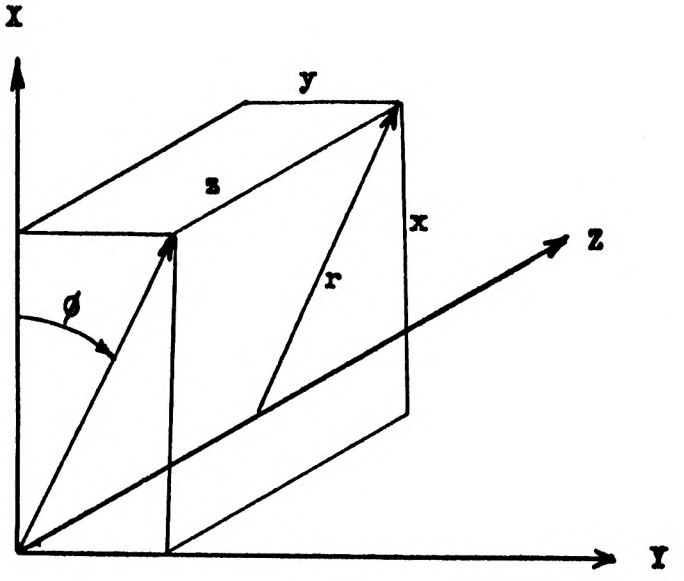

COORDINATE SYSTEM

Fig. 1.3

Section II

ADMITTANCE TRANSFORMATIONS

The field method for obtaining the propagation constants associated with a given physical configuration consists of getting expressions for the admittances of the given structure and the given beam in terms of propagation constants and then equating the two expressions. The resultant equation is then solved for values of the propagation constant. The equation usually is a complicated transcendental equation. In cylindrical symmetry the expressions will involve Bessel functions of complex arguments.

The first step in getting an expression for the circuit admittance is to derive a transformation which will transform admittance from one radius to another. Expressions will be derived for both, TE and TM modes of propagation. Space will be assumed isotropic and homogeneous except for abrupt changes at boundary surfaces. Each region of space will be characterized by a μ and an ϵ. As stated in the previous section, it will be assumed that there is no variation with ϕ. Time and z variation is expressed by the factor $e^{j\omega t - \gamma z}$.

The Maxwell curl equations can then be written in the following manner

$$\begin{aligned} E_\phi + j\omega\mu H_r &= 0 \\ \frac{1}{r}\frac{\partial}{\partial r}(r E_\phi) + j\omega\mu H_z &= 0 \\ \frac{\partial H_z}{\partial r} + H_r + j\omega E_\phi &= 0 \end{aligned} \qquad (2.1)$$

and

$$\begin{aligned} \gamma H_\phi - j\omega E_r &= 0 \\ \frac{1}{r}\frac{\partial}{\partial r}(r H_\phi) - j\omega\varepsilon E_z &= J_z \\ \frac{\partial E_z}{\partial r} + \gamma E_r - j\omega\mu H_\phi &= 0 . \end{aligned} \tag{2.2}$$

The assumption that electrons are restricted to motion along the z direction is indicated in equations (2.2) by the inclusion of a current term only in the second equation of the set of three.

(2.1) gives the equations which determine the field components of a TE wave if H_z is given. It is important to note that these equations are independent of the presence or absence of an electron beam.

(2.2) gives the equations which determine the field components of a TM wave if E_z is given. These equations include the effect of a beam. If no beam is present, J_z is to be set equal to zero. Otherwise, J_z is determined from the electric field and the equations of motion.

The explicit expressions for the other field components in terms of E_z and H_z are for TM waves

$$\begin{aligned} E_r &= \frac{1}{p^2}\gamma\frac{\partial E_z}{\partial r} \\ H_\phi &= \frac{j\omega}{p^2}\frac{\partial E_z}{\partial r} , \end{aligned} \tag{2.3}$$

where

$$p^2 = -(\gamma^2 + k^2) \tag{2.4}$$

$$k^2 = \omega^2\mu\varepsilon . \tag{2.5}$$

and similarly for TE waves,

$$E_{\phi} = -\frac{j\omega\mu}{p^2}\frac{\partial H_z}{\partial r} \qquad (2.6)$$

$$H_r = \frac{\gamma}{p^2}\frac{\partial H_z}{\partial r} .$$

One obtains the wave equations for H_z and E_z by means of the usual methods from (2.1) and (2.2) respectively. Substitution of the first equation of (2.6) into the second of (2.1) gives

$$-\frac{1}{r}\frac{\partial}{\partial r}\left(r\frac{j\omega\mu}{p^2}\frac{\partial H_z}{\partial r}\right) + j\omega\mu H_z = 0 ,$$

$$\frac{1}{r}\frac{\partial}{\partial r}\left(r\frac{\partial H_z}{\partial r}\right) - p^2 H_z = 0 . \qquad (2.7)$$

Similarly, if one substitutes the second equation of (2.3) into the second equation of (2.2), then

$$\frac{1}{r}\frac{\partial}{\partial r}\left(r\frac{j\omega}{p}\frac{\partial E_z}{\partial r}\right) - j\omega\varepsilon E_z = J_z ,$$

or

$$\frac{1}{r}\frac{\partial}{\partial r}\left(r\frac{\partial E_z}{\partial r}\right) - p^2 E_z = \frac{p^2}{j\omega\varepsilon} J_z . \qquad (2.8)$$

In the absence of a beam, $J_z = 0$, and the last equation can be written as

$$\frac{1}{r}\frac{\partial}{\partial r}\left(r\frac{\partial E_z}{\partial r}\right) - p^2 E_z = 0 . \qquad (2.8a)$$

Therefore, it is seen, E_z and H_z satisfy the same radial propagation equation. This equation is the modified Bessel equation of zero order and of argument pr. This means that the solution of the radial equation is a linear combination of modified Bessel functions. It is implicit in this argument that p^2 is a positive number. This means that $\gamma^2 + k^2$ is a negative real number. k is the rationalized wave

number of a uniform plane wave in the medium under consideration. It corresponds to the velocity of light in that medium. (2.4) gives

$$\gamma^2 = -k^2 - p^2 \quad . \tag{2.9}$$

Therefore, γ^2 is a negative real number of absolute value greater than k^2. This means that the wave is slower than the speed of light in the medium under consideration. If γ is not quite pure imaginary as required above, p^2 will not be pure real. This means that an increasing or decreasing wave which is expressed by γ being complex, does not have a radial variation corresponding to a purely real p. In other words, the general case of increasing and decreasing waves on a slow propagating circuit will have radial variations corresponding to modified Bessel functions of complex argument. If the rate of increase or decrease is small in one wavelength, the arguments of these modified Bessel functions will be almost purely real.

The TE and TM admittances are defined by

$$Y^{(1)} = \frac{H_z}{E_\phi} , \qquad Y^{(2)} = \frac{H_\phi}{E_z} \quad . \tag{2.10}$$

$Y^{(1)}$ is the TE admittance, and

$Y^{(2)}$ is the TM admittance.

Normalized admittances can also be defined by

$$Y_r^{(1)} = -\sqrt{\frac{\mu}{\varepsilon}}\ Y^{(1)} , \qquad Y_r^{(2)} = \sqrt{\frac{\mu}{\varepsilon}}\ Y^{(2)} . \tag{2.10a}$$

The general solution for H_z is

$$H_z = A\, I_o(pr) + B\, K_o(pr) \,. \tag{2.11}$$

Using equations (2.6), E_ϕ and H_r can be written

$$E_\phi = -\frac{j\omega\mu}{p}\left[A\, I_1(pr) - B\, K_1(pr)\right] \tag{2.12}$$

$$H_r = \frac{\gamma}{p}\left[A\, I_1(pr) - B\, K_1(pr)\right] \,. \tag{2.13}$$

If at a radius a ,

$$\frac{H_z(a)}{E_\phi(a)} = Y^{(1)}(a) \,, \tag{2.14}$$

then

$$\frac{A\, I_o(pa) + B\, K_o(pa)}{-\frac{j\omega\mu}{p}\left[A\, I_1(pa) - B\, K_1(pa)\right]}$$

and

$$\frac{A\, I_o(pb) + B\, K_o(pb)}{-\frac{j\omega\mu}{p}\left[A\, I_1(pb) - B\, K_1(pb)\right]} = Y^{(1)}(b)$$

at a radius b .

The first equation gives

$$A\left[I_o(pa) - \frac{j\omega\mu}{p}\, I_1(pa)\, Y^{(1)}(a)\right] = B\left[-K_o(pa) + \frac{j\omega\mu}{p}\, K_1(pa)\, Y^{(1)}(a)\right] .$$

This equation is satisfied if

$$B = I_o(pa) + \frac{j\omega\mu}{p}\, I_1(pa)\, Y^{(1)}(a)$$

and

$$A = -K_o(pa) + \frac{j\omega\mu}{p}\, K_1(pa)\, Y^{(1)}(a) \,.$$

One then finds the admittance at radius b to be

$$Y^{(1)}(b) = -\frac{p}{j\omega\mu}\;\frac{I_o(pb) + K_o(pb)\left[\dfrac{I_o(pa) + \frac{j\omega\mu}{p} I_1(pa)\, Y^{(1)}(a)}{-K_o(pa) + \frac{j\omega\mu}{p} K_1(pa)\, Y^{(1)}(a)}\right]}{I_1(pb) - K_1(pb)\left[\dfrac{I_o(pa) + \frac{j\omega\mu}{p} I_1(pa)\, Y^{(1)}(a)}{-K_o(pa) + \frac{j\omega\mu}{p} K_1(pa)\, Y^{(1)}(a)}\right]} \tag{2.15}$$

and the normalized admittance defined by (2.10a) to be

$$Y_r^{(1)}(b) = -j\frac{p}{k}\;\frac{I_o(pb) + K_o(pb)\left[\dfrac{I_o(pa) - j\frac{k}{p} I_1(pa)\, Y_r^{(1)}(a)}{-K_o(pa) - j\frac{k}{p} K_1(pa)\, Y_r^{(1)}(a)}\right]}{I_1(pb) - K_1(pb)\left[\dfrac{I_o(pa) - j\frac{k}{p} I_1(pa)\, Y_r^{(1)}(a)}{-K_o(pa) - j\frac{k}{p} K_1(pa)\, Y_r^{(1)}(a)}\right]} \tag{2.16}$$

The transformation for the TM admittance is found in the same manner. The general solution for E_z is

$$E_z = A\, I_o(pr) + B\, K_o(pr) \tag{2.17}$$

from which one finds

$$E_r = \frac{\gamma}{p}\left[A\, I_1(pr) - B\, K_1(pr)\right] \tag{2.18}$$

$$H_\phi = \frac{j\omega\varepsilon}{p}\left[A\, I_1(pr) - B\, K_1(pr)\right]. \tag{2.19}$$

These expressions give

$$\frac{j\omega\varepsilon}{p}\;\frac{\left[A\, I_1(pa) - B\, K_1(pa)\right]}{\left[A\, I_o(pa) + B\, K_o(pa)\right]} = Y^{(2)}(a)$$

$$\frac{\frac{j\omega\varepsilon}{p}\left[A\, I_1(pb) - B\, K_1(pb)\right]}{A\, I_o(pb) + B\, K_o(pb)} = Y^{(2)}(b)$$

$$A\left[\frac{j\omega\varepsilon}{p} I_1(pa) - I_o(pa)\, Y^{(2)}(a)\right] = B\left[\frac{j\omega\varepsilon}{p} K_1(pa) + K_o(pa)\, Y^{(2)}(a)\right]$$

$$Y^{(2)}(b) = \frac{j\omega\varepsilon}{p} \frac{I_1(pb) - K_1(pb)\left[\dfrac{\frac{j\omega}{p} I_1(pa) - I_o(pa)\, Y^{(2)}(a)}{\frac{j\omega}{p} K_1(pa) + K_o(pa)\, Y^{(2)}(a)}\right]}{I_o(pb) + K_o(pb)\left[\dfrac{\frac{j\omega}{p} I_1(pa) - I_o(pa)\, Y^{(2)}(a)}{\frac{j\omega}{p} K_1(pa) + K_o(pa)\, Y^{(2)}(a)}\right]} \qquad (2.20)$$

$$Y_r^{(2)}(b) = \frac{jk}{p} \frac{I_1(pb) - K_1(pb)\left[\dfrac{I_1(pa) - \frac{p}{jk} I_o(pa)\, Y_r^{(2)}(a)}{K_1(pa) + \frac{p}{jk} K_o(pa)\, Y_r^{(2)}(a)}\right]}{I_o(pb) + K_o(pb)\left[\dfrac{I_1(pa) - \frac{p}{jk} I_o(pa)\, Y_r^{(2)}(a)}{K_1(pa) + \frac{p}{jk} K_o(pa)\, Y_r^{(2)}(a)}\right]}. \qquad (2.21)$$

One has available now, expressions which relate the admittances at any two radii of a cylindrical symmetrical system. (2.15) and (2.20) give the expressions for transforming admittances. (2.16) and (2.21) give the corresponding information for transforming normalized admittances. Cases of special interest are those where one of the radii associated in the transformation is either infinite or zero. In such cases, certain terms become insignificant with respect to others, and the transformation is a function of the finite radius alone.

For the TE waves with a infinite

$$Y^{(1)}(b) = \frac{p}{j\omega\mu} \frac{K_o(pb)}{K_1(pb)}, \qquad Y_r^{(1)}(b) = -\frac{p}{jk} \frac{K_o(pb)}{K_1(pb)}. \qquad (2.22)$$

For the TE waves with a zero

$$Y^{(1)}(b) = -\frac{p}{j\omega\mu}\frac{I_o(pb)}{I_1(pb)}, \quad Y_r^{(1)}(b) = \frac{p}{jk}\frac{I_o(pb)}{I_1(pb)}. \tag{2.23}$$

For the TM waves with a infinite

$$Y^{(2)}(b) = -\frac{j\omega\varepsilon}{p}\frac{K_1(pb)}{K_o(pb)}, \quad Y_r^{(2)}(b) = -\frac{jk}{p}\frac{K_1(pb)}{K_o(pb)}. \tag{2.24}$$

And finally, for TM waves with a zero

$$Y^{(2)}(b) = \frac{j\omega\varepsilon}{p}\frac{I_1(pb)}{I_o(pb)}, \quad Y_r^{(2)}(b) = \frac{jk}{p}\frac{I_1(pb)}{I_o(pb)}. \tag{2.25}$$

These relationships can also be found by noting that any solution valid to infinity in the radial direction cannot contain Bessel functions of the first kind, and that solutions containing $r = 0$ cannot contain Bessel functions of the second kind.

Section III

HELIX CONSTRAINT

The relationships derived in the previous section merely determine the admittance transformations. If one equates the expressions for admittances, either those of (2.22) and (2.23) or (2.24) and (2.25) at some radius b one finds that only the value $p = \infty$ and $p = 0$ will satisfy these relationships. Irrespective of the physical significance of these waves, their velocities would be out of the range of interest with regard to traveling-wave interaction. Their velocities correspond to zero and the velocity of light respectively.

In order to get waves of interest, it is necessary to introduce structures that modify the admittances in some manner that will permit the propagation constants to fall within the range of interest. For instance, a conducting pipe at some given radius would fix the admittance at that radius to be infinite. This will result in TE or TM waves with phase velocities greater than that of light to exist in the region outside or inside the pipe. Other structures will have similar effects on the admittances.

One of the most interesting and useful structures that one can use is a helix. In order to simplify the discussion, an approximation to a real helix will be used. It is assumed that a helix can be replaced by an anisotropically conducting surface at the radius of the helix. The surface conducts perfectly in the direction of the helix, and it does not conduct at all perpendicularly to this direction. This has been called a sheath helix in the literature. Such a sheath helix is illustrated schematically by the helix in Fig. 4.1 . Conduction takes place

along the θ direction, that is, in the direction that makes an angle θ with the circular section cut by a plane perpendicular to the axis.

The effect of a helix is to act as a constraint on the values of the admittances immediately inside the outside the helix.

One can write down the boundary conditions.

$$E_{z_i} \sin\theta + E_{\phi_i} \cos\theta = 0 \qquad (3.1)$$

$$E_{z_o} \sin\theta + E_{\phi_o} \cos\theta = 0 \qquad (3.2)$$

$$E_{z_i} = E_{z_o} \quad (E_{\phi_i} = E_{\phi_o}) \qquad (3.3)$$

$$H_{z_i} \sin\theta + H_{\phi_i} \cos\theta = H_{z_o} \sin\theta + H_{\phi_o} \cos\theta \ . \qquad (3.4)$$

The subscripts designate the components of the field and whether it is the component just inside or just outside the sheath helix. Suitable substitutions are made to get expressions in terms of the admittances rather than in terms of the field components.

(3.4) becomes

$$Y_i^{(1)} E_{\phi_i} \sin\theta + Y_i^{(2)} E_{z_i} \cos\theta = Y_o^{(1)} E_{\phi_o} \sin\theta + Y_o^{(2)} E_{z_o} \cos\theta \ . \qquad (3.5)$$

(3.1) and (3.2) can be written

$$E_{\phi_i} = - E_{z_i} \tan\theta \ , \quad E_{\phi_o} = - E_{z_o} \tan\theta \ .$$

These equations, in conjunction with (3.3) are substituted into (3.5) to get

$$- Y_i^{(1)} E_{z_i} \tan\theta \sin\theta + Y_i^{(2)} E_{z_i} \cos\theta =$$

$$= - Y_o^{(1)} E_{z_i} \tan\theta \sin\theta + Y_o^{(2)} E_{z_i} \cos\theta$$

$$(Y_o^{(1)} - Y_i^{(1)}) \tan^2\theta = Y_o^{(2)} - Y_i^{(2)} \quad . \tag{3.6}$$

Obviously, the same relationship will hold for the normalized admittances except for the change of sign associated with the definitions.

$$(Y_{r_o}^{(1)} - Y_{r_i}^{(1)}) \tan^2\theta = Y_{r_i}^{(2)} - Y_{r_o}^{(2)} \quad . \tag{3.7}$$

Section IV

THE LOSSLESS HELIX

In order to get some insight as to how the admittance transformations and the helix constraint are to be used, the TM admittance of a lossless helix will be determined at a radius b smaller than the radius of the sheath helix a. This will give the admittance expression found by Chu and Jackson (R-1). Using the admittance expressions will enable one, however, to do away with much of the laborious algebraic manipulation required to keep track of the separation constants of the usual field matching technique.

The system under consideration is depicted in Fig. 4.1. The beam is of radius b. One wants to have an expression for the circuit admittance at radius b as a function of propagation constant, or, equivalently of p*. This expression is then used to match the admittance of the electron beam. The expressions for the TE admittances just inside and outside the helix and for the TM admittance just outside the helix are determined from equations (2.23), (2.22), and (2.24) respectively.

$$
\begin{aligned}
Y_{r_i}^{(1)} &= \frac{p}{jk}\,\frac{I_o(pa)}{I_1(pa)} \\
Y_{r_o}^{(1)} &= -\frac{p}{jk}\,\frac{K_o(pa)}{K_1(pa)} \\
Y_{r_o}^{(2)} &= -\frac{jk}{p}\,\frac{K_1(pa)}{K_o(pa)} \ .
\end{aligned}
\tag{4.1}
$$

*Sometimes p will be called a propagation constant here even though it is related to the actual propagation constant γ by $p^2 = -\gamma^2 - k^2$. This will be done only when no ambiguity will arise by doing so.

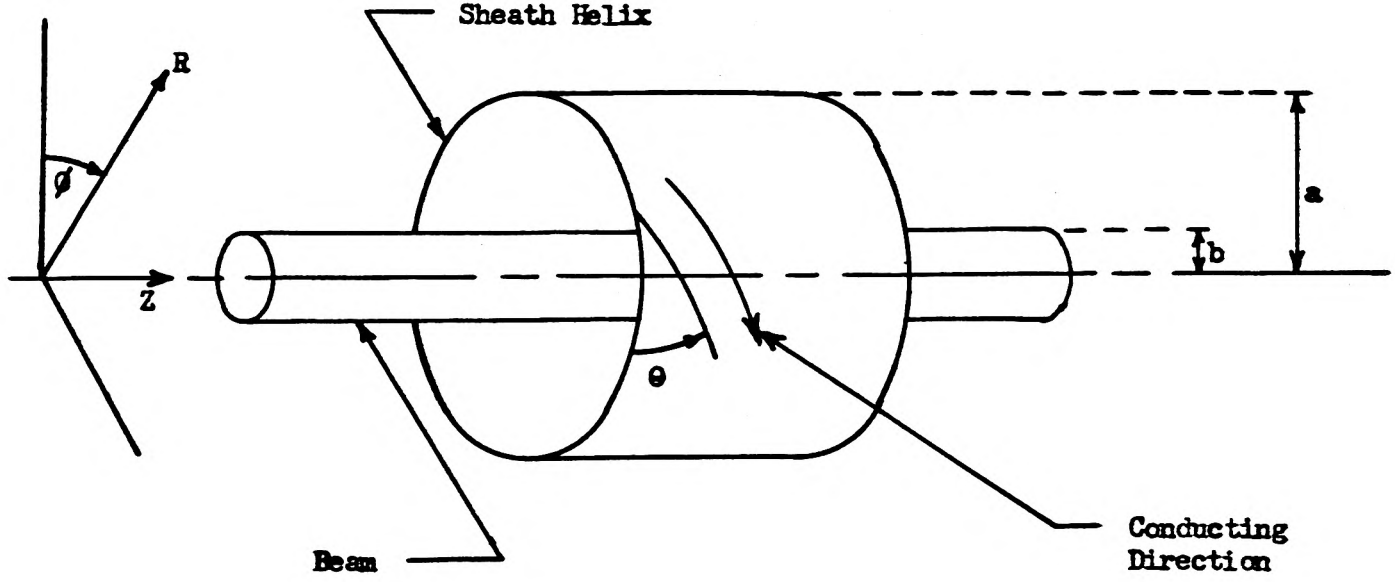

SHEATH HELIX WITH CONCENTRIC BEAM

Fig. 4.1

Substituting these expressions in the helix constraint (3.7) yields

$$Y^{(2)}_{r_i}(a) = -\frac{jk}{p}\frac{K_1(pa)}{K_0(pa)} + j\frac{p}{k}\left[\frac{K_0(pa)}{K_1(pa)} + \frac{I_0(pa)}{I_1(pa)}\right]\tan^2\theta \,.$$

By use of the Wronskian identity

$$I_0(z)\,K_1(z) + I_1(z)\,K_0(z) = \frac{1}{z} \,, \tag{4.2}$$

(4.1) can be written as

$$Y^{(2)}_{r_i}(a) = -j\frac{ka}{pa}\frac{K_1(pa)}{K_0(pa)} + \frac{j}{ka}\frac{\tan^2\theta}{I_1(pa)\,K_1(pa)} \,. \tag{4.3}$$

The transformation (2.21) then gives the admittance at b .

$$Y^{(2)}_r(b) = \frac{jka}{pa}\,\frac{I_1(pb) - K_1(pb)\;\dfrac{I_1(pa) + \dfrac{K_1(pa)\,I_0(pa)}{K_0(pa)} - \dfrac{pa}{(ka)^2}\dfrac{\tan^2\theta\, I_0(pa)}{I_1(pa)\,K_1(pa)}}{\dfrac{pa}{(ka)^2}\dfrac{\tan^2\theta\,K_0(pa)}{I_1(pa)\,K_1(pa)}}}{I_0(pb) + K_0(pb)\;\dfrac{I_1(pa) + \dfrac{K_1(pa)\,I_0(pa)}{K_0(pa)} - \dfrac{pa}{(ka)^2}\dfrac{\tan^2\theta\, I_0(pa)}{I_1(pa)\,K_1(pa)}}{\dfrac{pa}{(ka)^2}\dfrac{\tan^2\theta\,K_0(pa)}{I_1(pa)\,K_1(pa)}}}$$

Use of the identity (4.2) shows that

$$I_1(pa) + \frac{K_1(pa)\,I_0(pa)}{K_0(pa)} = \frac{1}{pa\,K_0(pa)} \,.$$

Substituting this expression into the expression for the admittance gives

$$Y^{(2)}_r(b) = j\frac{ka}{pa}\,\frac{I_1(pb) - K_1(pb)\;\dfrac{\left(\frac{ka}{pa}\right)^2\cot^2\theta\, I_1(pa)\,K_1(pa) - I_0(pa)K_0(pa)}{K^2_0(pa)}}{I_0(pb) + K_0(pb)\;\dfrac{\left(\frac{ka}{pa}\right)^2\cot^2\theta\, I_1(pa)\,K_1(pa) - I_0(pa)K_0(pa)}{K^2_0(pa)}} \,. \tag{4.4}$$

This is just the expression derived by Chu and Jackson.

Section V

THE LOSSY WIRE HELIX

In practice, helices are not made from perfectly conducting materials. In fact, consideration of the conductivity of the helix material may be secondary to the consideration of other necessary properties.

The real helix made from lossy wire will be approximated by a sheath helix with imperfect conductivity along the direction of conduction. The way such a lossy helix would enter into the calculation of the propagation constants would be through the helix constraint on the admittances. The equation of constraint corresponding to (3.6) or (3.7) could be found. However, in order to illustrate the labor saved by use of the admittance transformations and equations of constraint, the field matching technique will be used to solve this problem.

The system under consideration is depicted in Fig. 4.1, the only change being that the helix no longer is to be assumed to have infinite conductivity.

For the TE wave in region 1 and 2

$$H_z = A_1 I_o(pr) \tag{5.1a}$$

$$H_r = A_1 \frac{\gamma}{p} I_1(pr) \tag{5.1b}$$

$$E_\phi = -A_1 \frac{j\omega\mu}{p} I_1(pr) , \tag{5.1c}$$

and for region 3, outside the helix

$$H_z = A_2 K_o(pr) \tag{5.2a}$$

$$H_r = A_2 \frac{\gamma}{p} K_1(pr) \tag{5.2b}$$

$$E_\phi = A_2 \frac{j\omega\mu}{p} K_1(pr) \tag{5.2c}$$

For the TM wave in region 2, between the beam and the helix

$$E_z = C_3 I_o(pr) + C_4 K_o(pr) \tag{5.3a}$$

$$E_r = \frac{\gamma}{p}\left[C_3 I_1(pr) - C_4 K_1(pr)\right] \tag{5.3b}$$

$$H_\phi = \left[\frac{j\omega}{p} C_3 I_1(pr) - C_4 K_1(pr)\right] \tag{5.3c}$$

outside the helix,

$$E_z = C_1 K_o(pr) \tag{5.4a}$$

$$E_r = -C_1 K_1(pr) \tag{5.4b}$$

$$H_\phi = -C_1 \frac{j\omega\varepsilon}{p} K_1(pr) \quad . \tag{5.4c}$$

Since there is no perfectly conducting direction, E is continuous across the helix. The boundary conditions are

$$E_{z_i} \cos\theta - E_{\phi_i} \sin\theta = E_{z_o} \cos\theta - E_{\phi_o} \sin\theta \tag{5.5}$$

$$E_{z_i} \sin\theta + E_{\phi_i} \cos\theta = E_{z_o} \sin\theta + E_{\phi_o} \cos\theta \tag{5.6}$$

$$H_{z_i} \sin\theta + H_{\phi_i} \cos\theta = H_{z_o} \sin\theta + H_{\phi_o} \cos\theta \tag{5.7}$$

$$H_{z_i} \cos\theta - H_{\phi_i} \sin\theta = H_{z_o} \cos\theta - H_{\phi_o} \sin\theta + \sigma\left[E_{z_o} \sin\theta + E_{\phi_o} \cos\theta\right] \tag{5.8}$$

where σ is the conductivity along the conducting direction. No current can flow normally to this direction. The arguments of the Bessel functions are taken to be pa unless otherwise indicated.

Substituting the values for the field components into the boundary conditions

$$[C_3 I_o + C_4 K_o] \sin\theta - A_1 \frac{j\omega\mu}{p} I_1 \cos\theta = C_1 K_o \sin\theta + A_2 \frac{j\omega\mu}{p} K_1 \cos\theta \tag{5.9}$$

$$[C_3 I_o + C_4 K_o] \cos\theta + A_1 \frac{j\omega\mu}{p} I_1 \sin\theta = C_1 K_o \cos\theta - A_2 \frac{j\omega\mu}{p} K_1 \sin\theta \tag{5.10}$$

$$A_1 I_o \sin\theta + \frac{j\omega\varepsilon}{p} [C_3 I_1 - C_4 K_1] \cos\theta = A_2 K_o \sin\theta - C_1 \frac{j\omega\varepsilon}{p} K_1 \cos\theta \tag{5.11}$$

$$A_1 I_o \cos\theta - \frac{j\omega\varepsilon}{p} [C_3 I_1 - C_4 K_1] \sin\theta = A_2 K_o \cos\theta + C_1 \frac{j\omega\varepsilon}{p} K_1 \sin\theta + \sigma \left[C_1 K_o \sin\theta + A_2 \frac{j\omega\mu}{p} K_1 \cos\theta\right]. \tag{5.12}$$

When these equations are solved for the matching constants, one gets

$$C_3 = C_1 \frac{K_o^2}{(\frac{ka}{pa})^2 \cot^2\theta K_1 I_1 - \frac{j\omega\varepsilon}{p} \frac{1+\cot^2\theta}{pa}} \tag{5.13}$$

$$C_4 = C_1 \frac{(\frac{ka}{pa})^2 \cot^2\theta K_1 I_1 - K_o I_o - j \frac{\omega\varepsilon}{\sigma p} \frac{1+\cot^2\theta}{pa}}{(\frac{ka}{pa})^2 \cot^2\theta K_1 I_1 - \frac{j\omega\varepsilon}{\sigma p} \frac{1+\cot^2\theta}{pa}} . \tag{5.14}$$

The admittance at radius b is then seen to be

$$Y_r^{(2)}(b) = j \frac{ka}{pa} \frac{I_1(pb) - K_1(pb)\left[\frac{(\frac{ka}{pa})^2 \cot^2\theta \; K_1(pa)I_1(pa) - K_o(pa)I_o(pa) - \frac{j\omega\varepsilon}{\sigma p} \frac{\csc^2\theta}{pa}}{K_o^2(pa)}\right]}{I_o(pb) + K_o(pb)\left[\frac{(\frac{ka}{pa}) \cot^2\theta K_1(pa)I_1(pa) - K_o(pa)I_o(pa) - \frac{j\omega\varepsilon}{\sigma p} \frac{\csc^2\theta}{pa}}{K_o^2(pa)}\right]} \tag{5.15}$$

or if a normalized conductivity is used

$$\sigma_r = \sqrt{\frac{\mu}{\varepsilon}}\,\sigma\,, \tag{5.16}$$

$$Y^{(2)}(b) = j\,\frac{ka}{pa}\,\frac{I_1(pb) - K_1(pb)\left[\dfrac{\left(\frac{ka}{pa}\right)^2 \cot^2\theta\, K_1(pa)I_1(pa) - K_o(pa)I_o(pa) - \dfrac{jka}{\sigma_r pa}\,\dfrac{\csc^2\theta}{pa}}{K_o^2(pa)}\right]}{I_o(pb) + K_o(pb)\left[\dfrac{\left(\frac{ka}{pa}\right)^2 \cot^2\theta\, K_1(pa)I_1(pa) - K_o(pa)I_o(pa) - \dfrac{jka}{\sigma_r pa}\,\dfrac{\csc^2\theta}{pa}}{K_o^2(pa)}\right]}\,. \tag{5.17}$$

Section VI

PERFECT HELIX WITH AN ANISOTROPIC ADMITTANCE SHEATH IMMEDIATELY OUTSIDE THE HELIX

The configuration under consideration in this section is depicted in Fig. 6.1 .

Y_1 is the surface admittance in the ϕ direction.

Y_2 is the negative of the admittance in the z direction. The minus sign is used in order to be consistent with the previous admittance definitions.

The expressions for the admittances just outside the admittance sheath are the same as those found in (4.1) except for the normalization.

$$Y^{(1)} = \frac{p}{j\omega\mu} \frac{K_o(pa)}{K_1(pa)} , \qquad Y^{(2)} = - \frac{j\omega\varepsilon}{p} \frac{K_1(pa)}{K_o(pa)} . \tag{6.1}$$

To find the TE and TM admittances just outside the helix, the admittances of the sheath are added to those of (6.1) with due consideration of the signs in the definition.

$$Y_o^{(1)} = \frac{p}{j\omega\mu} \frac{K_o(pa)}{K_1(pa)} + Y_1 , \qquad Y_o^{(2)} = - \left[\frac{j\omega\varepsilon}{p} \frac{K_1(pa)}{K_o(pa)} + Y_2 \right] . \tag{6.2}$$

The TE admittance just inside the helix is

$$Y_i^{(1)} = - \frac{p}{j\omega\mu} \frac{I_o(pa)}{I_1(pa)} . \tag{6.3}$$

Application of the helix constraint (3.6) yields

$$Y_i^{(2)} = - \frac{\tan^2\theta}{j\omega\mu a\, I_1(pa)\, K_1(pa)} - Y_1 \tan^2\theta - \frac{j\omega\varepsilon}{p} \frac{K_1(pa)}{K_o(pa)} . \tag{6.4}$$

The admittance transformation is applied to (6.4) to get the expression for the admittance at the beam radius. The result of this transformation

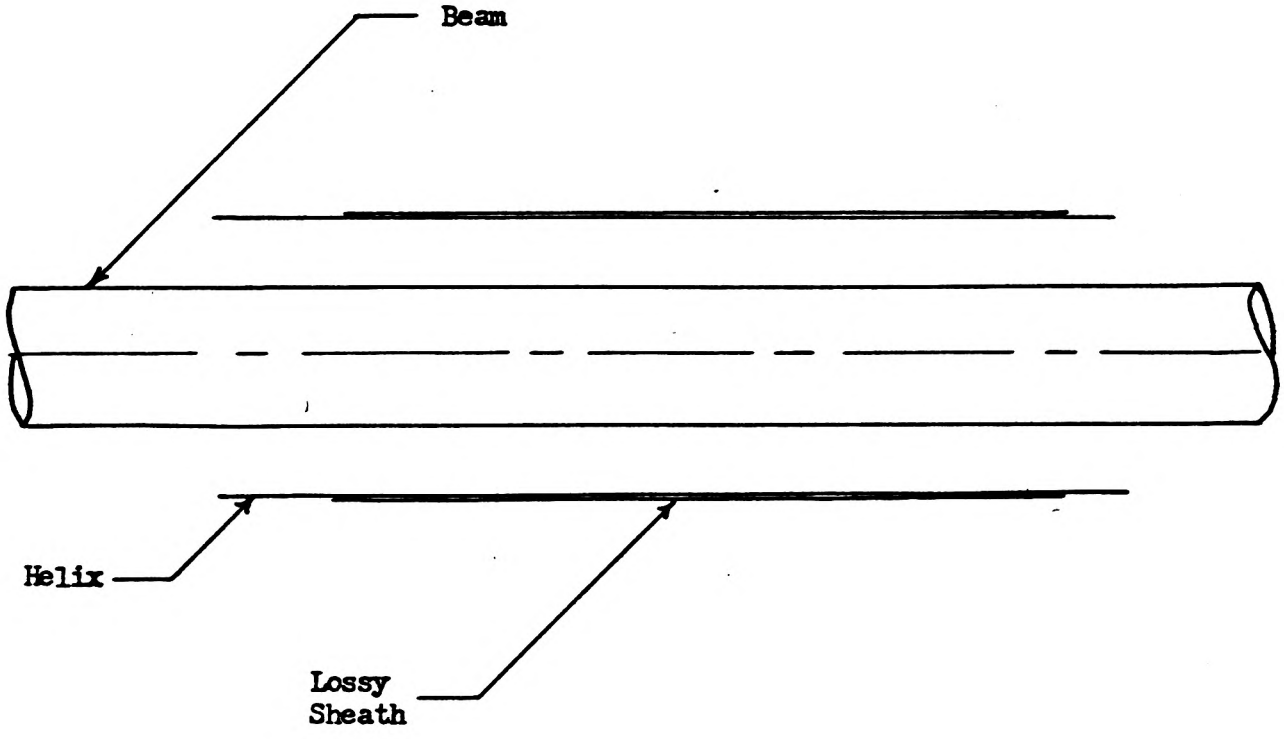

Helix with Anisotropic Lossy Sheath

Fig. 6.1

is

$$Y^{(2)}(b) = j\frac{ka}{pa}$$

$$\frac{I_1(pr) - K_1(pr)\left[\dfrac{(\frac{ka}{pa})^2 \cot^2\theta I_1(pa)K_1(pa) - I_o(pa)K_o(pa) - j\omega\mu a\cot^2\theta(Y_2 + Y_1\tan^2\theta)I_1(pa)K_1(pa)I_o(pa)K_o(pa)}{K_o^2(pa)\left[1 + j\omega\mu a I_1(pa)\,K_1(pa)\cot^2\theta\,(Y_2 + Y_1\tan^2\theta)\right]}\right]}{I_o(pr) + K_o(pr)\left[\dfrac{(\frac{ka}{pa})^2\cot^2\theta I_1(pa)K_1(pa) - I_o(pa)K_o(pa) - j\omega\mu a\cot^2\theta(Y_2 + Y_1\tan^2\theta)I_1(pa)K_1(pa)I_o(pa)K_o(pa)}{K_o^2(pa)\left[1 + j\omega\mu a I_1(pa)\,K_1(pa)\cot^2\theta\,(Y_2 + Y_1\tan^2\theta)\right]}\right]} \qquad (6.5)$$

Setting $Y_{r1} = \sqrt{\frac{\mu}{\varepsilon}}\,Y_1$ and $Y_{r_2} = \sqrt{\frac{\mu}{\varepsilon}}\,Y_2$ (6.6)

$$Y^{(2)}_{(b)} = j\frac{ka}{pa}$$

$$\frac{I_1(pr) - K_1(pr)\left[\dfrac{(\frac{ka}{pa})^2 \cot^2\theta I_1(pa)K_1(pa) - I_o(pa)K_o(pa) - jka\cot^2\theta(Y_2 + Y_1\tan^2\theta I_1(pa)K_1(pa)I_o(pa)K_o(pa)}{K_o^2(pa)\left[1 + jka\, I_1(pa)\, K_1(pa)\cot^2\theta(Y_2 + Y_1\tan^2\theta)\right]}\right]}{I_o(pr) + K_o(pr)\left[\dfrac{(\frac{ka}{pa})^2 \cot^2\theta I_1(pa)K_1(pa) - I_o(pa)K_o(pa) - jka\cot^2\theta(Y_2 + Y_1\tan^2\theta) I_1(pa)K_1(pa)I_o(pa)K_o(pa)}{K_o^2(pa)\left[1 + jka\, I_1(pa)\, K_1(pa)\cot^2\theta\,(Y_2 + Y_1\tan^2\theta)\right]}\right]} \qquad (6.7)$$

Section VII

PERFECT HELIX WITH AN ANISOTROPIC ADMITTANCE SHEATH AT A GREATER RADIUS THAN THAT OF THE HELIX

Obviously, the result of a calculation would depend a good deal upon the model chosen to represent a traveling-wave tube. Perhaps a suitable representation is shown in Fig. 7.1 .

The difference in the capacitivity and permeability in the region between the helix and the admittance sheet indicates that a medium other than vacuum can be considered to surround the helix. One may wish to represent the glass envelope of a traveling-wave tube in this manner. Other configurations can also be used, depending upon the complexity of the calculations that one is willing to handle. For instance, a conducting pipe may surround the entire structure, or there may be a region of vacuum between the helix and the dielectric. When handling a problem which deals with several media, it must be remembered that k and p are also functions of the particular medium. Unnormalized admittances are continuous across dielectric boundaries. Normalized admittances could be used by using $\sqrt{\frac{\mu_o}{\varepsilon_o}}$ as a normalizing factor instead of $\sqrt{\frac{\mu}{\varepsilon}}$.

If the circuit admittances are to be computed by digital computers of suitable capacity, the introduction of complicated arrangements of cylindrical regions should not cause any trouble. The machine can be programmed to repeat the transformations as often as required. If it is desired to get an analytical expression for the admittance, the task is straightforward but very tedious. In fact, it is impractical to consider hand calculations for obtaining admittance values at many

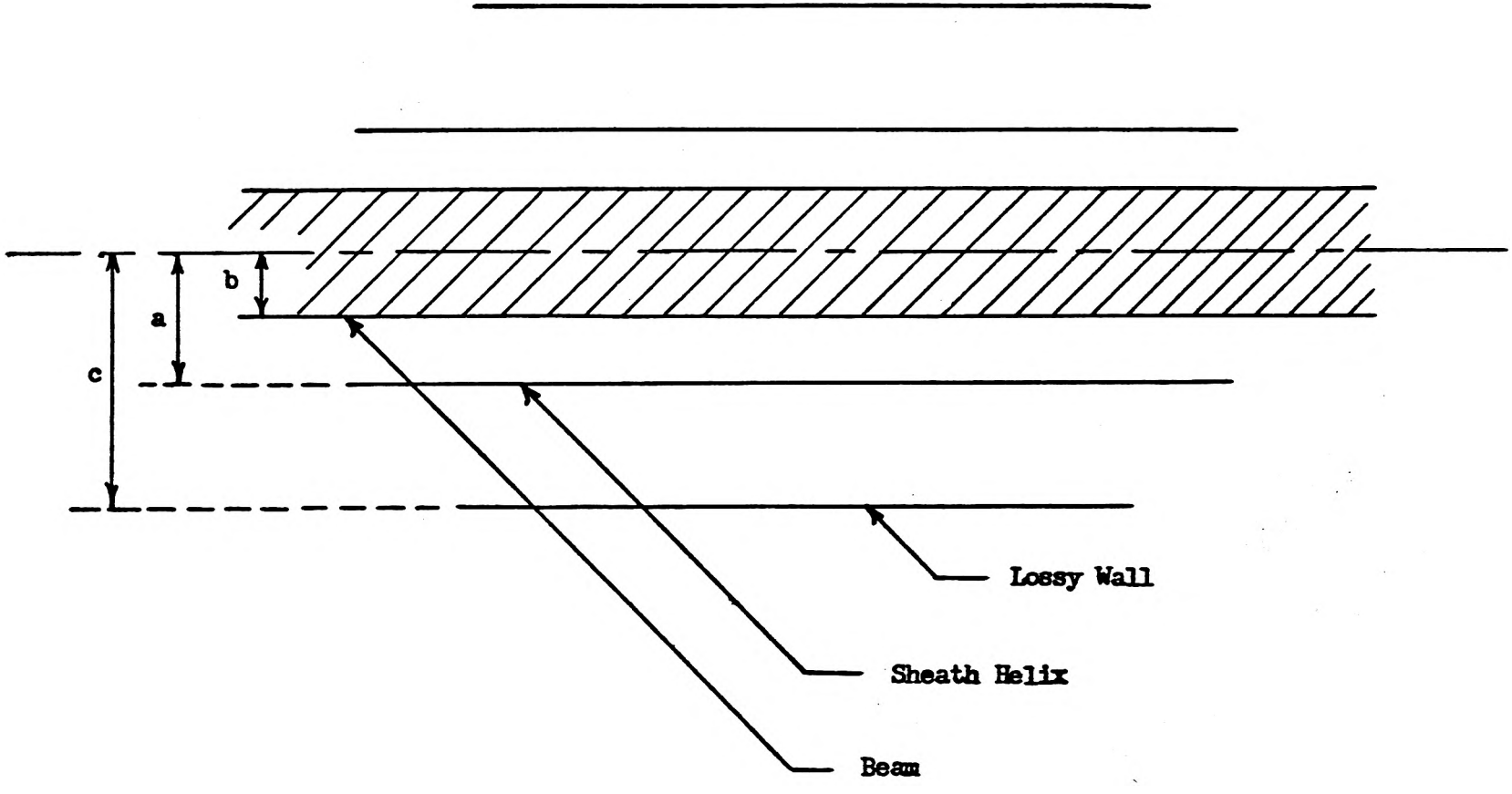

TRAVELING-WAVE TUBE WITH AN ATTENUATING WALL

Fig. 7.1

points in the complex p plane.

An expression has been obtained for the TM admittance of the structure depicted in Fig. 7.1 at the inner surface of the helix under the condition that all the volume is vacuum. In order to get the admittance at the beam surface, another admittance transformation is required. Such an expression can be obtained, but it would be quite unmanageable. No additional physical insight would be obtained by the use of such an unwieldy expression. The admittance function is found as described below.

The admittances outside the sheath at radius c are found from (2.22) and (2.24). They are

$$Y_o^{(1)}(c) = \frac{p}{j\omega\mu} \frac{K_o(pc)}{K_1(pc)} \tag{7.1}$$

$$Y_o^{(2)}(c) = -\frac{j\omega\varepsilon}{p} \frac{K_1(pc)}{K_o(pc)} \tag{7.2}$$

To get the admittance just inside the admittance sheet, the parallel admittance of the admittance sheath and the free space admittance is taken.

$$\begin{aligned} Y_i^{(1)}(c) &= \frac{p}{j\omega\mu} \frac{K_o(pc)}{K_1(pc)} + Y_1 \\ Y_i^{(2)}(c) &= -\left[\frac{j\omega\varepsilon}{p} \frac{K_1(pc)}{K_o(pc)} + Y_2\right] \end{aligned} \tag{7.3}$$

Using the transformations (2.15) and (2.20), these admittances are transformed to the helix radius.

$$Y_o^{(1)}(a) = -\frac{p}{j\omega\mu}$$

$$\frac{I_o(pa) + K_o(pa)\left[\dfrac{\frac{j\omega\mu}{p}\left[\frac{p}{j\omega\mu}\frac{K_o(pc)}{K_1(pc)} I_1(pc) + Y_1 I_1(pc)\right] + I_o(pc)}{\frac{j\omega\mu}{p}\left[\frac{p}{j\omega\mu}\frac{K_o(pc)}{K_1(pc)} K_1^2(pc) + Y_1 K_1(pc)\right] - K_o(pc)}\right]}{I_1(pa) - K_1(pa)\left[\dfrac{\frac{j\omega\mu}{p}\left[\frac{p}{j\omega\mu}\frac{K_o(pc)}{K_1(pc)} I_1(pc) + Y_1 I_1(pc)\right] + I_o(pc)}{\frac{j\omega\mu}{p}\left[\frac{p}{j\omega\mu}\frac{K_o(pc)}{K_1(pc)} K_1^2(pc) + Y_1 K_1(pc)\right] - K_o(pc)}\right]}$$

which, after simplification and the use of (4.2) becomes

$$Y_o^{(1)}(a) = \frac{p}{j\omega\mu}\,\frac{K_o(pa) + j\omega\mu c\, Y_1 K_o(pc)\left[I_o(pa)K_1(pc) + K_o(pa)I_1(pc)\right]}{K_1(pa) - j\omega\mu c Y_1 K_o(pc)\left[I_1(pa)K_o(pc) - K_1(pa)I_1(pc)\right]}\,. \tag{7.4}$$

Similarly, after suitable simplification

$$Y_o^{(2)}(a) = -\frac{j\omega\varepsilon}{p}\,\frac{K_1(pa) + \frac{p^2c}{j\omega\varepsilon} K_o(pc)Y_2\left[K_o(pc)I_1(pa) + I_o(pc)K_1(pa)\right]}{K_o(pa) + \frac{p^2c}{j\omega\varepsilon} K_o(pc)Y_2\left[I_o(pc)K_o(pa) - K_o(pc)I_o(pa)\right]}\,. \tag{7.5}$$

Inside the helix, the TE admittance is the same as has already been computed by means of (2.23)

$$Y_i(a) = -\frac{p}{j\omega\mu}\,\frac{I_o(pa)}{I_1(pa)}\,. \tag{7.6}$$

Application of the helix constraint (3.6) yields

$$Y_i^{(2)}(a) =$$

$$-\frac{j\omega\varepsilon}{p}\,\frac{K_1(pa)+\frac{p^2c}{j\omega\varepsilon}\,K_o(pc)\,Y_2\left[K_o(pc)\,I_1(pa)+I_o(pc)\,K_1(pa)\right]}{K_o(pa)+\frac{p^2c}{j\omega\varepsilon}\,K_o(pc)\,Y_2\left[I_o(pc)\,K_o(pa)-K_o(pc)\,I_o(pa)\right]} \tag{7.7}$$

$$-\frac{p\tan^2\theta}{j\omega\mu}\left[\frac{I_o(pa)}{I_1(pa)}+\frac{K_o(pa)+j\omega\mu c\,Y_1\,K_o(pc)\left[I_o(pa)K_1(pc)+K_o(pa)I_1(pc)\right]}{K_1(pa)-j\omega\mu c\,Y_1\,K_o(pc)\left[I_1(pa)K_1(pc)-K_1(pa)I_1(pc)\right]}\right].$$

This can be written in terms of normalized admittance

$$Y_{r_i}^{(2)}(a) = j\,\frac{pa}{ka}\tan^2\theta$$

$$\left[\frac{I_o(pa)}{I_1(pa)}+\frac{K_o(pa)+jkc\,Y_{r_i}\,K_o(pc)\left[I_o(pa)\,K_1(pc)+K_o(pa)\,I_1(pc)\right]}{K_1(pa)-jkc\,Y_{r_i}\,K_o(pc)\left[I_1(pa)\,K_1(pc)-K_1(pa)\,I_1(pc)\right]}\right]$$

$$-j\,\frac{ka}{pa}\,\frac{K_1(pa)-j(\frac{pa}{ka})pc\,Y_{r_2}\left[K_o(pc)\,I_1(pa)+I_o(pc)\,K_1(pa)\right]}{K_o(pa)-j(\frac{pa}{ka})pc\,Y_{r_2}\left[I_o(pc)\,K_o(pa)-K_o(pc)\,I_o(pa)\right]}\,. \tag{7.8}$$

This admittance could be transformed again to get an expression for the admittance at the beam radius. This will not be done because of the reasons given at the beginning of this section.

Section VIII

DYNAMICS OF THE ELECTRON BEAM

Much of this section is devoted to the derivation of the results of Chu and Jackson (R-1) and of Birdsall and Whinnery (R-4). They are derived here in order to have the expressions in a desirable form.

One starts with equation (2.8) which is rewritten here.

$$\frac{1}{r}\frac{\partial}{\partial r}\left(r\frac{\partial E_z}{\partial r}\right) - p^2 E_z = \frac{p^2}{j\omega\varepsilon} J_z \,. \tag{8.1}$$

In addition, the equation of continuity and the linearized equation of motion are to be used. The equation of continuity is

$$\frac{\partial \rho}{\partial t} = -\frac{\partial J_z}{\partial z} \,, \tag{8.2}$$

which is equivalent to

$$j\omega\rho = \gamma J_z \,, \tag{8.3}$$

where ρ and J_z are the alternating charge and current densities respectively. The equation of motion is

$$\frac{dv}{dt} = \frac{e}{m} E_z \,, \tag{8.4}$$

where e is the algebraic charge of the particle and m is the mass. Relativistic effects are neglected.

The operator $\frac{d}{dt}$ can be replaced by

$$\frac{d}{dt} = \frac{dz}{dt}\frac{\partial}{\partial z} + \frac{\partial}{\partial t} \,. \tag{8.5}$$

Linearization of the equation of motion takes place by setting $\frac{dz}{dt} = u_o$. The equation of motion can then be written as

$$-u_o \gamma v + j\omega v = \frac{e}{m} E_z , \tag{8.6}$$

where v is the alternating velocity of the electrons, and u_o is the direct velocity of the electrons.

To terms of the first order,

$$J_z = \rho u_o + \rho_o v , \tag{8.7}$$

where ρ_o is the direct charge density.

Substitution of (8.3) into (8.7) gives

$$J_z = \frac{\rho_o v}{1 - \frac{\gamma u_o}{j\omega}} . \tag{8.8}$$

Now, use of (8.6) gives J_z entirely in terms of E_z.

$$J_z = \frac{e \rho_o}{m (1 - \frac{\gamma u_o}{j\omega})(j\omega - \gamma u_o)} E_z . \tag{8.9}$$

The right hand side of (8.1) can be written as

$$p^2 \frac{e \rho_o}{m \varepsilon u_o^2} E_z \frac{1}{(j \frac{\omega}{u_o} - \gamma)^2} = \frac{\beta_p^2 p^2}{(\gamma - j\beta_e)^2} E_z . \tag{8.10}$$

where

$$\beta_p^2 = \frac{e \rho_o}{m \varepsilon u_o^2} , \tag{8.11}$$

the plasma wave number squared, and

$$\beta_e = \frac{\omega}{u_o} , \tag{8.12}$$

the wave number at the electron velocity.

Equation (6.1) can then be written

$$\frac{1}{r}\frac{\partial}{\partial r}\left(r\frac{\partial E_z}{\partial r}\right) - p^2\left[1 + \frac{\beta_p^2}{(\gamma - j\beta_e)^2}\right]E_z = 0 . \tag{8.13}$$

This equation is just a modified Bessel equation of zero order. The solution for E_z is of the form $I_o(\ r)$, where

$$\eta^2 = p^2\left[1 + \frac{\beta_p^2}{(\gamma - j\beta_e)^2}\right] . \tag{8.14}$$

The H_ϕ that is associated with this value of E_z is found by using equation (2.3).

$$H_\phi = \frac{j\omega\varepsilon\eta}{p^2} I_1(\eta r)\, E_z(r=0) . \tag{8.15}$$

The admittance of the beam at its surface is then seen to be

$$Y^{(2)}(b) = \frac{j\omega\varepsilon\eta}{p^2}\frac{I_1(\eta b)}{I_o(\eta b)} . \tag{8.16}$$

The normalized admittance is

$$Y_r^{(2)}(b) = j\frac{ka}{pa}\frac{\eta b}{pb}\frac{I_1(\eta b)}{I_o(\eta b)} . \tag{8.17}$$

Section IX

OBTAINING PROPAGATION CONSTANTS

This section will describe the straightforward procedure that one would adopt to get all the discrete propagation constants of a propagating structure with cylindrical symmetry and a coaxial electron beam.

The propagation constants correspond to the solutions of the equation obtained by setting the circuit admittance at the beam radius $Y_r^{(2)}(b)$ equal to the electronic admittance (8.17). Let the circuit admittances at b be designated by $y_b(pa)$ and $y_{rb}(pa)$ for the unnormalized and normalized admittances respectively. The matching equation is written

$$j \frac{ka}{pa} \frac{\eta b}{pb} \frac{I_1(\eta b)}{I_o(\eta b)} = y_{rb}(pa) , \tag{9.1}$$

which can also be written as

$$\eta b \frac{I_1(\eta b)}{I_o(\eta b)} = - j \frac{pa}{ka} pb \; y_{rb}(pa) . \tag{9.2}$$

The term $\eta b \frac{I_1(\eta b)}{I_o(\eta b)}$ is a function of ηb alone. It can be plotted in the complex ηb plane by means of two overlaid contour maps.

Birdsall and Whinnery (R-4) have published such plots with slightly different labels for the coordinate axes. Their contours consist of a set for the magnitude of the function and another set for the phase of the function. See Fig. 9.1. The plot is a universal curve for all electron beams.

In order to obtain values of the propagation constants, contour maps of the beam admittance and the circuit admittance can be drawn in

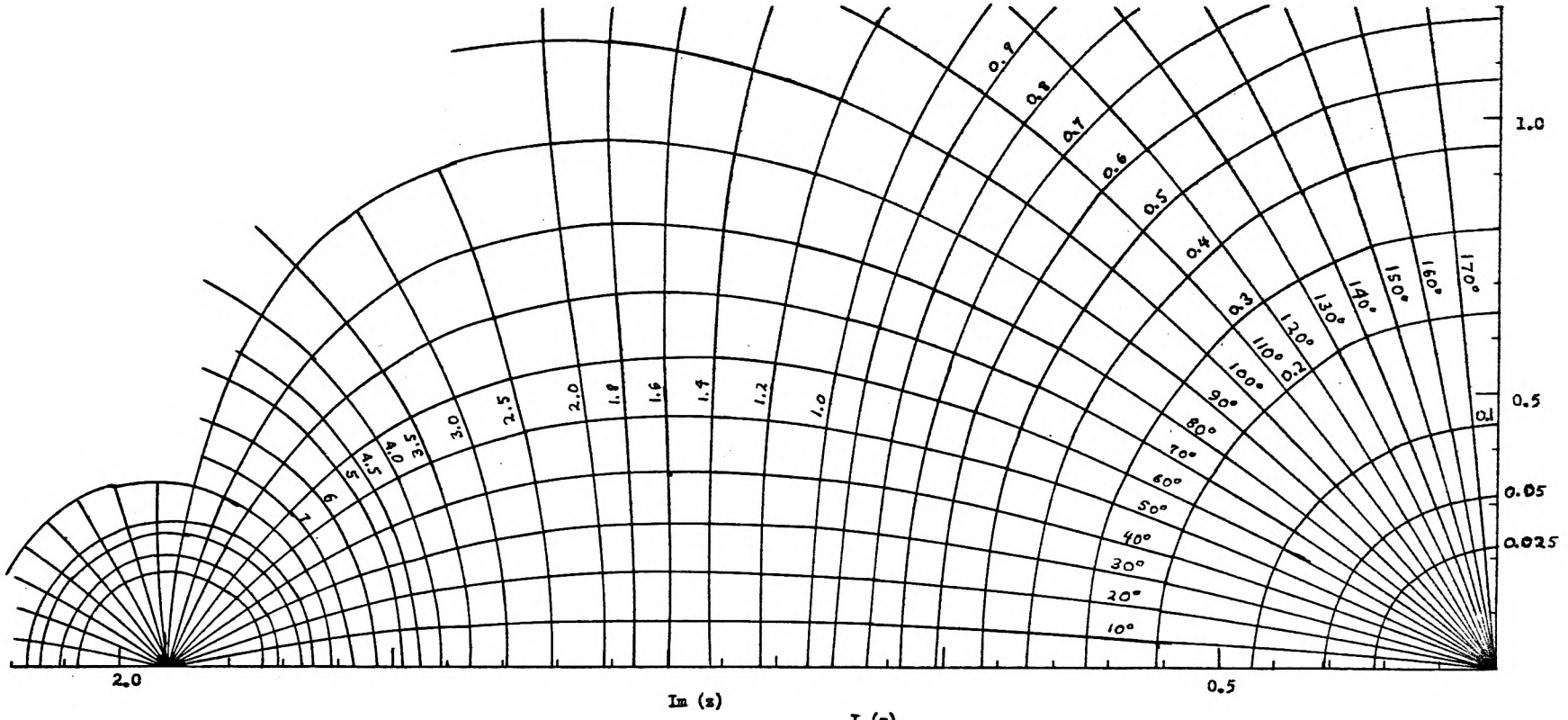

Contours of Constant Amplitude and Phase of $z\,\frac{I_1(z)}{I_0(z)}$

Fig. 9.1

either the pa plane or the ηb plane. In fact, if some other variable is convenient, a completely different plane may be chosen for the plots. The intersections of the beam and circuit admittances can then be found.

If the intersections are to be found in the pa plane, the values of pa are conveniently linked with the propagation constants through equation (2.4). Since relativistic effects are neglected,

$$p^2 \approx -\gamma^2 , \tag{9.3}$$

and (8.14) can then be written as

$$(\eta a)^2 = (pa)^2 \left[1 - \frac{(\beta_p a)^2}{(pa - \beta_e a)^2}\right] . \tag{9.4}$$

This equation enables one to make the calculations using pa as the independent variable rather than first using γa and then computing corresponding values of pa.

If intersections are to be found in the ηb plane, some further calculation is necessary to find the propagation constants in terms of these intersections. Equation (9.4) will have to be solved for the values of pa that correspond to each ηb which is a solution.

It must be noted that if the determination of the admittance intersections takes place in the pa plane, there will be an infinite number of intersections in the vicinity of $pa = \beta_e a$. This is seen from (9.4) and (9.1). As pa approaches $\beta_e a$, $(\eta a)^2$ approaches infinity. This means that the left hand term of (9.1) ranges through entire range of complex values twice each time ηa ranges approximately over an annulus of radius difference π, in the complex plane. That is, pa is an infinitely multiply-valued function of $\eta b \frac{I_1(\eta b)}{I_0(\eta b)}$. This means

that if one wants to determine the propagation constants in the pa plane, only one branch of the beam admittance function should be plotted on each set of circuit curves. Furthermore, if one wants to obtain the values of the difference between the propagation constant and β_e accurately, that is $p - \beta_e$, then the plots will have to be suitably expanded in the vicinity of $pa = \beta_e a$.

The advantage of working in the ηb plane is that the region in the vicinity of $p = \beta_e$ is mapped conformally over the entire complex plane. This means that all the mode intersections will be sufficiently far apart to handle easily.

The universal beam plot will require that a different circuit plot be drawn for every possible beam. That is, in order to use the ηb plane, a different set of curves will have to be drawn in the ηb plane to represent the circuit admittance for every set of beam characteristics even though the circuit characteristics remain unchanged. Similarly, if one works in the pa plane, a different set of beam curves is required for each change in beam characteristics. The latter procedure may be preferable if all one wants is the determination of the principal modes. If computation and curve plotting is done by machine, the same program can be used to calculate electronic curves in the pa plane for beams of widely ranged parameters. Calculation of the circuit admittance will tend to be strongly dependent upon the particular structure being considered, with considerably more calculation time required to get one point.

Section X

DESCRIPTION OF THE ADMITTANCE FUNCTIONS, RELATIONSHIP TO PIERCE-FLETCHER THEORY

Chu and Jackson (R-1) have described the admittance function of a helix. They have drawn a graph which shows the behavior of the admittance for real values of pa. See Fig. 10.1. This is a plot of the function $Y_r^{(2)}$ given in equation (4.4). The only singularities and zeros of the function occur for real pa. The reason for this is that an infinite or zero admittance corresponds to no transfer of energy between the beam and the helix. That is, either H_ϕ or E_z is zero at the beam surface for a zero or pole of the admittance. If there is no transfer of energy, there can be no gain or decay of the wave, and therefore, p will have to be real.

Examination of (4.4) will show, taking into account the behavior of the K functions for small values, that $pa = 0$ corresponds to a logarithmic branch point with a double pole. That is, the behavior is like $\frac{1}{z^2 \log z}$ near $z = 0$. There also is a zero at $pa = p'a$, and a pole at $pa = p_p a$. Furthermore, as pa approaches infinity, the value of the admittance will approach zero.

The description given above corresponds to a lossless helix with the admittance measured at a radius which is less than that of the helix. Examination of (4.4) shows that if $a = b$, then there will be no pole corresponding to p_p. The function will then have a zero corresponding to p' and will have a pole at infinity. See Fig. 10.2. Setting $b = a$ in (4.4) gives back (4.3). The significance of this fact is that

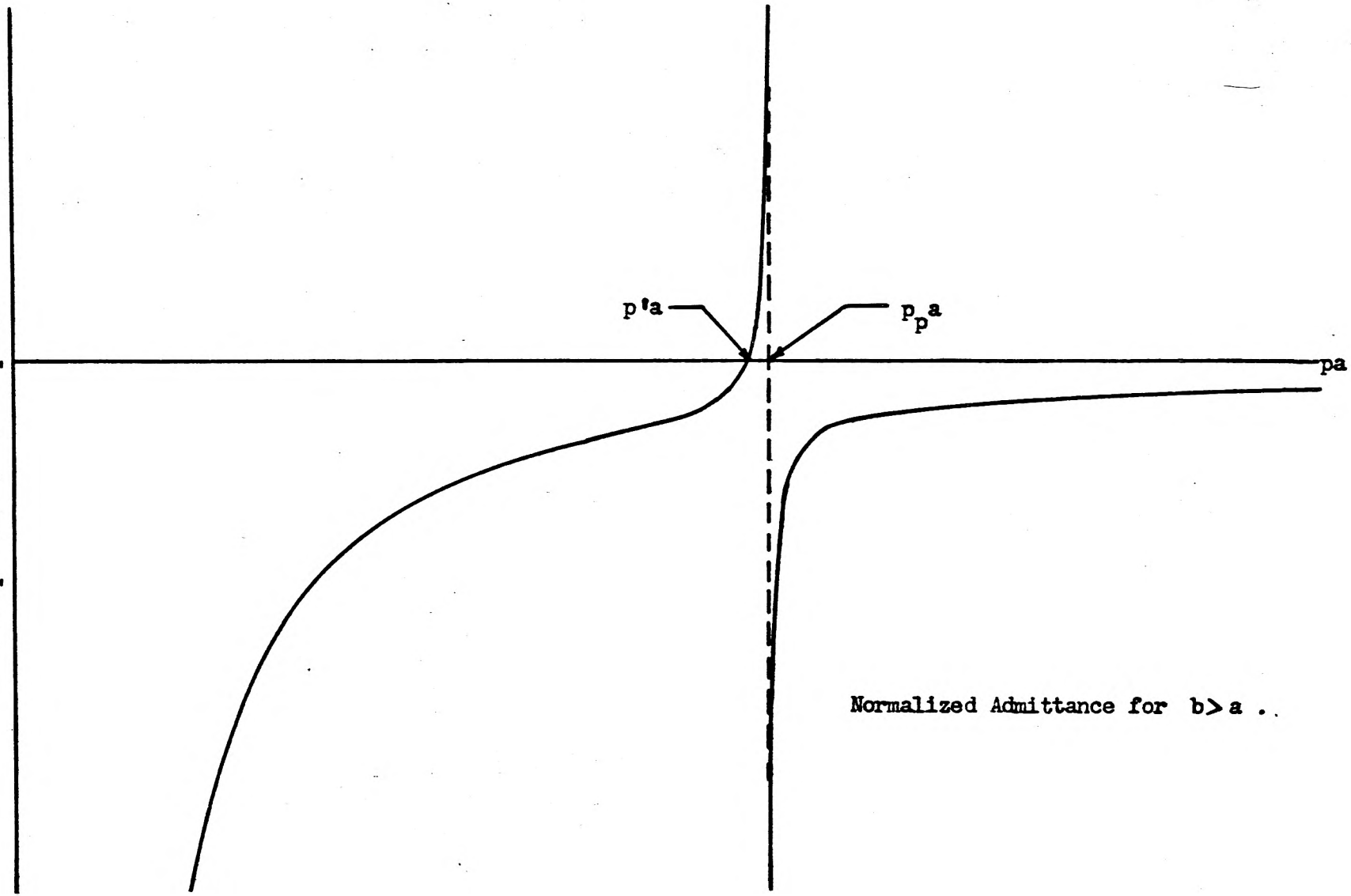

Normalized Admittance for b > a . .

Fig. 10.1

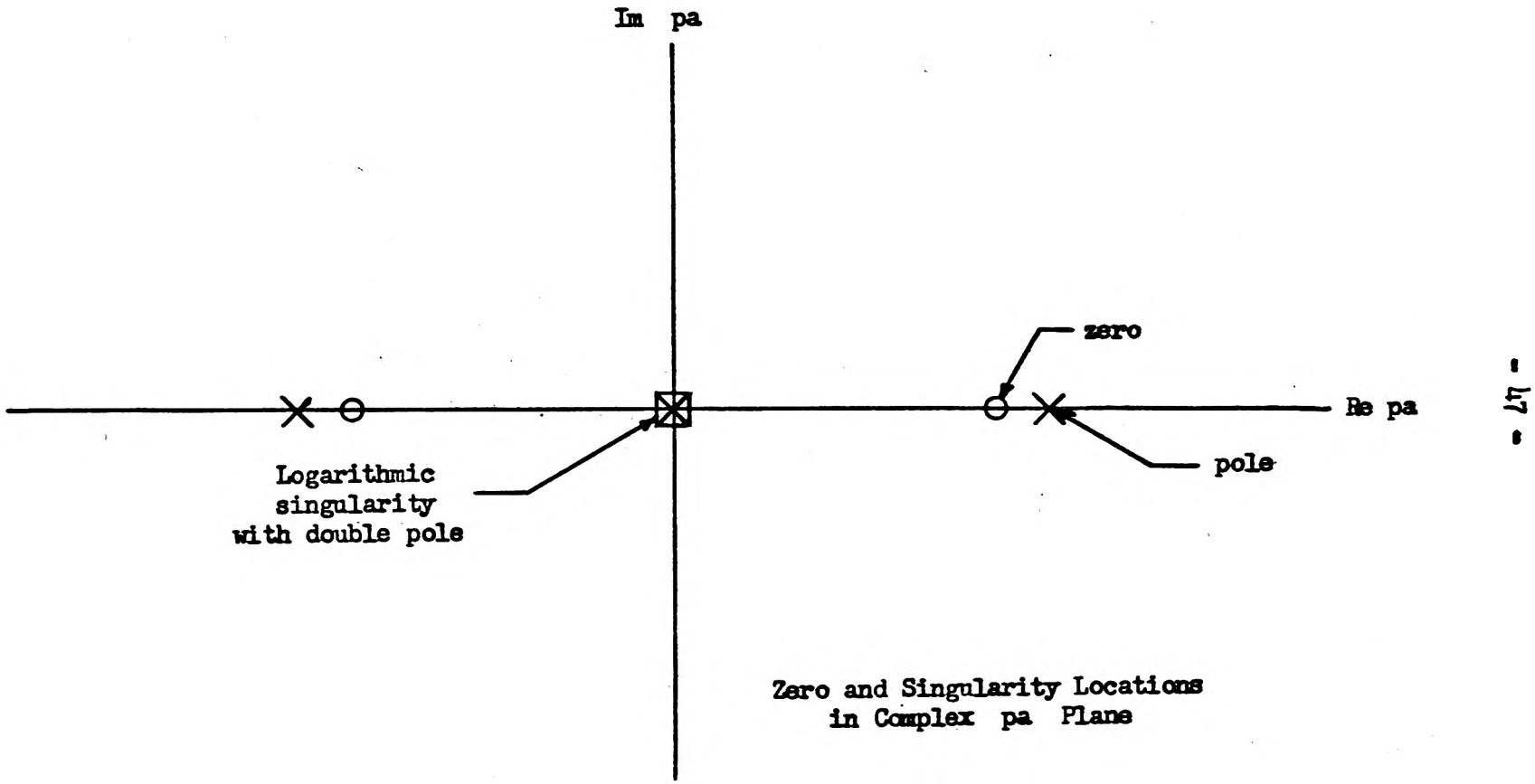
Im pa
zero
Re pa
pole
Logarithmic
singularity
with double pole
Zero and Singularity Locations
in Complex pa Plane

Fig. 10.2

a pole in the admittance function does not appear unless the admittance is transformed to a radius smaller than that of the helix.

Fletcher (R-6) in his theory which enables the calculation of the Pierce parameters in terms of the results from field theory uses an admittance function Y_c which is defined by

$$Y_c = Y^{(2)} - \frac{j\omega\varepsilon}{p} \frac{I_1(pb)}{I_o(pb)} \quad . \tag{10.1}$$

A normalized Y_{rc} can also be defined by

$$Y_{rc} = Y_r^{(2)} - \frac{jka}{pa} \frac{I_1(pb)}{I_o(pb)} \quad . \tag{10.2}$$

The second terms in equations (10.1) and (10.2) correspond to the TM admittance of a cylinder of some medium out to the radius b. Thus, the equation $Y_c = 0$ expresses the condition for cold propagation. The location of the zero of Y_c has a slightly larger value of pa than the location of the zero for $Y^{(2)}$. This can be seen by plotting $\frac{ka}{pa} \frac{I_1(pb)}{I_o(pb)}$ on the same graph as $\text{Im } Y_r^{(2)}$ and finding their intersection for real pa. One advantage of using Y_c is that the location of the zero $p_o a$ is not a function of the radius of the beam. The location of the pole is unchanged because $j \frac{ka}{pa} \frac{I_1(pb)}{I_o(pb)}$, is finite everywhere along the real pa axis. $j \frac{ka}{pa} \frac{I_1(pb)}{I_o(pb)}$ becomes zero as pa approaches infinity. Therefore, the asymptotic behavior of Y_c is just the same as that for $Y^{(2)}$. It also is constant near $pa = 0$ so that the nature of the singularity of Y_c in that region is also the same as that of $Y^{(2)}$.

The physical basis for the statements made above in regard to the

location of p_p is as follows. The location of the pole corresponds to the propagation constant of a helix with a sheath located at $r = b$ which conducts only in the z direction. Such a sheath would fix the TM admittance at $r = b$ to be infinite. Such a surface may be made experimentally by scratching longitudinal grooves into a thin dielectric cylinder which has been coated with a conducting material. It is obvious, that such a surface would cause a large deviation in the propagation constant from that of a helix alone if its radius were large with respect to that of the helix radius. In fact, if it were at the helix radius, it would completely short the helix. If b were very small, there would be very little effect on the propagation constant.

The pole will move in from infinity to some finite location as the difference in radii of the helix and beam surface increases when measured in terms of pa. In fact, for large values of $p_o a$ and reasonable values of b/a, the $p_p a$ will be very close to $p_o a$.

In order to get an estimate of the location of the pole and zero, one may use the transformation (2.21). Setting the numerator of (2.21) equal to zero determines the value of $p'a$. In order to get a simple expression not involving Bessel functions, the Bessel functions are replaced by their asymptotic values. This makes the result dependent on the values of pa and pb being sufficiently large for the approximation to hold. The approximation is, for the purposes at hand, quite good for arguments as small as 2 and useful for arguments as small as 1. The result of this approximation is

$$\frac{y_{ra}(p'a)}{jka} = \frac{\tanh p'a\,(1-\frac{b}{a})}{p'a} \quad . \tag{10.3}$$

Similarly, the location of the pole is found by setting the denominator of (2.21) equal to zero and making the same approximations.

$$\frac{y\, r_a\, (p_p a)}{jka} = \frac{\coth pa\,(1-\frac{b}{a})}{pa} \qquad (10.4)$$

For large x, $\tanh x$ approaches unity; $\coth x$ approaches unity. The right hand sides of equations (10.3) and (10.4) will be close to each other under large argument conditions. Since p_o lies between p' and p_p, they all will fall close to each other for large values of $p_o a$ and reasonable values of b/a, for instance $b/a = 1/2$. It is also obvious, even though equations (10.3) and (10.4) do not strictly apply, that for small $p_o a$ the pole may be quite removed from the zero.

The discussion up to this point has been limited to the lossless helix. Similar consideration in regard to zero and pole locations will hold in regard to other lossless systems such as an iris loaded waveguide. It is of importance to know what effect the introduction of loss would have.

It must be that the introduction of loss does not change the system very drastically. The location of the pole and zero discussed above are shifted. It is obvious that they are shifted in such a manner that the $p_o a$ and $p_p a$ correspond to decaying propagation constants--they just correspond to measurements of the propagation constants taken respectively with and without the presence of a z conductive sheath at the beam radius. $\frac{\partial Y_c}{\partial(pa)}$ at any pa will in general be a function that depends upon the conductivity parameters. In the region of interest, the particular model by which loss is taken into account does not in

itself influence the general shape of an admittance contour map. The reasoning behind this conclusion is purely physical although it is believed that a rigorous basis should not be difficult to find. It may be argued that the introduction of additional paralleling admittance by means of lossy surfaces does not change the character of the admittances by very much. The transformations will have a tendency to become independent of the admittance when the difference in the radii is large in units of pa. This has been illustrated in the derivation of (2.22), (2.23), (2.24), and (2.25). Furthermore, the singularities are introduced by means of the transformations themselves. For instance, it has already been seen that there is no pole in the vicinity of the zero for the lossless helix when the beam radius is taken equal to the helix radius. The calculations made have indicated that the loss shows up on the circuit admittance map as a combination rotation and stretching of the admittance contours with also some translation of the region of interest.

It has been mentioned that the locations of the zero and pole correspond to measurements of propagation constants without and with a unidirectional sheath placed at the beam radius. This provides an experimental method of determining these constants. For instance, a loaded waveguide will have many possible modes. Nevertheless, the location of each pole and zero of the admittance function could be found by measuring the propagation constants with and without such a sheath. As already stated, one can approximate such a sheath by scratching insulating lines on a metalized surface. The widths of the conducting lines should be small compared to their spacing which should also be

small. It is also interesting, experimentally, to know the value of $\frac{\partial Y_c}{\partial(pa)}_{p=p_o}$. This can be determined in several ways. Perhaps one of the best is to use a perturbation method. In this method, a finite section of the structure is used, and the shifts in the resonant frequencies are observed when small metallic objects are placed inside the structure. From this information, knowledge of the fields associated with each mode can be determined.

From a knowledge of the three quantities, $p_o a$, $p_p a$, and $\frac{\partial Y_c}{\partial(pa)}_{p=p_o}$ Fletcher has shown that one can calculate the parameters required by the Pierce theory. His equations, in the notation used here are

$$\frac{2Q}{\beta_e a} = \left(1 + \left(\frac{ka}{p_o a}\right)^2\right)^{-1/2} \frac{p_o a}{(p_p a)^2 - (p_o a)^2} \tag{10.5}$$

$$\frac{1}{K} = -j\pi p_o a\, p_o b \left(1 + \left(\frac{ka}{pa}\right)^2\right)^{3/2} \left(\frac{\partial Y_c}{\partial(pa)}\right)_{p=p_o} . \tag{10.6}$$

Since relativistic effects are neglected, the factors $1 + \left(\frac{ka}{p_o a}\right)^2$ may be set equal to unity. The resulting equations are

$$\frac{2Q}{\beta_e a} = \frac{p_o a}{(p_p a)^2 - (p_o a)^2} \tag{10.7}$$

$$\frac{1}{K} = -j\pi p_o a\, p_o b \left(\frac{\partial Y_c}{\partial(pa)}\right)_{p=p_o} \tag{10.8}$$

In order to get these relationships, Fletcher first considers the performance of a thin hollow beam at radius b. He notes that the electric field acting on the beam is a constant throughout the beam so that

$$Y_c = \frac{H\phi_o - H\phi_i}{E_z} = \frac{1}{2\pi b} \frac{i}{E_z} , \tag{10.9}$$

where i is the alternating current in the beam. The Pierce electronic equation holds for a beam where E_z is the same for all electrons with the same value of z at any time.

$$i = \frac{j\beta_e}{(j\beta_e - \gamma)^2} \frac{I_o}{2V_o} E_z . \tag{10.10}$$

Therefore, equation (10.9) can be written

$$Y_c = \frac{1}{2\pi b} \left(\frac{i}{E_z}\right)_{\text{electronic}} \tag{10.11}$$

The Pierce circuit equation is

$$E_z = -\left[\frac{\gamma^2 \gamma_o K}{\gamma^2 - \gamma_o^2} + \frac{2j\,QK\gamma^2}{\beta_e}\right] i . \tag{10.12}$$

Using (2.4), (10.12) can be written

$$Y'_c = \frac{1}{2\pi b} \frac{(p_o^2 - p^2)\beta_e}{jK(p^2 + k^2)\left[(p_o^2 + k^2)^{1/2}\beta_e + 2Q(p_o^2 - p^2)\right]} = \frac{1}{2\pi b} \frac{i}{E_z} . \tag{10.13}$$

Using the value of $\left(\frac{i}{E_z}\right)_{\text{electronic}}$ in (10.13) gives the equation for the propagation constants for the Pierce theory.

The propagation constants obtained by the two methods would be the same if the left hand sides of the equations (10.11) and (10.13) were identical. They are not identical, but under certain conditions they approximate one another in the region which corresponds to the range of the propagation constants.

Fig. 10.1 can be taken as a typical plot of Y_c if the point p'a were relabeled $p_o a$ and the normalizing factor taken out. A typical plot of the left hand side of (10.13) is shown in Fig. 10.3.

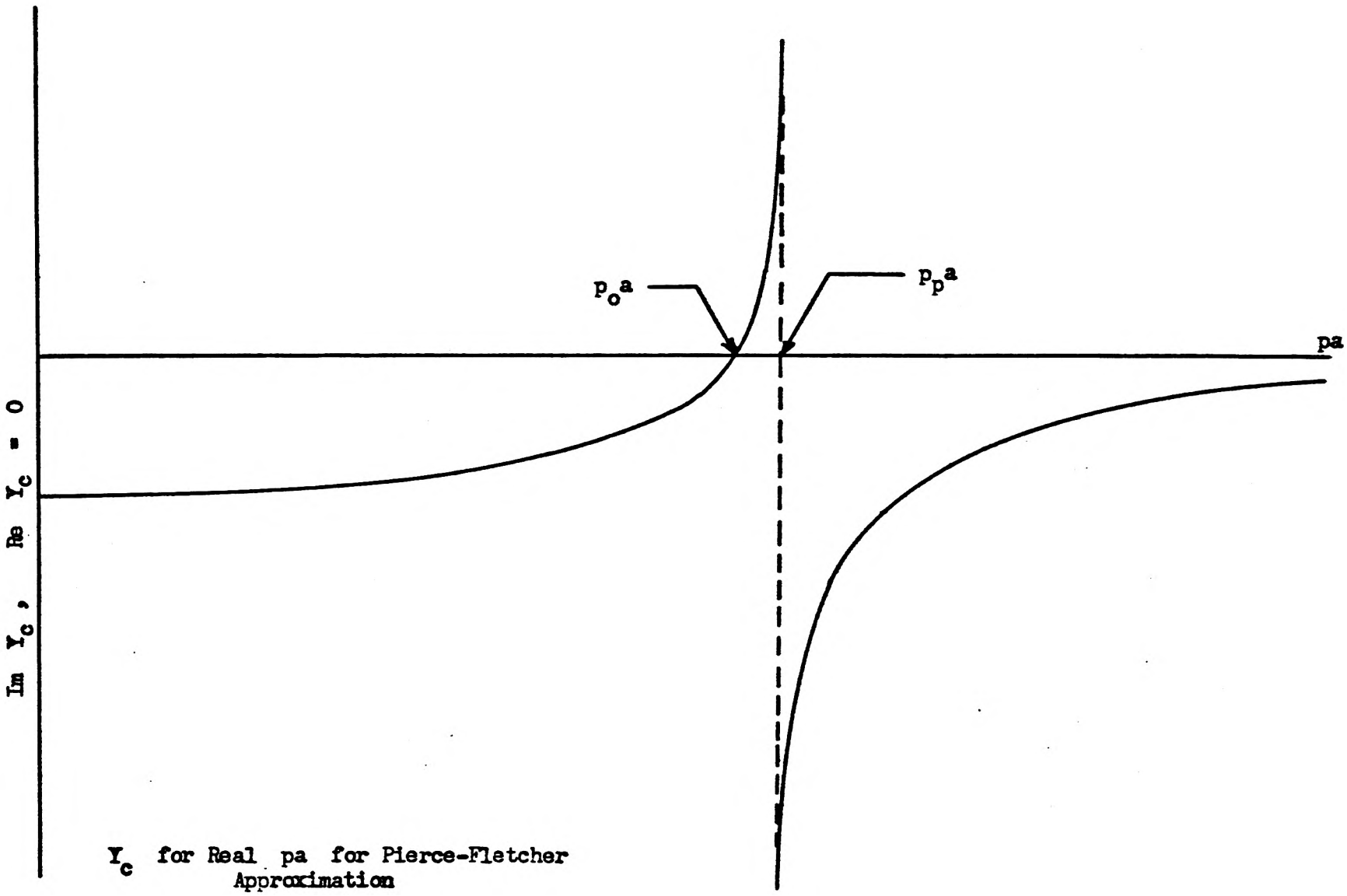

Y_c for Real pa for Pierce-Fletcher Approximation

Fig. 10.3

There are simple poles at $p = \pm jk$ on the imaginary axis, and another pole for which

$$(p_o^2 + k^2)^{1/2} \beta_e + 2Q(p_o^2 - p^2) = 0 \quad .$$

There also is a zero at $p = p_o$. As pa approaches infinity, the function approaches zero. At $pa = 0$ the function is finite and has zero slope.

The propagation constants of a traveling-wave tube will be in the vicinity of the cold circuit propagation constant, near $p_o a$ in the complex pa plane. Under the conditions that the pole is close to the zero, the left hand side Y'_c could be matched to Y_c by choosing the parameters K and Q so that the poles coincide and that the slope at $p = p_o$, $\frac{\partial Y}{\partial (pa)}_{p = p_o}$, are equal for both Y_c and Y'_c . This matching results in the equations which Fletcher uses to define Q and K , that is (10.5) and (10.6) .

Fletcher treats the case of a thick beam by finding an equivalent thin beam. The current and radius of the thin beam will be smaller than for the solid beam. Fletcher presents a plot which gives these values as functions of $\beta_e b$.

If loss is present, the same procedure still holds. The poles can be made to coincide by the proper choice of Q , and the impedance parameter K is determined by the slope at $p_o a$. In the case of loss, however, these parameters will not be real. This means, that in the Pierce theory, the assumption that loss can be represented by the loss factor d is not correct. d represents only the effect that loss plays by its effect on p_o . It is necessary to account for the change

that occurs in Q and K as well. Some crude attempts have been made along this line by stating that the introduction of loss reduces the impedance. Since the space charge parameter Q enters into gain calculations rather strongly, Q must also be considered to change. The Pierce notation can still be used to describe such situations, but the advantages of C, Q, and K being real numbers disappear. It becomes a difficult task indeed to calculate sets of universal gain curves in terms of the Pierce parameters.

The validity of the Pierce theory will also depend to a large extent upon just how well Y'_c compares to Y_c. A comparison of the admittance plots indicates that the requirements for the approximation to be good are that the pole and zero be close together and that the propagation constants of the complete structure fall close to the pole and zero.

The conditions that determine the separation of the pole and zero have been discussed earlier in this section. In the case of a solid beam, the pole and zero will be closer together than in a thin hollow beam of the same radius because the equivalent thin beam has a reduced radius.

The propagation constants will differ greatly from those corresponding to p_o when the reduced plasma wave number β_q is a considerable fraction of p_o. If β_q is sufficiently large, the admittances for these propagation constants will differ considerably from each other.

The conclusions to be reached from the discussion of this section are:

The Pierce theory is subject to error when $p_o a$ is small, of the

order of unity. This is because the pole and zero will usually be widely separated under such conditions. Also, the effect of the singularities near the origin will play an important role in making for a poor approximation.

The Pierce theory may fail if large β_q is used because the propagation constants will fall outside the validity of the Fletcher approximation.

These conditions would be likely to occur for high power tubes where one tries to get small β_e corresponding to small p_o, and large current densities corresponding to large β_p.

In the case of lossy circuits, the Pierce theory with the proper parameters can be used to describe the tube operation to the same degree that it can be used to describe lossless operation, but one must be prepared to deal with complex parameters.

Section XI

HIGHER ORDER MODES

As has been pointed out in Section IX, the higher order modes have values of pa which differ only slightly from the value of $\beta_e a$. In order to operate traveling-wave tubes efficiently, the electron injection velocity must be greater than the cold helix velocity. For such operation $\beta_e a$ is smaller than $p_o a$ by approximately $\beta_q a$. Therefore, none of the higher order modes will have propagation constants which lie very close to the pole of $Y_r^{(2)}$. Under such circumstances, to the first approximation,

$$Y_r^{(2)}(pa) \simeq Y_r^{(2)}(\beta_e a) . \tag{11.1}$$

Equating electronic admittance to circuit admittance, using (8.17),

$$j \frac{ka}{pa} \frac{\eta b}{pb} \frac{I_1(\eta b)}{I_o(\eta b)} = Y_r^{(2)}(\beta_e a) . \tag{11.2}$$

If, after this equation is solved for the propagation constants, a better set of values is desired, the procedure may be repeated using the newly found propagation constants for a second iteration.

The behavior of the function $w = z \frac{I_1(z)}{I_o(z)}$ has to be investigated. The function w has a double zero at the origin. It also has simple poles and zeros alternating on the imaginary axis. A picture of this behavior can be formed by noting that w is asymptotic to $-j z \tan j(z - \frac{j\pi}{a})$ along the imaginary z axis.

Obviously, the point at infinity is an essential singularity. There are no other zeros or singularities in the complex plane. The double

zero at the origin will be seen to be the key to the number and behavior of the lowest order modes of a traveling-wave tube amplifier.

The function w can be approximated in the vicinity of each of its simple zeros by a Taylor series. If the first term of the Taylor series is a good approximation, then one can easily see that the function will take on all the complex values of small absolute value $< \epsilon$ near its zeros. The permissible size of ϵ is determined by the error that can be tolerated in representing w by the first term of its Taylor expansion. For zeros of large argument, the first term of the Taylor series expansion is a very good approximation indeed. It turns out that in the cases of interest, the approximation will be very good even for the first order zero. In any event, the validity of the representation by the first term can be checked by computing the correction introduced by the second term of the Taylor expansion.

w can be approximated by the first term of the Taylor or Laurent series in the vicinities of its zeros and poles.

$$z \frac{I_1(z)}{I_o(z)} \simeq \frac{z^2}{2} \quad \text{near} \quad z = 0 \ . \tag{11.3}$$

$$z \frac{I_1(z)}{I_o(z)} \simeq z_n(z - z_n) \quad \text{near} \quad z_n \tag{11.4}$$

$$\text{where} \quad I_1(z_n) = 0, \quad z_n \neq 0 \ .$$

$$z \frac{I_1(z)}{I_o(z)} \simeq \frac{z_k}{z - z_k} \quad \text{near} \quad z_k \tag{11.5}$$

$$\text{where} \quad I_o(z_k) = 0 \ .$$

Substitution of the approximation (11.4) into (11.2) and using expression (9.4) results in

$$z_n \left[pb\left(1 - \frac{(\beta_p a)^2}{(pa - \beta_e a)^2}\right)^{1/2} - z_n \right] = -j \frac{\beta_e^2 ab}{ka} Y_r^{(2)}(\beta_e a) \qquad (11.6)$$

where z_n is the n^{th} zero of $I_1(z_n)$.

It can be assumed that pb can be replaced by $\beta_e b$ whenever it does not occur in a difference term. When that equation is solved, one gets

$$pa = \beta_e a \pm \frac{\beta_p a}{\left[1 - \frac{1}{(\beta_e b)^2}\left(z_n + \frac{\beta_e^2 ab}{jka\, z_n} Y_r^{(2)}(\beta_e a)\right)^2\right]^{1/2}} . \qquad (11.7)$$

If a more accurate solution is desired, the value of pa from (11.7) and the admittance for this value can be put into (11.6) which is then solved again for pa . By iteration of this procedure, the propagation constants of the higher order modes can be calculated to any degree of accuracy desired. Even the first approximation, however, should be very good.

It can now be seen that in the case of a lossless structure, the higher order modes will not be either growing or decaying. For lossless circuits, the admittance $Y_r^{(2)}$ is purely imaginary for purely real pa . Therefore, the solution of (11.7) is pure real. The z_n are imaginary. Real values of pa correspond to constant amplitude waves.

Similarly, complex values of $Y_r^{(2)}(\beta_e a)$ corresponding to lossy structures will result in an increasing and a decreasing wave. The rate of gain drops off rapidly with the increasing size of z_n .

Another way of showing that the higher order waves for a lossless circuit are of constant amplitude without the use of the approximations involved in (11.7) exists. If one plots the admittance of the beam and the admittance for the circuit as functions of ηa , one gets a plot such

as in Fig. 11.1 . Since both the circuit and beam admittances are pure imaginary, there will be intersections as shown which correspond to purely real pa , and therefore, to constant amplitude waves.

The location of a double order zero at the origin means that if one equates the $Y_r^{(2)}(\beta_e a)$ to the approximation (11.3) two values of ηa will be solutions corresponding to four values of pa . The double zero, in effect, doubles the number of modes of the system associated with it. Actually, $Y_r^{(2)}$ is a function of pa and the electronic admittance cannot be equated to the circuit admittance evaluated at one point alone. If there is any appreciable gain, the resultant values for pa of the lowest modes will be removed from one another to such an extent that $Y_r^{(2)}$ cannot be represented by a constant. Nevertheless, it is obvious that there still will be four solutions corresponding to the double zero.

It is also obvious from equation (11.7) that the higher order modes for lossy structures will consist of pairs of growing and decaying waves. In most cases, however, the rate of gain will be insignificant to the rates of gain of the principal modes. Examination of (11.7) indicates that the rate of gain will become small very rapidly as a function of the order of the mode.

The small gains will mean that the various space charge waves will be almost entirely independent of the structure that is involved. This will be seen to be of possible importance in consideration of attenuator saturation effects.

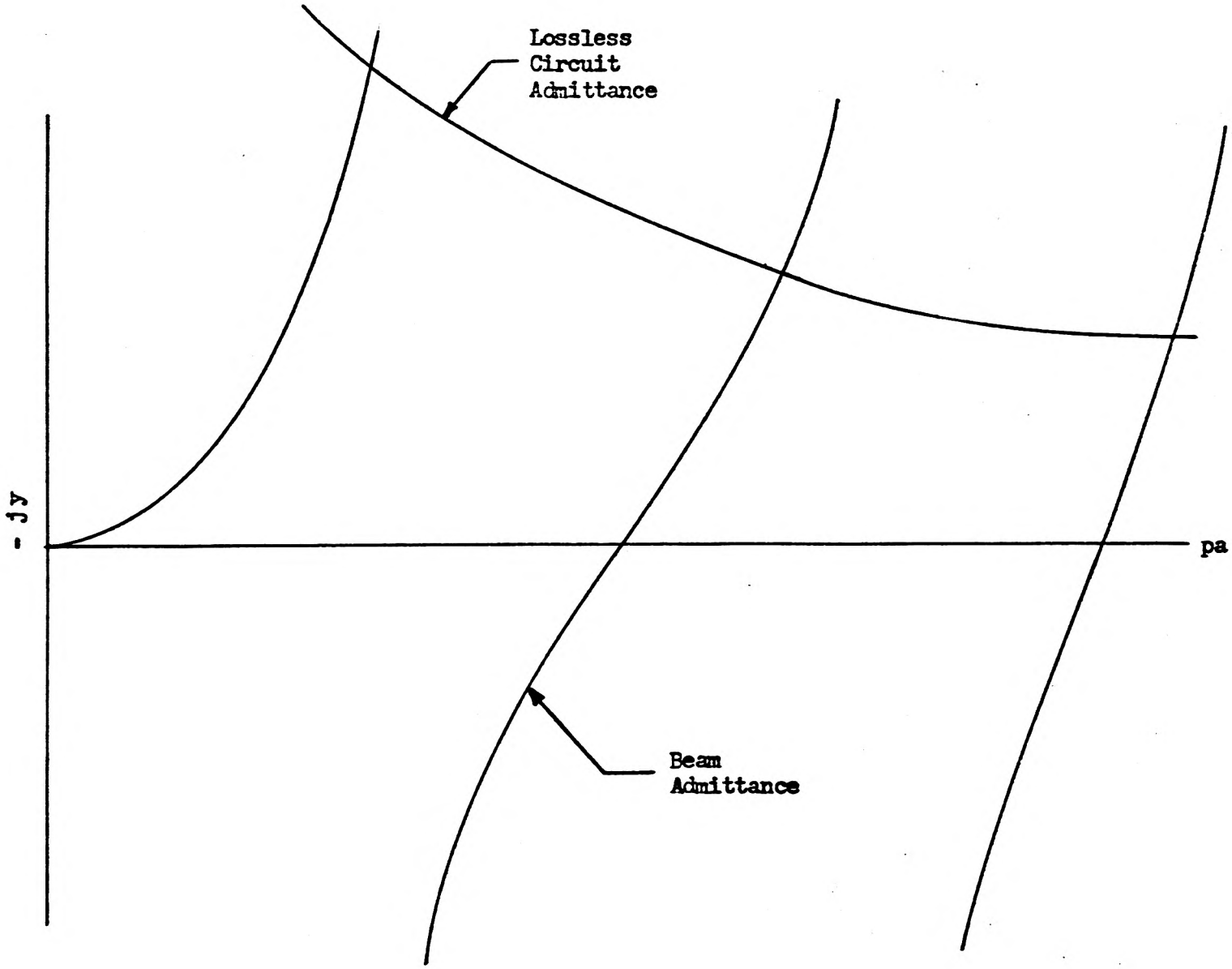

Beam and Lossless Circuit Admittances for Purely Real pa

Fig. 11.1

Section XII

EXCITATION OF NEW LOWEST ORDER WAVES AT A DISCONTINUITY OF A TRAVELING-WAVE TUBE CIRCUIT

If a traveling-wave tube consists of several sections of differing properties such as one may find in a tube with an attenuator placed between two lossless sections, it is important to be able to determine what the amplitudes of the waves in the various sections are. In general, this is a very difficult problem. As an approximation, one can match current density, electric field, and velocity on the axis of an electron beam at the point where the two circuits join. In this way one need only use the three lowest forward modes of a traveling-wave tube in order to provide the matching.

It usually can be assumed that at the end of any particular section the increasing wave has grown to be so large that the others can be neglected. If this is not true, the method described below is still valid if the excitations of the three waves are added together.

The current density and velocity in a modulated electron beam can be expressed in terms of E_z for each wave. These relationships are found from (8.6) and (8.9).

$$J_z = -j\omega\varepsilon \frac{\beta_p^2}{(\beta_e - p)^2} E_z , \tag{12.1}$$

$$v = -j \frac{\frac{e}{m} E_z}{u_o(\beta_e - p)} . \tag{12.2}$$

The matching conditions are

$$E_1 + E_2 + E_3 = E_{in} \,, \tag{12.3}$$

$$v_1 + v_2 + v_3 = v_{in} \,, \tag{12.4}$$

$$J_1 + J_2 + J_3 = J_{in} \,, \tag{12.5}$$

where the subscripts refer to the three waves of the region the beam is entering; the subscript "in" refers to the incident wave.

Using (12.1) and (12.2) the matching conditions (12.4) and (12.5) can be written entirely in terms of the electric field components.

$$\frac{E_1}{\beta_e - p_1} + \frac{E_2}{\beta_e - p_2} + \frac{E_3}{\beta_e - p_3} = \frac{E_{in}}{\beta_e - p_{in}} \,. \tag{12.6}$$

$$\frac{E_1}{(\beta_e - p_1)^2} + \frac{E_2}{(\beta_e - p_2)^2} + \frac{E_3}{(\beta_e - p_3)^2} = \frac{E_{in}}{(\beta_e - p_{in})^2} \,. \tag{12.7}$$

There are three simultaneous equations in three unknowns which can be solved for the amplitudes of the modes excited in the section the beam is entering. Since the expressions are symmetrical in subscripts 1, 2, and 3, solving for E_1 is sufficient. The other quantities are obtained by a permutation of indices.

$$E_1 = \frac{\begin{vmatrix} 1 & 1 & 1 \\ \frac{1}{\beta_e - p_{in}} & \frac{1}{\beta_e - p_2} & \frac{1}{\beta_e - p_3} \\ \frac{1}{(\beta_e - p_{in})^2} & \frac{1}{(\beta_e - p_2)^2} & \frac{1}{(\beta_e - p_3)^2} \end{vmatrix}}{\begin{vmatrix} 1 & 1 & 1 \\ \frac{1}{\beta_e - p_1} & \frac{1}{\beta_e - p_2} & \frac{1}{\beta_e - p_3} \\ \frac{1}{(\beta_e - p_1)^2} & \frac{1}{(\beta_e - p_2)^2} & \frac{1}{(\beta_e - p_3)^2} \end{vmatrix}} E_{in} \tag{12.8}$$

The numerator of this expression, which is called N_1, is found to be

$$N_1 = \frac{(p_{in} - p_2)\,(p_2 - p_3)\,(p_3 - p_{in})}{(\beta_e - p_{in})^2 (\beta_e - p_2)^2 (\beta_e - p_3)^2} \quad . \tag{12.9}$$

Similarly, the denominator, which is called D, is found to be

$$D = \frac{(p_1 - p_2)\,(p_2 - p_3)\,(p_3 - p_1)}{(\beta_e - p_1)^2 (\beta_e - p_2)^2 (\beta_e - p_3)^2} \quad . \tag{12.10}$$

$$E_1 = \frac{N_1}{D} = \frac{(p_2 - p_{in})\,(p_3 - p_{in})\,(\beta_e - p_1)^2}{(p_2 - p_1)\,(p_3 - p_1)\,(\beta_e - p_{in})^2}\; E_{in} \quad . \tag{12.11}$$

Use of (12.1) gives

$$\frac{J_1}{J_{in}} = \frac{(\beta_e - p_{in})^2}{(\beta_e - p_1)^2}\; \frac{E_1}{E_{in}} \tag{12.12}$$

which becomes, with aid of (12.11)

$$\frac{J_1}{J_{in}} = \frac{(p_2 - p_{in})\,(p_3 - p_{in})}{(p_2 - p_1)\,(p_3 - p_1)} \tag{12.13}$$

Equations (12.12) and (12.13) can be written in terms of the Pierce incremental propagation constants, the δ's . They are defined by

$$\beta = -j\gamma = \beta_e(1 + j\,C\,\delta) \tag{12.14}$$

Therefore (12.12) and (12.13) can be written in the form

$$\frac{J_1}{J_{in}} = \frac{\delta_{in}^2}{\delta_1^2} \frac{E_1}{E_{in}} \tag{12.15}$$

and

$$\frac{J_1}{J_{in}} = \frac{(\delta_2 - \delta_{in})(\delta_3 - \delta_{in})}{(\delta_2 - \delta_1)(\delta_3 - \delta_1)} \tag{12.16}$$

Section XIII

BUNCHING EFFECTS OF HIGHER ORDER SPACE CHARGE MODES

The possibility exists that higher order modes excited at a discontinuity in the characteristics of a propagating circuit cause portions of an electron beam to saturate even though the amplitudes of the lowest modes, those usually of interest, are relatively small. In fact, the amplitudes of the lowest modes at saturation may be much smaller than they would have to be in order to cause saturation by themselves. Because of the difficulty in calculating the effect of these modes, the equations derived in this section should not be taken too literally. The results derived can only be taken as a qualitative description of an effect of importance. Further, but very involved calculations are possible which can put this explanation on a rigorous basis.

The configuration to be assumed for the following analysis is shown in Fig. 13.1 .

It is assumed that the beam fills the helix and the conducting pipe, both of radius a . The conducting pipe replaces the lossy section of a traveling-wave tube. There is no variation with ϕ . The treatment of the attenuator section as a conducting drift tube will be discussed later to a somewhat greater extent. Restriction is made to the linearized problem, in the manner of Chu and Jackson (R-1), and Birdsall and Whinnery (R-4). A wave has been excited on the first helix in such a way that only the increasing wave has any substantial amplitude at the junction of sections 1 and 2. The electromagnetic wave on this helix is terminated at the junction (by something similar to a Maxwell demon)

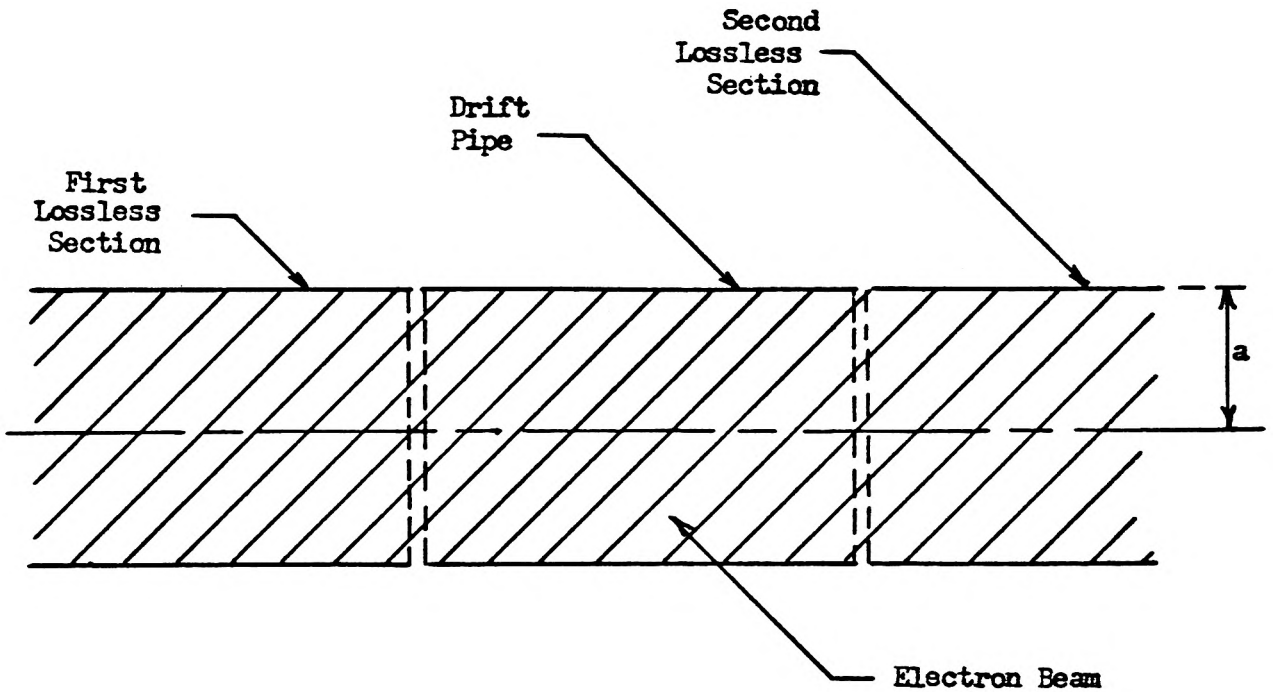

DRIFT PIPE REPRESENTATION OF AN ATTENUATOR

Fig. 13.1

leaving only the modulated electron beam to carry signal beyond this point. The behavior of the electron stream in the second region is analyzed according to the methods of Birdsall and Whinnery. After the electron beam leaves the conducting drift space it enters the second helix which is terminated at the junction. The modes of this helix are determined by the methods of Chu and Jackson. The excitation problem has been treated by Sollfrey (R-5), but is in a form that is unsuited for calculation. It must be emphasized that the type of saturation effects considered here do not arise in a beam of infinitesimal diameter. The effects are directly due to the finite diameter of the beam. Therefore, if the mechanism described here is important, the nonlinear analyses up to date completely neglect this effect (R-7,8).

In what follows, it will be necessary to be able to expand the function $I_o(kr)$ as a summation of $J_o(\tau_n r)$.

$$I_o(kr) = \sum_{n=1}^{\infty} A_n J_o(\tau_n r) \qquad \text{where } J_o(\tau_n a) = 0 \tag{13.1}$$

where

$$A_n = \frac{2}{[a J_1(\tau_n a)]^2} \int_o^a r I_o(kr) J_o(\tau_n r)\, dr . \tag{13.2}$$

This can be written

$$A_n = \frac{2}{[a J_1(\tau_n a)]^2} \int_o^a r J_o(jkr) J_o(\tau_n r)\, dr , \tag{13.3}$$

because

$$I_\nu(z) = j^{-\nu} J_\nu(jz) \tag{13.4}$$

Lommel (R-9) has shown that

$$(\alpha^2 - \beta^2) \int_0^x x\, J_n(\alpha x)\, J_n(\beta x)\, dx$$
$$= x\left[J_n(\alpha x)\frac{d}{dx} J_n(\beta x) - J_n(\beta x)\frac{d}{dx} J_n(\alpha x)\right]. \qquad (13.5)$$

Restricting (13.5) to $n = 0$, and replacing β by jk and $\alpha = \tau_n$, one gets

$$(\tau_n^2 + k^2) \int_0^a r\, J_o(jkr)\, J_o(\tau_n r)\, dr$$
$$= a\left\{J_o(\tau_n r)\frac{d}{dr} I_o(kr) - I_o(kr)\frac{d}{dr} J_o(\tau_n r)\right\}_{r=a}. \qquad (13.6)$$

Therefore,

$$A_n = \frac{2\tau_n I_o(ka)}{a(\tau_n^2 + k^2) J_1(\tau_n a)} \quad . \qquad (13.7)$$

The assumption is made that the radial distributions of alternating current density and velocity in the electron beam take on the same radial form as that of the longitudinal electric field propagating on the cold sheath helix, the form $I_o(p_o r)$ $I_o(\beta_e r)$.

The incident velocity and current densities on the axis at the junction of the sheath helix and the drift pipe are designated by the complex quantities v_o and i_o respectively. Their distributions are given by

$$v = v_o I_o(\beta_e r) \qquad (13.8)$$

and

$$i = i_o I_o(\beta_e r) \quad . \qquad (13.9)$$

Equation (8.13) describes the radial behavior of the longitudinal field. The conducting pipe establishes the boundary conditions. (8.13) can be written in the form

$$\frac{1}{r}\frac{\partial}{\partial r}\left(r\frac{\partial E_z}{\partial r}\right) + (p^2 - k^2)\left[\frac{\beta_p{}^2}{(p-\beta_e)^2} - 1\right] E_z = 0 . \qquad (13.10)$$

The solutions for the field will contain cut-off modes for typical parameters. These will not be important. The other solutions, the important ones, will correspond to the plasma waves on a beam in a conducting pipe. These modes will have values of p which are close to β_e. Under this condition, (13.10) can be written

$$\frac{1}{r}\frac{\partial}{\partial r}\left(r\frac{\partial E_z}{\partial r}\right) + \beta_e^2\left[\frac{\beta_p^2}{(p-\beta_e)^2} - 1\right] E_z = 0 . \qquad (13.11)$$

Let τ_n be defined by

$$\tau_n^2 = \beta_e^2\left[\frac{\beta_p^2}{(p_n-\beta_e)} - 1\right] . \qquad (13.12)$$

The solution for p_n is

$$p_n = \beta_e \pm \frac{\beta_p}{\left(1 + \frac{\tau_n^2}{\beta_e^2}\right)^{1/2}} , \qquad (13.13)$$

where p_n is one of the allowable values of p in (13.10). To find the equation for determining these p_n, one notes that the solution to (13.10) is

$$E_z = J_o(\tau_n r) . \qquad (13.14)$$

The condition that E_z be zero at the surface of the conducting pipe is then given by

$$J_o(\tau_n a) = 0 . \qquad (13.15)$$

Thus, there are two waves corresponding to each of an infinite number of values of n, one that is faster and one that is slower than the speed

of the electrons. These will be designated by p_{1n} and p_{2n} respectively.

One now tries to expand i and v in series;

$$i = \sum_{n=1}^{\infty} J(\tau_n a)\left[A_{1n}\, e^{-jp_{1n} z} + A_{2n}\, e^{-jp_{2n} z}\right]; \tag{13.16}$$

$$v = \sum_{n=1}^{\infty} J(\tau_n a)\left[B_{1n}\, e^{-jp_{1n} z} + A_{2n}\, e^{-jp_{2n} z}\right]. \tag{13.17}$$

The coefficients can be determined from (13.8) and (13.9) and the work deriving (13.7)

$$A_{1n} + A_{2n} = \frac{2i_o \tau_n I_o(\beta_e a)}{a(\tau_n^2 + \beta_e^2) J_1(\tau_n a)} \quad . \tag{13.18}$$

$$B_{1n} + B_{2n} = \frac{2v_o \tau_n\, I_o(\beta_e a)}{a(\tau_n^2 + \beta_e^2)\, J_1(\tau_n a)} \quad . \tag{13.19}$$

Use of (8.8) relates the A's and B's .

$$\begin{aligned} B_{in} &= \frac{(1 - \frac{p_{1n}}{\beta_e})}{\rho_o} A_{1n} \, . \\ B_{2n} &= \frac{(1 - \frac{p_{2n}}{\beta_e})}{\rho_o} A_{2n} \, . \end{aligned} \tag{13.20}$$

(13.18) through (13.31) yield

$$A_{1n} = - \frac{2\tau_n\, I_o(\beta_e a)\left[\, v_o\, \rho_o\, \beta_e - i_o(\beta_e - p_{2n})\right]}{a(\tau_n^2 + \beta_e^2)\; J_1(\tau_n a)\; (p_{1n} - p_{2n})} \, , \tag{13.21}$$

$$A_{2n} = \frac{2\tau_n I_o(\beta_e a)\left[v_o \rho_o \beta_e - i_o(\beta_e - p_{1n})\right]}{a(\tau_n^2 + \beta_e^2) J_1(\tau_n a)\ (p_{1n} - p_{2n})}, \qquad (13.22)$$

with similar expressions for B_{1n} and B_{2n}.

Taking into account

$$\beta_e - p_{1n} = p_{2n} - \beta_e = \frac{\beta_p}{(1 + \frac{\tau_n^2}{\beta_e^2})^{1/2}}, \qquad (13.23)$$

i can be expressed by

$$i = \sum_{n=1}^{\infty} \frac{2\tau_n I_o(\beta_e a) J_o(\tau_n r)}{a(\tau_n^2 + \beta_e^2) J_1(\tau_n a)} e^{-j\beta_e z}$$

$$\left[i_o \cos \frac{\beta_p z}{(1 + \frac{\tau_n^2}{\beta_e^2})^{1/2}} + je^{j\frac{4\pi}{3}} (1 + \frac{\tau_n^2}{\beta_e^2})^{1/2} v_o \rho_o \frac{\beta_e}{\beta_p} \sin \frac{\beta_p z}{(1 + \frac{\tau_n^2}{\beta_e^2})^{1/2}} \right], \qquad (13.24)$$

and v by

$$v = \sum_{n=1}^{\infty} \frac{2\tau_n I_o(\beta_e a) J_o(\tau_n r)}{a(\tau_n^2 + \beta_e^2) J_1(\tau_n a)} e^{-j\beta_e z}$$

$$\left[v_o \cos \frac{\beta_p z}{(1 + \frac{\tau_n^2}{\beta_e^2})^{1/2}} + j \frac{i_o}{\rho_o} \frac{\beta_p}{\beta_e} \sin \frac{\left(\frac{\beta_p z}{(1 + \frac{\tau_n^2}{\beta_e^2})^{\frac{1}{2}}}\right)}{(1 + \frac{\tau_n^2}{\beta_e^2})^{1/2}} \right]. \qquad (13.25)$$

(13.24) and (13.25) give the current density and velocity at any point in the drift tube. The problem of determining the excitation caused by such distributions on another section of lossless helix still remains. The solution of this problem is very difficult indeed (R-5). In order to get an answer, many assumptions are made which are not rigorously justified. It is not known just how much error these assumptions introduce.

One treats the principal modes of the helix as if they were three of a complete orthogonal set of modes. One then uses the usual method for getting the component of the incident distribution which contributes to these modes. It is then assumed that the rest of the distribution sets up space charge waves, the remaining modes, on the helix.

The "I_o" component of the current is then duly defined by

$$f_{I_o} = \frac{\int_o^a f(r)\, I_o(\beta_e r)\, r\, dr}{\int_o^a I_o(\beta_e r)^2\, r\, dr} \quad . \tag{13.26}$$

In order to determine the magnitude of this component it will be necessary to evaluate two integrals.

$$\int_o^a J_o(\tau_n r)\, I_o(\beta_e r)\, r\, dr = \frac{a\tau_n\, I_o(\beta_e a)\, J_1(\tau_n a)}{\tau_n^2 + \beta_e^2} , \tag{13.27}$$

and

$$\int_o^a I_o(\beta_e r)^2\, r dr = a^2\, \frac{\left[I_o(\beta_e a)\right]^2 - \left[I_1(\beta_e a)\right]^2}{2} \quad . \tag{13.28}$$

(13.27) has been determined already by the derivation of (13.7).

To get (13.28) one starts with another Lommel integral (R-9)

$$2\alpha^2 \int_0^x x \left[J_n(\alpha x)\right]^2 dx = (\alpha^2 x^2 - n^2)\left[J_n(\alpha x)\right]^2 + x \frac{d}{dx}\left[J_n(\alpha x)\right]^2 . \quad (13.29)$$

Taking $n = 0$, $\alpha = jk$, and putting $x = a$ yields the desired result.

Application of (13.26) to the current distribution at z which is given by (13.24), the "I_o" component of the current is found to be

$$i_{I_o} = \frac{4\left[I_o(\beta_e a)\right]^2}{\left[I_o(\beta_e a)\right]^2 - \left[I_1(\beta_e a)\right]^2} \sum_{n=1}^{\infty} \frac{(\tau_n a)^2 e^{-j\beta_e z}}{(\tau_n a)^2 + (\beta_e a)^2} \quad (13.30)$$

$$\left[i_o \frac{\cos \beta_p z}{(1 + \frac{\tau_n^2}{\beta_e^2})^{1/2}} + j (1 + \frac{\tau_n^2}{\beta_e^2})^{1/2} v_o \rho_o \frac{\beta_e}{\beta_p} \sin \frac{\beta_p z}{(1 + \frac{\tau_n^2}{\beta_e^2})^{1/2}} \right] .$$

Similarly, the "I_o" component of the velocity distribution can be found.

$$v_{I_o} = \frac{4\left[I_o(\beta_e a)\right]^2}{\left[I_o(\beta_e a)\right]^2 - \left[I_1(\beta_e a)\right]^2} \sum_{n=1}^{\infty} \frac{(\tau_n a)^2 e^{-j\beta_e z}}{(\tau_n a)^2 + (\beta_e a)^2} \quad (13.31)$$

$$\left[v_o e^{j\phi} \cos \frac{\beta_p z}{(1 + \frac{\tau_n^2}{\beta_e^2})^{1/2}} + j \frac{i_o}{\rho_o} \frac{\beta_p}{\beta_e} \frac{\sin\left(\frac{\beta_p z}{(1 + \frac{\tau_n^2}{\beta_e^2})^{1/2}}\right)}{(1 + \frac{\tau_n^2}{\beta_e^2})^{1/2}} \right]$$

The further assumption that the electric field is zero at the input to the second helix permits the determination of the amplitudes of the three principal traveling-wave tube modes which are excited.

If the characteristics of the wave incident upon the drift tube

are known, in this case the incident wave is assumed to be an increasing traveling-wave tube wave, the velocity and current are related. In order to simplify the calculations, it is assumed that the current and velocity are related to each other as in an increasing traveling-wave tube wave under small C and small QC conditions. (R-3)

$$\frac{v}{i} = -j \left[\frac{j\beta_e - \gamma}{\beta_e \rho_o} \right], \tag{13.32}$$

$$-\gamma = -j\beta_e + \beta_e C \left(\frac{3}{2} - \frac{j}{2} \right). \tag{13.33}$$

for the increasing wave. Therefore

$$\frac{v}{i} = \frac{C}{\rho_o} e^{j\frac{4\pi}{3}}.$$

The expressions for v and i, (13.23) and (13.24) can be written entirely in terms of i_o.

$$i = 2i_o I_o(\beta_e a) e^{-j\beta_e z} \sum_{n=1}^{\infty} \frac{\tau_n a}{(\tau_n a)^2 + (\beta_e a)^2} \frac{J_o(\tau_n r)}{J_1(\tau_n a)} \tag{13.34}$$

$$\left[\cos \frac{\beta_p z}{\left(1 + \frac{\tau_n^2}{\beta_e^2}\right)^{1/2}} + je^{j\frac{4\pi}{3}} \left(1 + \frac{\tau_n^2}{\beta_e^2}\right)^{1/2} C \frac{\beta_e}{\beta_p} \sin \frac{\beta_p z}{\left(1 + \frac{\tau_n^2}{\beta_e^2}\right)^{1/2}} \right].$$

$$v = 2 I_o(\beta_e a) \frac{i_o}{\rho_o} e^{-j\beta_e z} \sum_{n=1}^{\infty} \frac{\tau_n a}{(\tau_n a)^2 + (\beta_e a)^2} \frac{J_o(\tau_n r)}{J_1(\tau_n a)} \tag{13.35}$$

$$\left[Ce^{j\frac{4\pi}{3}} \cos \frac{\beta_p z}{\left(1 + \frac{\tau_n^2}{\beta_e^2}\right)^{1/2}} + j \frac{\beta_p}{\beta_e} \frac{1}{\left(1 + \frac{\tau_n^2}{\beta_e^2}\right)^{1/2}} \sin \frac{\beta_p z}{\left(1 + \frac{\tau_n^2}{\beta_e^2}\right)^{1/2}} \right].$$

(13.30) and (13.31) can also be rewritten

$$\frac{i_{I_o}}{i_o} = \frac{4\left[I_o(\beta_e a)\right]^2 e^{-j\beta_e z}}{\left[I_o(\beta_e a)\right]^2 - \left[I_1(\beta_e a)\right]^2} \sum_{n=1}^{\infty} \frac{(\tau_n a)^2}{(\tau_n a)^2 + (\beta_e a)^2} \tag{13.36}$$

$$\left[\cos \frac{\beta_p z}{\left(1 + \frac{\tau_n^2}{\beta_e^2}\right)^{1/2}} + e^{j\frac{\pi}{6}} C \frac{\beta_e}{\beta_p} \left(1 + \frac{\tau_n^2}{\beta_e^2}\right)^{1/2} \sin \frac{\beta_p z}{\left(1 + \frac{\tau_n^2}{\beta_e^2}\right)^{1/2}} \right].$$

$$\frac{v_{I_o}}{i_o} = \frac{4\left[I_o(\beta_e a)\right]^2 e^{-j\beta_e z}}{\rho_o \left[I_o(\beta_e a)\right]^2 - \left[I_1(\beta_o a)\right]^2} \sum_{n=1}^{\infty} \frac{(\tau_n a)^2}{\left[(\tau_n a)^2 + (\beta_e a)^2\right]^2} \tag{13.37}$$

$$\left[Ce^{j\frac{4\pi}{3}} \cos \frac{\beta_p z}{\left(1 + \frac{\tau_n^2}{\beta_e^2}\right)^{1/2}} + j \frac{\beta_p}{\beta_e} \frac{\sin \frac{\beta_p z}{\left(1 + \frac{\tau_n^2}{\beta_e^2}\right)^{1/2}}}{\left(1 + \frac{\tau_n^2}{\beta_e^2}\right)^{1/2}} \right]$$

The expression for the current density (44) has two terms. The first is that due to initial current modulation; the second, which contains the factor C, is that due to initial velocity modulation. $\left(1 + \frac{\tau_n^2}{\beta_e^2}\right)^{1/2}$ increases without bound as one considers larger and larger n. The wavelengths of the modes become greater and greater with larger and larger n in proportion to the value of $\left(1 + \frac{\tau_n^2}{\beta_e^2}\right)^{1/2}$. The current amplitude due to current modulation starts at a maximum, but the current amplitude due to velocity modulation starts at zero and increases with z. Furthermore, since $\left(1 + \frac{\tau_n^2}{\beta_e^2}\right)^{1/2}$ appears as a

factor in the term due to velocity modulation, the amplitudes of these terms increase without bound as n is taken larger and larger. But the value of z for which these terms reach their maximum also increases with n. For large enough values of $\beta_e a$, $\beta_e a$ = about 3, the coefficients in the expansion for $I_o(\beta_e r)$ first increase and then decrease slowly to zero for increasing n. If one were to observe the current due to initial velocity modulation at a large value of z, one would find that for low values of n, the current in each mode would increase faster than the coefficients of the expansion of $I_o(\beta_e r)$, that is as higher and higher values of n are considered, the values of these terms would decrease because of the increasing wavelengths of the sine envelope of the current due to velocity modulation.

The expression for the velocity also contains two terms. The first, containing a factor C, represents velocity due to initial velocity modulation. The second represents velocity due to initial current modulation. Here there are no terms with amplitudes that increase without bound as n increases without bound.

These equations should not be taken to mean that many physical quantities become infinite. The equations merely indicate that the bunching ability of high order space charge waves is very large. In order to realize large bunched current densities from small initial velocity modulation it would be necessary to use a very long drift tube. The current density will fall off away from the axis. Different parts of the beam will have opposite phases. Also, when one considers the combined effect of bunching of many space charge waves, it must be realized that there will be much cancellation of the actual current densities

because the phases of the current density associated with the various space charge waves will vary considerably from one another. For these reasons, the current density does not become quite as large as an initial cursory consideration may indicate.

As a disturbance travels down the drift space with an initial $I_o(\beta_e r)$ radial distribution, the individual components change phase with increasing z. The radial distribution profile changes radically with z. For example, the lowest order mode, because of its relatively short wavelength, changes phase by 180^o before the phases of the other modes change substantially. See Fig. 1.2. For larger values of z, the phase shifts for the other modes also become significant. In addition, the current arising out of the velocity modulation of the higher order modes begins to get significant. All this contributes to a jagged radial current distribution profile.

The problem as it now stands is to determine the current densities and other quantities along a sheath helix containing an electron beam, excited by the distributions of current and velocity found at the end of the drift space considered above. Once the current distribution in the stream for the second helix has been found, criteria for saturation can be established. It will be shown that the current which is to be considered is not that of the usable signal alone.

If one were to examine the secular equation for the propagation constants found by Chu and Jackson for an electron stream filling the helix, one would find an infinity of modes with purely imaginary propagation coefficients, in pairs, clustered about a limit point $j\beta_e$. These correspond to the plasma waves of a finite diameter beam in empty space

but modified slightly by the presence of the helix.

An assumption is made now. There are "I_o components" in the current and velocity profiles at the end of the drift tube. These parts, together with the zero electric field excite the increasing, decreasing and constant forward waves of the simple circuit theory. "What is left over" continues to propagate in the form of plasma waves mentioned in the preceding paragraph. The radial distribution profile of these plasma waves will be quite jagged.

In the linear problem, the "I_o" part of the input signal will split into three forward waves, one of which will grow exponentially to be much greater than any of the others at an appreciable distance down the helix. The remainder of the input will propagate as plasma waves with all the bunching and debunching processes that are associated with them. Furthermore, because of the jaggedness of the current and velocity radial distribution profiles at the input of the helix, the "I_o" part that increases will be a relatively small fraction of the peaks in the profile--perhaps a fifth of the profile peak. See Fig. 13.2 . The remainder of the input, that is, the plasma waves with no "I_o" component, will be called <u>hash</u> from now on. It will be assumed that the hash cannot ever give rise to usable signal as it proceeds down the tube. Since the amplitude of the "I_o" part of the input at the second helix is a small fraction of the hash level, the hash will cause current saturation in the stream while the useful signal is still many decibels below the hash. That is, increasing the excitation of the first helix will cause a nonlinear cessation of amplification in the second helix even though the electron stream is not fully modulated by useful signal.

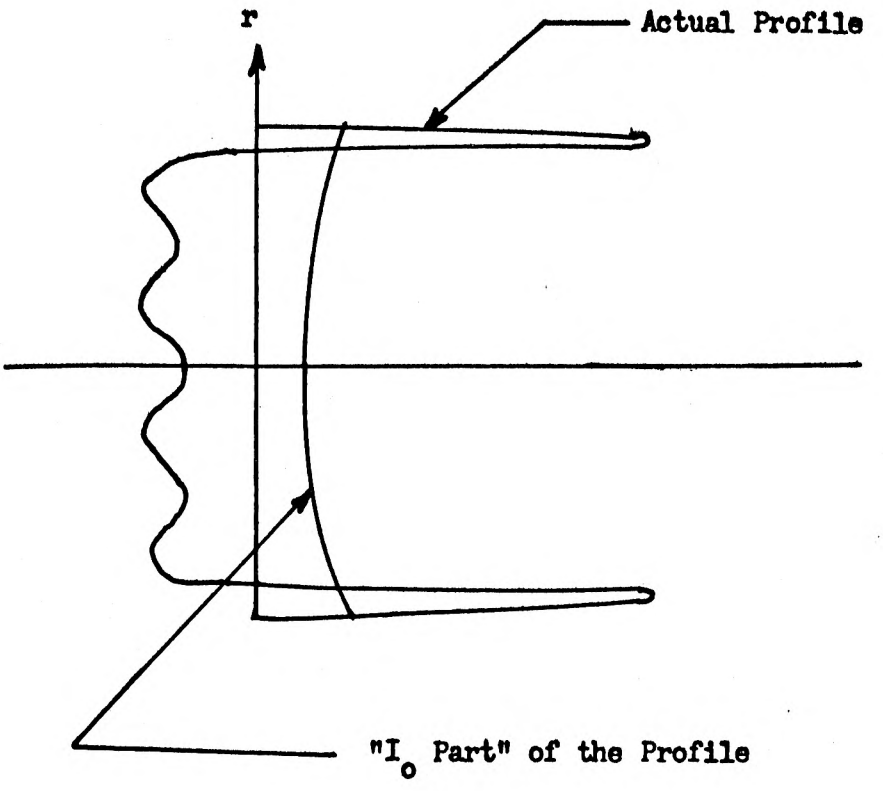

Fig. 13.2

To carry the argument one step further, consider the graphs of Fig. 13.3 . Fig. 13.3 is based on a rough calculation for a tube of β_e = 2.65 radians/meter for 1600 volt electrons and with β_p = 27.6 radians/meter. Operation is at 3000 mc. The length of the drift space was taken to be about 0.15 meters--equivalent to one-half a space charge wavelength for the lowest order drift space mode. This corresponds to a reversal of the $J_o(\Gamma_1 r)$ component at the end of the drift space. The hash amplitudes were calculated only at the start of the second helix and at the point one space charge wavelength from the start of the second helix. Then various rates of growth with distance were assumed for the hash. It is the author's guess that the hash would grow at a rate between a 1/2 and 1 power variation with distance along the helix. The difference in the results obtained by choice of either one or the other of these variations is less than the other errors which are involved. The assumption of continued growth of the hash is based on the differing degrees to which bunching takes place for the higher order modes, the fact that the bunching distance increases with the order of the mode, and the continued bunching taking place inside the helix.

It is now necessary to interpret the graphs of Fig. 13.3 . At the start of the second helix, the hash is about 12 db. above the signal level. For a reasonably high rate of gain, the signal will be larger than the hash at some distance down the second helix. If the input is increased until nonlinear operation takes place at the end of the drift tube, the signal will never be able to grow out of the hash. In order to get the full output available from the beam, the tube must be long enough so that the signal is out of the hash at the end of the tube.

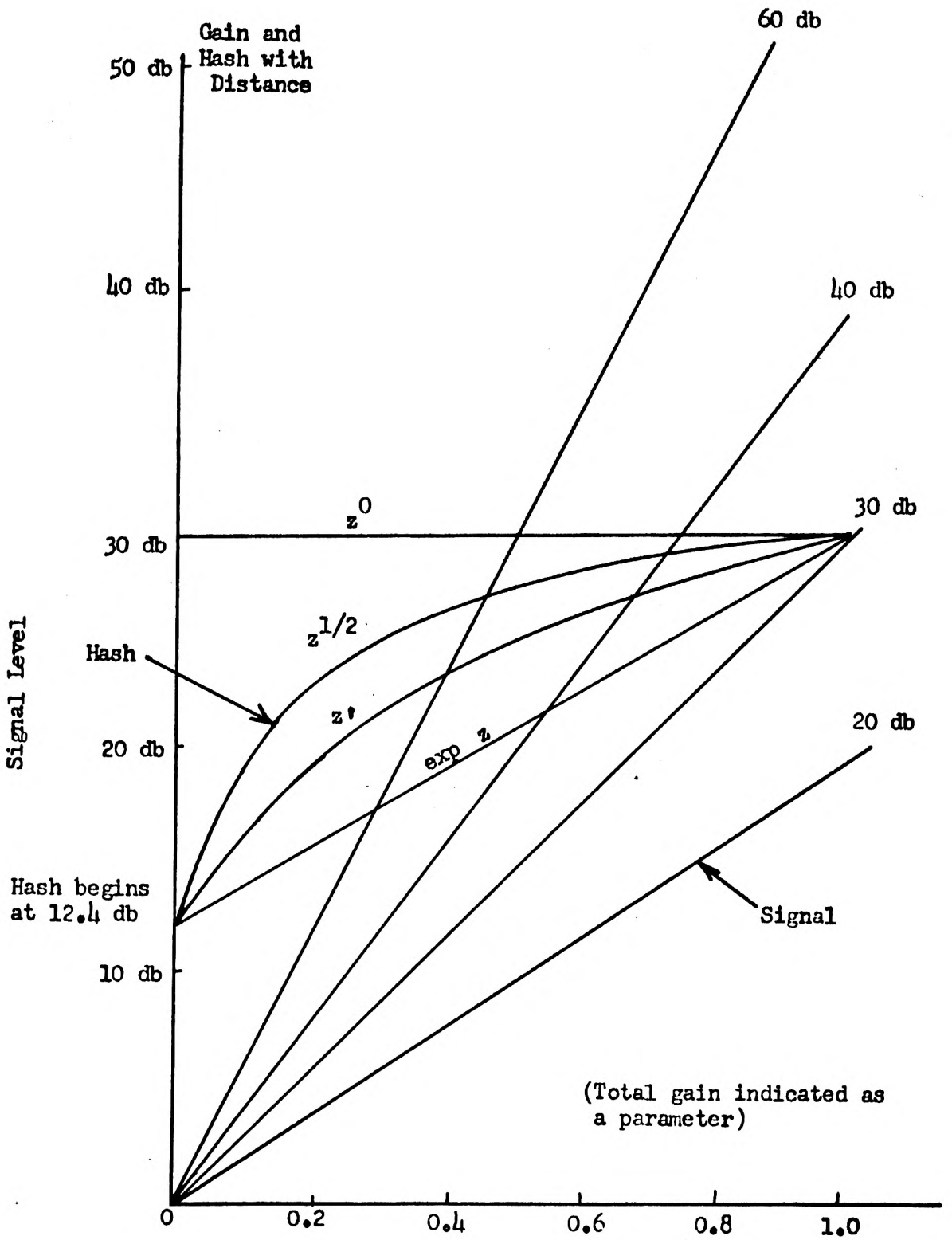
Gain and
Hash with
Distance
50 db
40 db
30 db
20 db
10 db
Signal Level
60 db
40 db
30 db
20 db
z^0
$z^{1/2}$
z
exp z
Hash
Hash begins
at 12.4 db
Signal
(Total gain indicated as
a parameter)
0
0.2
0.4
0.6
0.8
1.0
z in Units of First Mode Space Charge Wavelengths

Fig. 13.3

Due to the jaggedness of the current profile, not all parts of the beam should saturate together. Saturation would then show up gradually as the input signal is increased and the various portions of the beam begin to saturate.

For the purposes of the preceding calculations it was assumed that the following was true.

1. The beam filled the helix.
2. The beam filled the drift tube.
3. The higher order plasma waves in the helix behaved as if a drift tube surrounded the beam.

The last assumption was made just to enable the rough calculation just described to be completed.

Actually, beams seldom fill the helix. In that case, the $I_o(\beta_e r)$ radial variation of velocity and current still holds for low C and no space charge effects.

The second assumption also has implicitly implied that the attenuator acts as a drift tube. Firstly, if the beam does not fill the drift tube, one can still find the propagation constants of the waves which exist on the electron beam. Calculations can be made by placing an imaginary pipe just around the beam and hoping that the results will not be badly off. Secondly, one can make an attempt to get expressions in place of (13.23) and (13.24) by a method similar to that of Sollfrey. In any event, it is known that general physical properties of the plasma waves are not greatly affected by the presence or absence of a conducting pipe surrounding the beam. Furthermore, it has been shown in Sections XI and XVI that admittance wall amplification is negligible for the higher order space charge waves.

The amplitudes of the current modes contributed by the current modulation at the beginning of the drift pipe do not change very much with distance. It can also be seen from (13.34) that any change will be toward a smaller contribution. Therefore, the amplitudes of these current modulation contributions cannot be any greater in order of magnitude than the amplitude of the initial current incident upon the drift tube. The worst that could happen is that some of the modes may reverse sign or change phase, but no current peaks much greater than this initial amplitude will result if the current at the end of the drift tube would be due to only the initial current modulation. If, however, the part due to initial velocity modulation is also included, the amplitude of the current at the end of the drift pipe due to this velocity modulation can be much greater than the amplitude contributed by the current modulation. In that case, current peaks will be built up which may be several times as great as the initial current amplitude at the beginning of the drift space.

In order for a contribution to the current in a particular mode due to velocity modulation to be significant, it is necessary from (13.34), that $(1 + \frac{\tau_n^2}{\beta_e^2})^{1/2} C \frac{\beta_e}{\beta_p}$ be comparable to unity. If $C \frac{\beta_e}{\beta_p}$ is of the order of unity, the term $(1 + \frac{\tau_n^2}{\beta_e^2})^{1/2}$ emphasizes the higher order mode effect of velocity modulation. The reason that very high order terms do not contribute very greatly is because of the $\sin \frac{\beta_p z}{(1+\frac{\tau_n^2}{\beta_e^2})^{1/2}}$ factor. Nevertheless, for very large n, the small argument expansion for the sine shows that the contribution to the current in that mode due to initial velocity modulation is $\frac{1}{\tau_n^a} C \frac{\beta_e}{\beta_p}$.

In view of these considerations, it must be realized that a tube with large $C\frac{\beta_e}{\beta_p}$ will be very susceptible to velocity modulation bunching saturation effects. A tube with small $C\frac{\beta_e}{\beta_p}$ will be rather immune. The former situation will apply to typical low power tubes whereas the latter will apply to typical high power tubes using small β_e, large β_p, large C, but with $\frac{C}{\beta_p}$ small.

Section XIV

SATURATION MECHANISMS

In the previous section, one mechanism by which saturation due to attenuators may occur was described. Because of the strong assumptions that were made to enable calculation, the validity of such calculations is quite open to question. Furthermore, it has been shown that mode bunching effects cannot account for saturation in some high power traveling-wave tubes.

The material culminating in Section IX indicates that growing waves can exist in attenuator sections of traveling-wave tubes. Based on calculations which will be described later, another mechanism with a stronger basis will be described in this section to account for attenuator saturation effects.

It is supposed that one has obtained all the propagation constants associated with all the various sections of a traveling-wave tube. One can use the methods of Section XII to follow the current density amplitude and the electric field amplitude of the increasing wave along the length of a traveling-wave tube. See Fig. 14.1 . The information is plotted on a logarithmic scale. In the lossless regions, the current and field are normalized so as to be represented by the same line. The straight line indicates an exponential buildup of the wave along the tube.

When the attenuator region is reached, a new set of waves is excited. The level of the current in the increasing wave in this region is greater than the incident level. The field that is associated with that current however is smaller. The current and field can then be plotted as two parallel lines with the field below the current. The slope of these

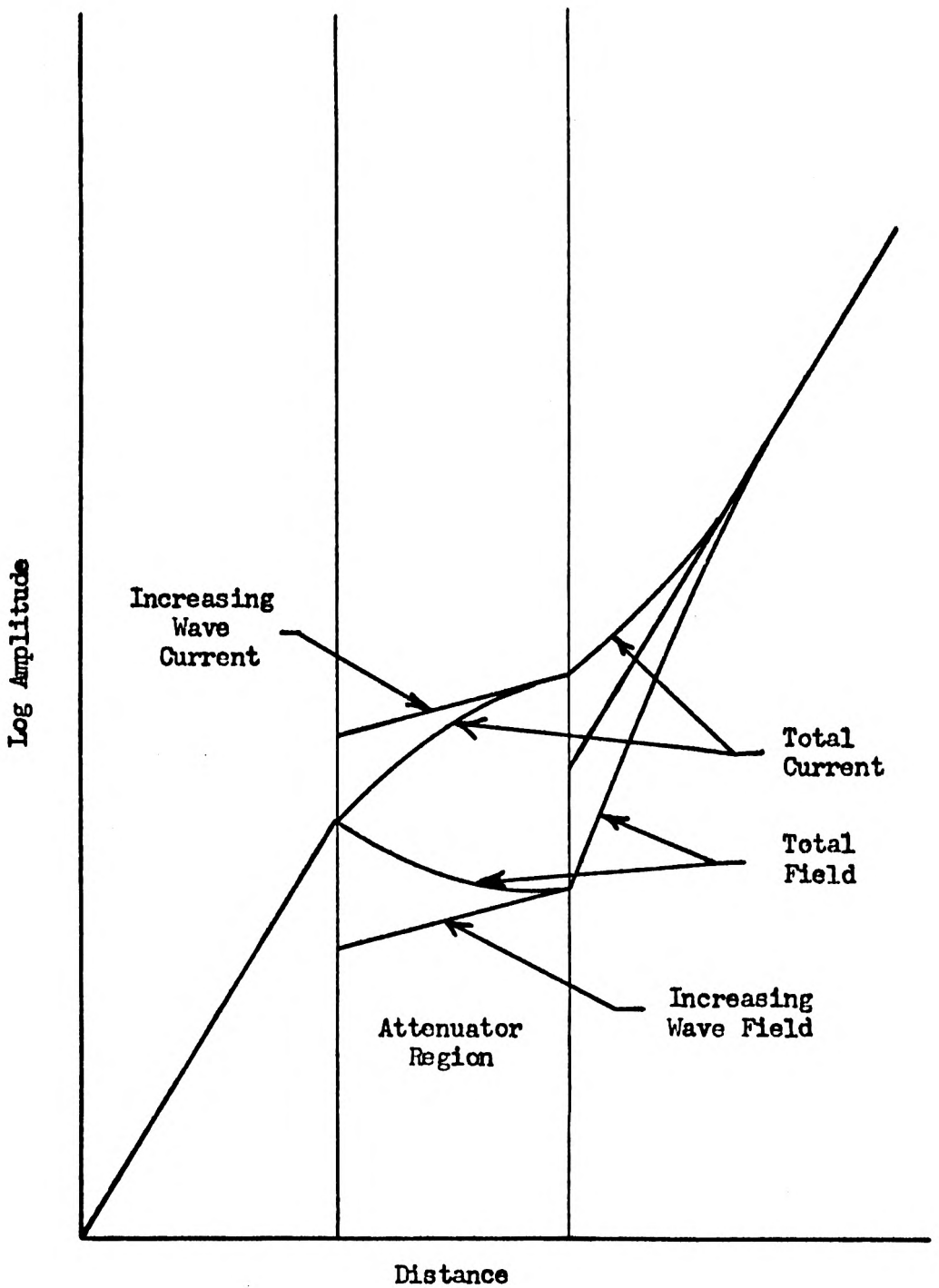

Behavior of Current and Field in an Attenuator

Fig. 14.1

lines will be somewhat smaller than the slope in the lossless region. This will indicate the loss of gain introduced by the conductive coating.

At the end of the attenuator region, a new lossless region begins. If one assumes that the gain and length of the attenuator region are sufficiently large so that only an increasing wave is incident upon the lossless region, it becomes an easy matter to calculate the amplitudes of the three waves set up in the new lossless region. Even if the gain and the length of the attenuator were not sufficiently long enough to give only an incident increasing wave, the calculations are still possible if one uses all the waves in the attenuator region. The use of only an increasing wave upon the attenuator lossless helix section will be simpler, however, for illustrative purposes.

The lines representing current and field in the increasing wave will again fall upon each other and have the same slope as they had in the first lossless section. The current in this increasing wave will be at a lower level than the level of the incident increasing wave from the attenuator.

Since the total field and current are continuous, it is easy to see that in the section of the second lossless helix near the attenuator, the current that corresponds to a given field is considerably greater than the current which corresponds to that field if only an increasing wave were present. It is, however, this larger current that causes saturation. Physically, one may argue that in the lossy region, the addition of conductance in parallel with the other admittance lowers the impedance of the structure. The lowered impedance means that a larger current will be present for a fixed amount of field.

From the point of view presented here, one sees that one way to make

a tube efficient is to make the gain of the lossless output section large enough so that only an increasing wave will be present at the point where the signal level on the tube becomes large enough to cause nonlinear operation.

Section XV

THE USE OF COMPUTING MACHINERY FOR CALCULATIONS

Digital computing machinery offers many advantages in obtaining suitable results. Primarily, the calculations are of such a nature that complete hand calculation is unfeasible. Furthermore, many Bessel functions of complex argument are needed for the calculation. The author knows of only one set of tables where such functions are available. The use of these tables would require much interpolation in addition to the table searching.

Machine computation is very useful if the same calculation must be repeated very many times. This is just what must be done in order to get enough information for plotting the various admittance functions. Transcendental functions of various kinds can be calculated by the machine as they are needed. Although this may seem like wasted effort, the avoidance of table searching more than compensates for the disadvantages. Plotting machines are also available which can take punched cards and plot points on a sheet of paper. They have not been used for the work described here.

The digital computing machinery available at the Institute at the present time is very meager indeed; only an I.B.M. punched card computer, 604, is available for use. This machine does have some additional features, however, which are not found on the standard 604 machine and which greatly increase its capabilities. Its chief defects are the following:

1. There is a lack of storage. The storage of the machine is very limited and this makes it necessary to punch out intermediate results. It is very difficult to work with complex numbers because the real part and imaginary part must be stored separately in individual storage units, thereby rapidly filling up the available storage. The number of places available in the storage is also limited. It limits one to quotients with no more than five significant figures.

2. Programming the machine is done by means of a board and patch cords. A limited number of steps is available for each pass of the cards. This means that for a very long calculation intermediate results must be punched out on cards. In order to store a program, the board which has the appropriate wiring must be stored. This is very difficult if there is not a sufficient number of boards available to meet the requirements of all the persons using the machine.

3. The machine is slow compared to more modern equipment.

In spite of all these disadvantages, any attempt to make the computations without a machine would appear hopeless.

In general, the author believes that further calculations using only the 604 should not be attempted. For this reason the entire set of programs will not be presented here. A sample program is given just to indicate the method. See Table 15.1 .

In order to make efficient calculations, other machines should be used. An I.B.M. 650 or the Electrodata "Datatron" should be suitable. An I.B.M. 701 would even be better. These machines are capable of storing program instructions in the same memory system as is used for storing numerical information. This enables long programs to be stored in the

Step No.			
1	Emit 4, RIFS2GS1 RI2	24	ROFS13, RIMQ
2	ROFS13, RIMQ	25	ROGS2, Mult +
3	ROFS13, Mult +	26	ROFS4, RIMQ
4	ROFS4, RIMQ	27	ROGS4, Mult -
5	ROFS4, Mult -	28	ROFS2GS1, Div
6	ROFS2GS1, Div	29	ROR
7	ROR	30	ROMQ, RI +
8	ROMQ, RIGS2	31	Emit 1, RI + RI5
9	ROFS13, RIMQ	32	ROGS2, RIMQ
10	ROFS4, Mult +	33	ROR, RIGS2
11	ROFS4, Mult +	34	ROFS4 , Mult +
12	ROFS2GS1, Div	35	ROGS4, RIMQ
13	ROR	36	ROFS13, Mult +
14	ROMQ, RIFS4	37	ROFS2GS1 Div.
15	ROGS2, RIFS13	38	ROR
16	Emit 2, RIGS3 RI2	39	ROMQ, RIGS4
17	RIGS4	40	ROGS3 RI +
18	Emit 1, RIGS2 RI5	41	Emit 1 RI -
19	ROGS3, RIMQ	42	RO, RIGS3
20	ROGS3, Mult +	43	Zero Test, R
21	ROR, RIFS2GS1	44	PU Prog. Rpt, PU GRP SUP
22	ROFS2GS1, RI + RI4		
23	ROR, RIFS2GS1		

Sup. Steps 1-18 from GRP SUP SUP. 44 from SUP on Zero
x,y,A,B in FS4, FS13, GS2, GS4 Rospectively
Calculation of $I_o(x + jy) = A + jB$

Table 15.1

machine. The machines mentioned all have storage capacities of at least several thousand words of ten decimal digits each, compared to less than ten words of fewer digits for the 604. Furthermore, once the machine has been progremmed from punched cards or tape, the card or tape with the program can be stored for future use leaving the machine free for other problems. Also, because of the large storage available, the machines are capable of being progremmed to get the required propagation constants by some process, possibly Newton's method, which does not require the plotting of contour maps of the admittance functions. The extra storage greatly increases the possibilities for machine computation.

Sollfrey has expressed the solution for the field quantities of a traveling-wave tube with arbitrary excitation in terms of a Laplace transform. The standard methods for evaluation of the inverse transform are quite impossible for this transform if one desires the rigorous answer. One can evaluate the inverse transform by a numerical integration. This will give the full effect of the higher order space charge waves as well as that of the continuum associated with a branch cut. Again, for such a process, a suitable general purpose computer with considerable storage would be necessary. A 701 or equivalent would probably be required to handle such a job.

Section XVI

CALCULATED RESULTS OF THE FIELD THEORY

A region of pa plane in the vicinity of $p_o a$ of the helix was chosen. This region was divided by a rectangular grid. For each intersection of the grid lines, values of the circuit admittance were calculated for various conductivities of the lossy coating. The admittance was calculated for a radius just inside the sheath helix. The results of Section V were used for this calculation. Once having determined the admittance of the circuit for a given pa , a point can be entered upon the complex admittance plane. When all such points have been entered, they can be joined together by lines to form a contour map relating the admittance to the propagation constant.

One performs a similar admittance calculation for the electron beam. The calculation can be repeated for various beams. The results of such calculations are plotted in the same manner as the results of the circuit admittance calculation. A given beam admittance value will be attained by an infinite number of propatation constants with a limit point corresponding to the velocity of the beam because of the essential singularity at β_e . The plot of interest corresponds to that region of pa which corresponds to the largest deviations from velocity synchronism which gives solutions.

In order to get the propagation constants corresponding to a given circuit and electron beam, one takes the corresponding plots and superimposes them. A light table is a convenient means for doing so. Then one determines the propagation constants which give the same values of

admittance on both maps, the electronic and the circuit maps. This can be done easily by finding the intersections between the corresponding contours of the real part of the propagation constants and then drawing a line through these points, doing the same thing for the imaginary contours, and then finding the intersection between the two lines so determined.

On a suitable computer, one would be able to program the machine to determine the propagation constants by means of an iterative procedure without the necessity of resorting to the drawing of admittance contour maps.

In any event, the final result will be the determination of the three principal forward waves associated with a traveling-wave tube. Using the results of Section XII one can calculate the amplitudes of the waves that are excited in various regions. It is assumed that all the other modes are not present in any appreciable amount.

Such calculations have been made for a helix with a conductive sheath at a radius double that of the helix. This relative value of radii was chosen in order to simulate to some degree the effects of dielectric loading. Several differing values of conductivity were chosen. The normalized conductivities used were 0, 0.5, 0.25, 0.1, and 0.05 for cases 0, 1, 2, 3, and 4 respectively. Other parameters were $ka = 0.153$, $\tan^2 \theta/ka = 0.1025$. The admittance maps for these cases appear in Figs. 16.1 through 16.5. The cold circuit propagation constants are listed in table 16.1. It is interesting to note that the cold circuit attenuation is a maximum for an intermediate value of conductance. This

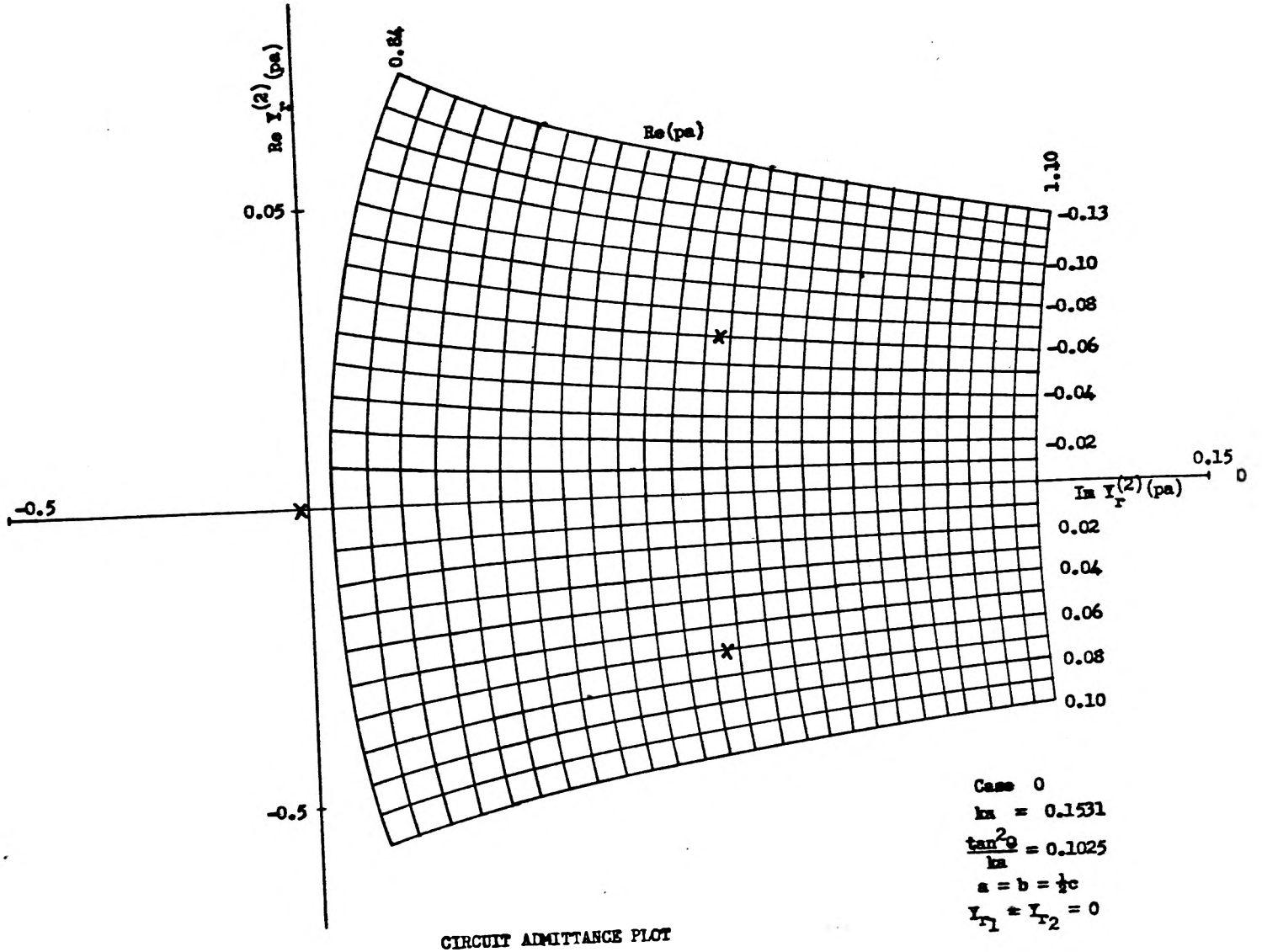

CIRCUIT ADMITTANCE PLOT

Fig. 16.1

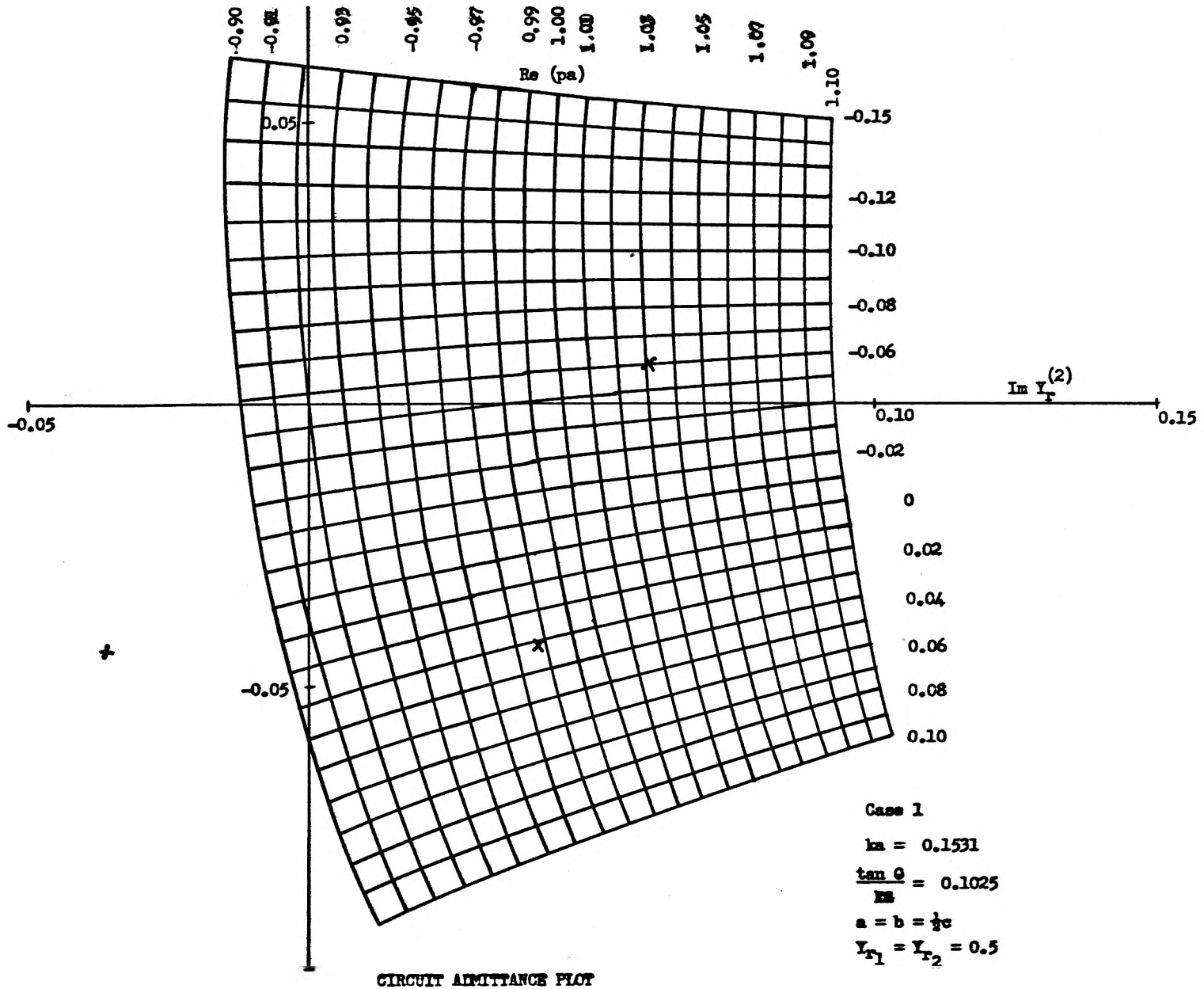

Case 1

ka = 0.1531

$\frac{\tan \theta}{ka} = 0.1025$

$a = b = \frac{1}{2}c$

$Y_{r_1} = Y_{r_2} = 0.5$

CIRCUIT ADMITTANCE PLOT

Fig. 16.2

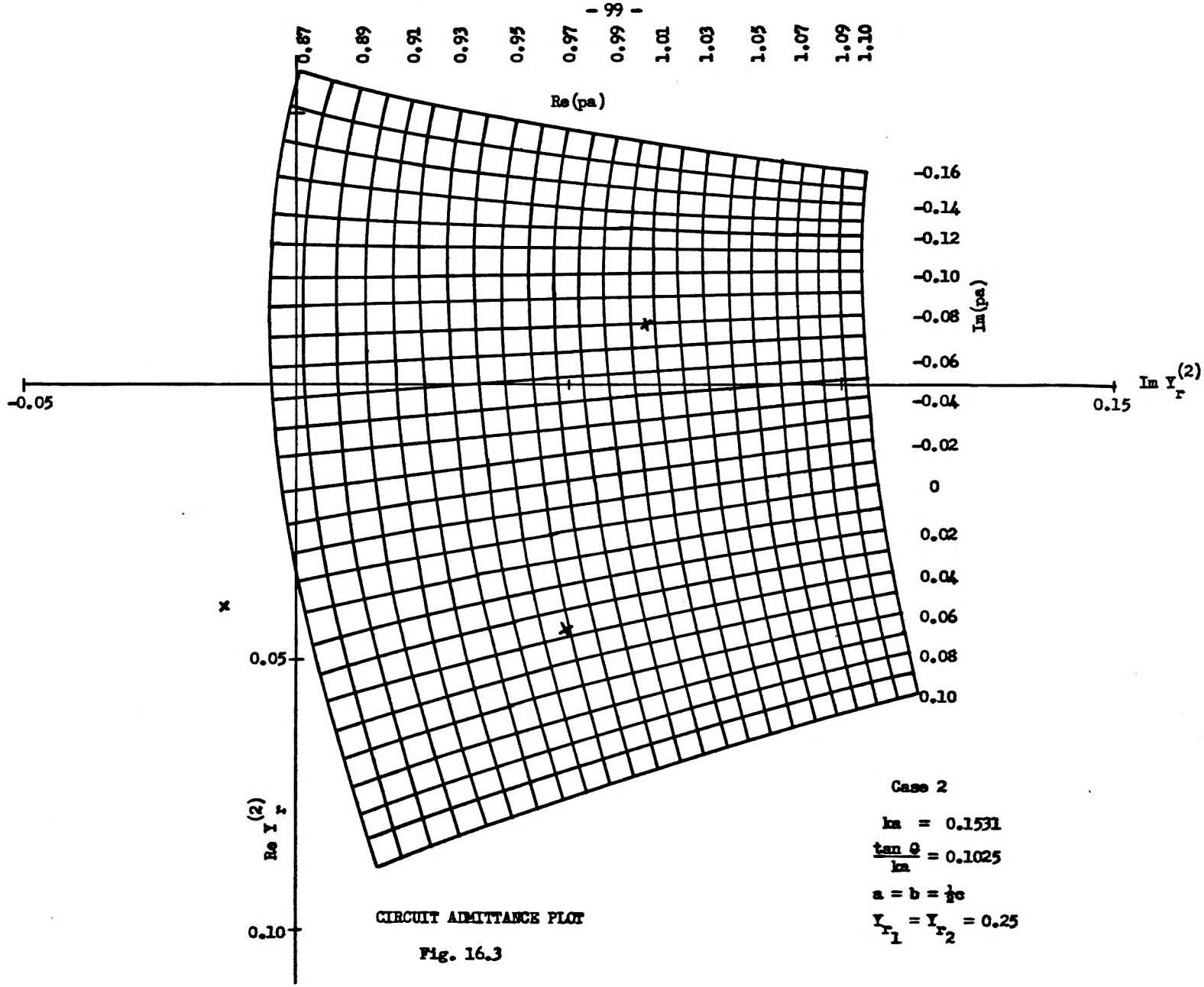

CIRCUIT ADMITTANCE PLOT

Fig. 16.3

Case 2

ka = 0.1531

$\frac{\tan \theta}{ka} = 0.1025$

a = b = $\frac{1}{10}$c

$Y_{r_1} = Y_{r_2} = 0.25$

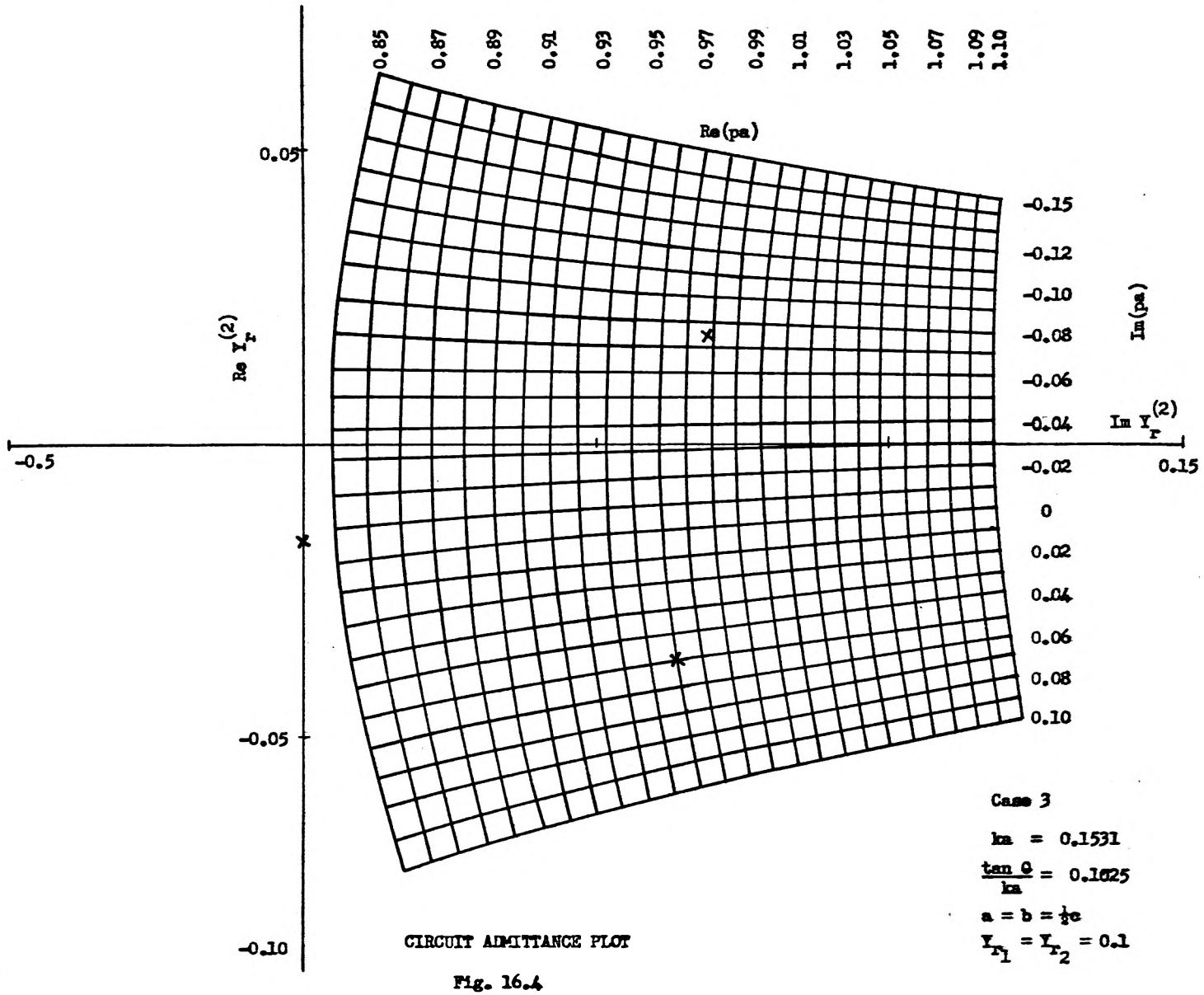

CIRCUIT ADMITTANCE PLOT

Fig. 16.4

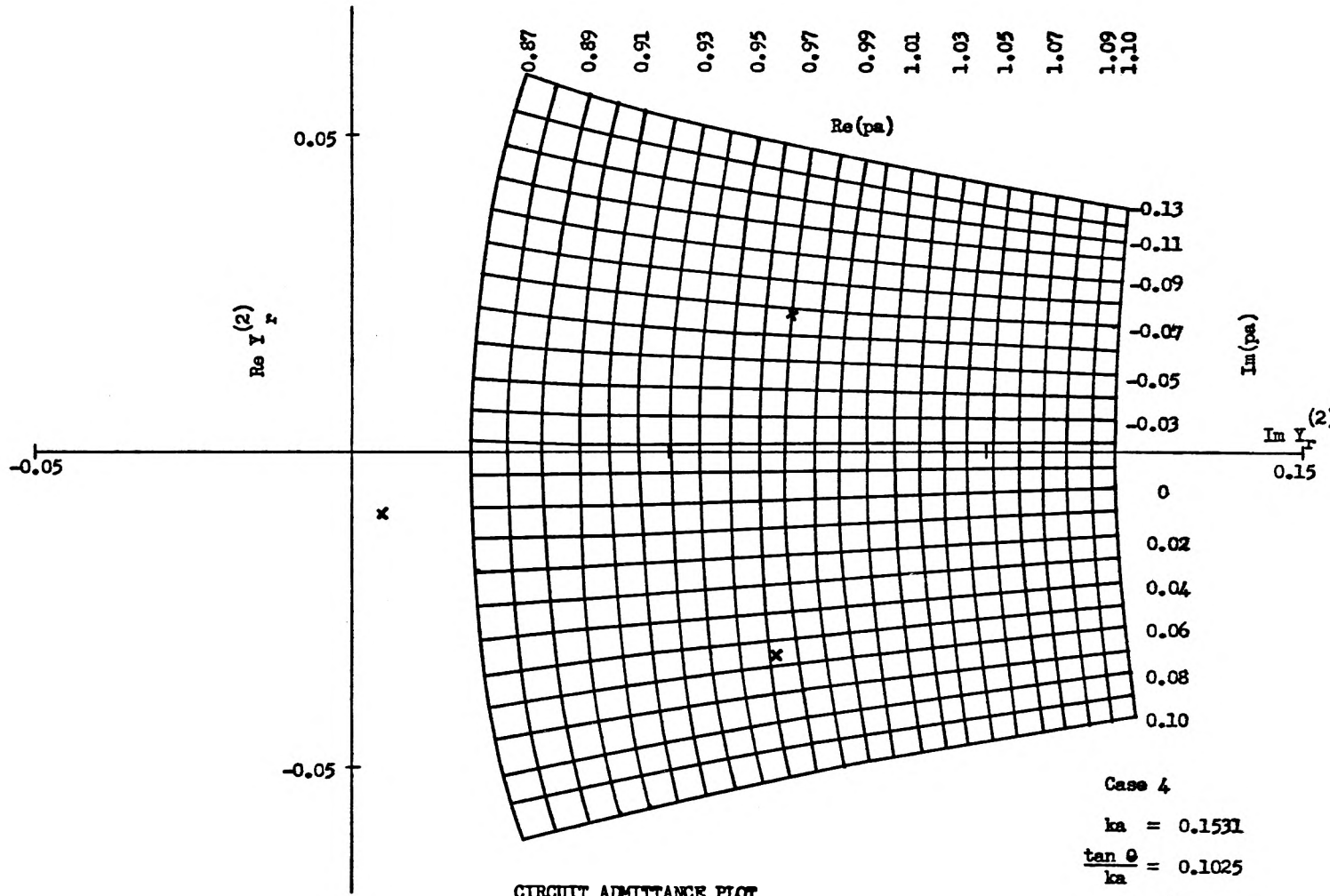

CIRCUIT ADMITTANCE PLOT

Fig. 16.5

Case 4

$ka = 0.1531$

$\frac{\tan \theta}{ka} = 0.1025$

$a = b = \frac{1}{2}c$

$Y_{r_1} = Y_{r_2} = 0.05$

Case	Normalized Admittance	Resistivity	$P_o a$	% Velocity Change	$\frac{\text{loss}}{\text{helix radius}}$
0	0		0.967 + j0.000	0	0
1	0.5	754	1.046 - j0.043	8	0.37
2	0.25	1510	1.014 - j0.052	5	0.45
3	0.1	3770	0.977 - j0.032	1	0.28
4	0.05	7540	0.97 - j0.017	small	0.15

Cold Circuit Properties

Table 16.1 $ka = 0.1513, \frac{\tan^2 \theta}{ka} = 0.1025, \quad c = 2a$

is to be expected when one considers the behavior if there were infinite conductivity at $r = c$. It is of importance to note that the velocity of propagation is lowered with increasing conductivity. Fig. 16.6 is an admittance map for an electron beam with $\beta_p a = 0.06$ and $\beta_e a = 0.900$, and $b = a$. The plot for positive imaginary pa is found by reflection by the imaginary admittance axis.

Figs. 16.1 through 16.5 have the intersections with Fig. 16.6 indicated. These intersections correspond to the propagation constants. Some of these intersections are not in the region for which calculations have been made. It is, nevertheless, rather easy to get a good estimate of where they ought to be by visual means. These propagation constants are listed in Table 16.2 .

It is of interest to determine saturation based on the mechanism described in Section XIV and the associated figure, Fig. 14.1 . The quantity of interest would be the ratio of the current to field in the attenuator region, compared to the ratio of current to field in the lossless region. If the current and field are normalized so as to fall on the same line in the lossless region as in Fig. 14.1, then the quantity of interest will be the difference in height between the two lines in the attenuator region, l , expressed in decibels. These quantities, and a few related ones have been calculated and are presented in Table 16.3 . The calculation is made for a traveling-wave tube using the structure corresponding to case 0 , for the lossless section. The attenuator section corresponds to the cases 1, 2, 3, and 4 .

In order to understand the saturation beyond the end of the attenuator on the basis of the discussion presented here, it is necessary

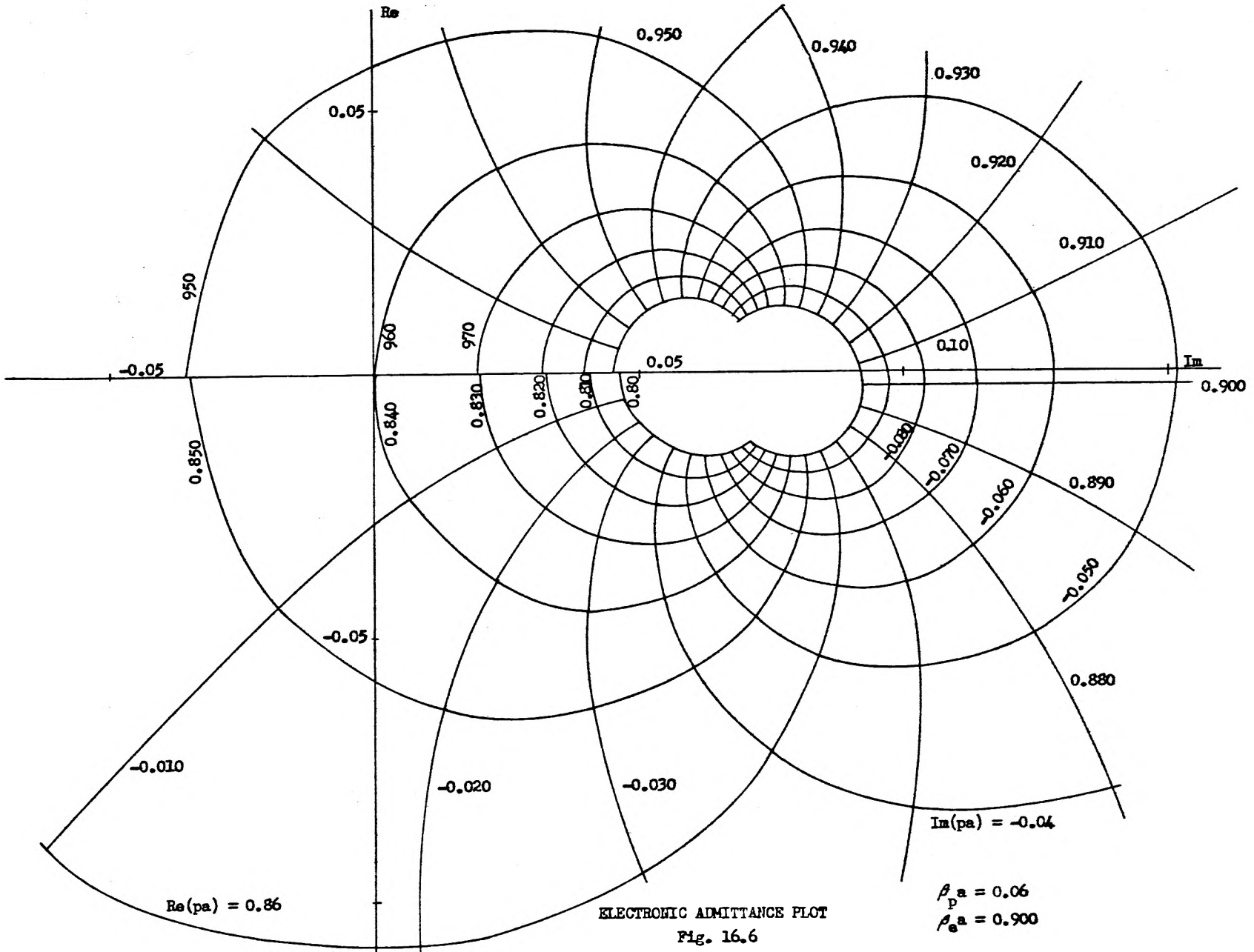

$\beta_p a = 0.06$
$\rho_e a = 0.900$

ELECTRONIC ADMITTANCE PLOT
Fig. 16.6

Case	Normalized Admittance	Gaining pa	Decaying pa	Fast pa
0	0	0.966 + j0.062	0.966 - j0.062	0.840 - j0.000
1	0.5	0.976 + j0.032	1.036 - j0.060	0.850 - j0.008
2	0.25	0.968 + j0.037	1.008 - j0.078	0.845 - j0.010
3	0.1	0.960 + j0.050	1.008 - j0.074	0.840 - j0.006
4	0.05	0.962 + j0.056	0.978 - j0.068	0.840 - j0.003

Traveling-Wave Tube Propagation Constants

Table 16.2

Case	$\frac{i_1}{i_{in}}$	$\frac{E_1}{E_{in}}$	$\frac{\beta_e - p_1}{\beta_e - p_{in}}^2$	
1	1.29	1.070	0.836	1.6 db
2	1.31	0.956	0.730	2.8 db
3	1.22	0.902	0.740	2.6 db
4	1.10	0.935	0.850	1.4 db

$$= 20 \log \frac{\text{Current at end of attenuator}}{\text{Electric field at end of attenuator}} \quad \frac{\text{Current of increasing wave(lossless)}}{\text{Field of increasing wave (lossless)}}$$

Table 16.3

to calculate the build up of current and field, the sum of the three forward waves. From such a procedure, one determines the degree to which the field and current is represented by the increasing wave alone. The three waves were summed for Case 2 for various distances beyond the end of the attenuator. The current to field ratios at these points were compared to the current to field ratio for a purely increasing wave. The results of these calculations are shown in Fig. 16.7 . This shows that the effects of the attenuator in changing the current to field ratios of the waves continue to be present at reasonable distances beyond the attenuator.

Experimental work done at the Hughes Aircraft Company (R-2) has shown that the attenuator loss in power output is about two or three decibels. Maximum power for typical operation is obtained beyond the end of the attenuator for their tubes. The calculation performed here indicates that the power loss should not be that great beyond the attenuator. It is believed that the discrepancy lies in the fact that the attenuator used in the Hughes tube is more closely coupled to the helix than the attenuator for which calculations have been made.

The maximum loss obtainable by the adjustment of the attenuator conductivity for the cases calculated here is about 3.0 db. per guide wavelength. The losses associated with the Hughes tube attenuator are about 8 or 9 db. per guide wavelength. The Hughes tube was constructed with a rather thin wall envelope. The envelope was thin enough so that even upon taking into account dielectric loading, the ratio of equivalent attenuator radius to helix radius ratio is considerably less than 2. For the calculations performed here, the ratio c/a was chosen to

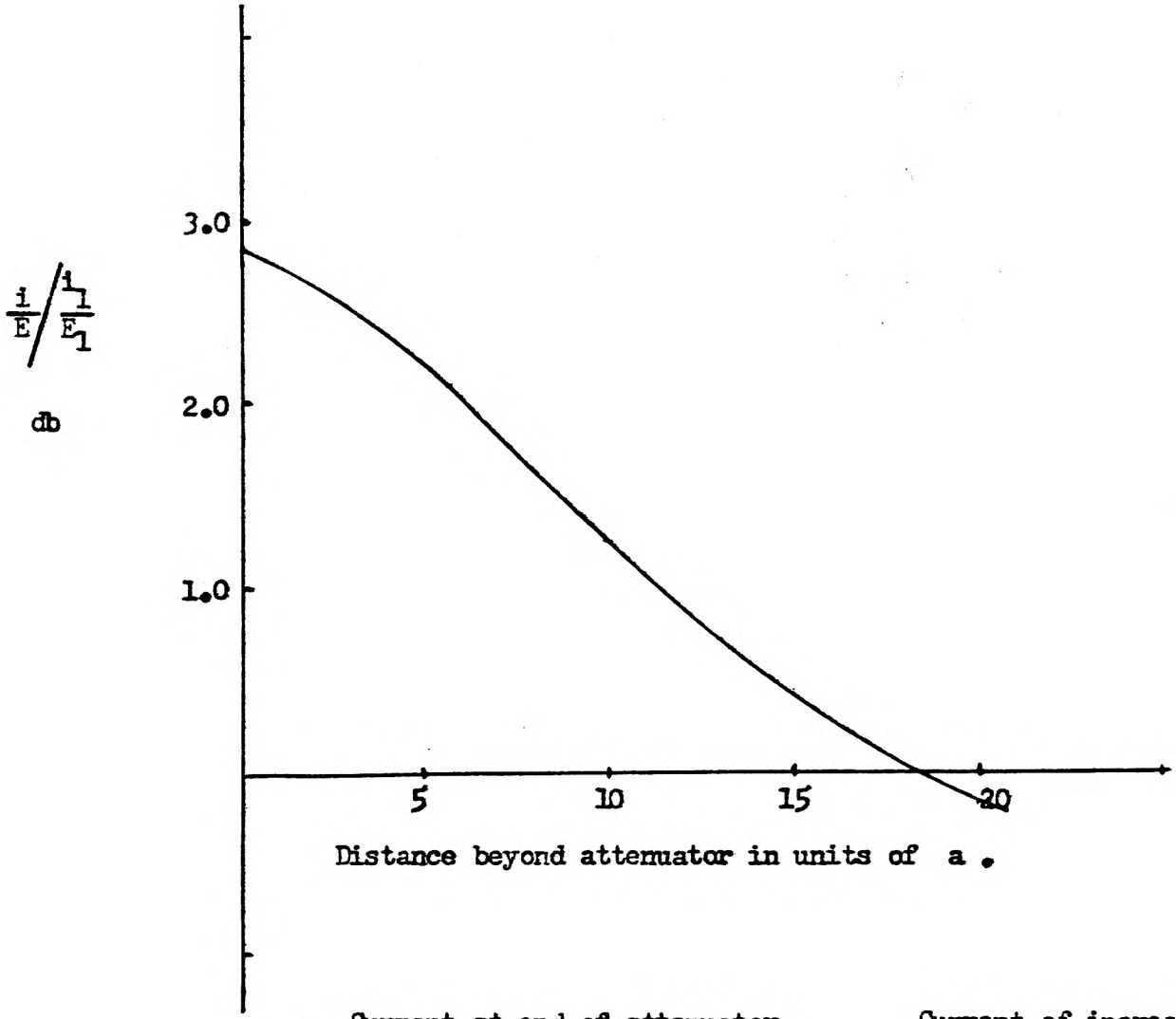

$\frac{\text{Current at end of attenuator}}{\text{Electric Field at end of attenuator}}$ $\frac{\text{Current of increasing wave}}{\text{Electric field of increasing wave}}$ vs. z

Fig. 16.7

be equal to 2 in order to emphasize the effect of dielectric loading.

An attenuator which is strongly coupled to the helix will introduce considerably more loss than one that is coupled more loosely. It is now easy to see why such an attenuator will have a stronger effect on the propagation constants. It then appears to be very likely that a more strongly coupled attenuator will cause the changes in the current to field ratios at the end of the attenuator to be larger than for a weakly coupled attenuator with the same conductivity. Such a situation would require more gain in order for the increasing wave to be much larger than the constant and decreasing waves since large changes in the propagation constants will excite large decaying and fast waves.

It is of interest to compare the results of the field calculations to those predicted by the Pierce-Fletcher theory. The values of K and Q that were used in the comparison were read directly off the graphs published by Fletcher. There may be considerable error introduced by such direct use of the curves.

The published curves correspond to a helix in empty space. That is, they do not strictly apply to lossy helices. But, in the absence of any better calculations, they were made to do. The introduction of loss is represented by d in the Pierce theory. Actually, introduction of loss also results in a change of phase velocity. This can be taken into account by the use of a complex d. This turns out, however, to be equivalent to using a value of b which corresponds to the lossy phase velocity. It is not correct to merely introduce a real d without simultaneously modifying b.

K and Q actually are complex numbers for lossy helices, and their

absolute values change as the circuit properties are changed: it is to be expected then, that there will be poorer agreement between the field and Pierce values for the propagation constants for lossy helix tubes. This is indeed found to be true. The discrepancy between the field and Pierce values for the increasing wave incremental propagation constants for the lossless case is about 5 percent. The corresponding discrepancy for the lossy Case 2 is about 10 percent. For the lossless case, the discrepancy is only slightly larger than the accuracy one can expect to get by reading values off the Fletcher curves. For the lossy case, the discrepancy becomes markedly larger than can be attributed to error in reading the curves. This indicates that the Pierce-Fletcher theory does not adequately account for the effects of loss.

The results of these calculations appear in Table 16.4 .

It is somewhat difficult to predict what the discrepancies between the Pierce and field theories will be for other parameters. Larger values of $\beta_e a$ will correspond to tubes which agree more closely to the Pierce-Fletcher theory if no loss is introduced. The absolute value of Q will be larger for such tubes, and the effect of loss on Q is presently quantitatively unknown. Larger currents will increase the incremental propagation constants which in turn will make the Fletcher approximation more inaccurate.

Finally, it is of interest to get an estimate of what kind of amplification can be expected in the higher order modes of a lossy helix traveling-wave tube. For Case 2, the admittance to be used for $pa = 0.900$, is $Y_r^{(2)} = -0.0320 + j0.0170$. The z_n corresponding to the first higher order mode is $j3.832$. Substitution of these values

PROPERTY	FIELD THEORY VALUE	PIERCE THEORY VALUE
Lossless and Lossy		
K	--	208
Q	--	0.261
I_o	75.8 ma	75.8 ma
V_o	7440	7440
C	--	0.0809
QC	--	0.0211
Lossless only		
b	--	0.92
δ increasing	0.851 - j0.906	0.812 - j0.870
Lossy only		
b	--	1.567
d	--	0.714
δ increasing	0.507 - j0.933	0.437 - j0.854
$\frac{E}{i} \Big/ \frac{E}{i}$ lossless	0.73	0.68

Table 16.4

into (11.7) results in

$$pa = 0.900 \pm 0.0136 + j0.00152$$

Therefore, the rate of gain for this mode is quite small indeed compared to the gain of the principal mode.

Section XVII

CALCULATED AND EXPERIMENTAL RESULTS FROM THE BUNCHING THEORY

Attempts have been made to find out the correlation between the experiment and the bunching theory of Section XIII. Calculations were made for a tube with the following parameters.

V_o = 650 V

I_o = 0.5 ma

$2b$ = 1.27 mm = beam diameter

$2a$ = 2.31 mm = mean helix diameter

λg = 0.518 cm

$\beta_e a$ = 1.4

β_p = 46.0/m

β_e = 1218/m

C = 0.034

QC = 0.11

It is assumed that a beam of radius a is incident upon the attenuator which is assumed to be equivalent to a drift pipe. The plasma frequency of the actual beam is assumed to be equal to the plasma frequency of the beam in a closely fitted drift pipe. With these assumptions, and the results of Section XIII, current and velocity profiles have been computed for the beam at various distances from the beginning of the drift pipe. These are illustrated in Figs. 17.1 through 17.4 . The calculations were made using a finite number of the space charge wave modes.

It is noted that the peaks of the distributions shown in Figs. 17.1 through 17.4 occur for values of r which are almost but not quite equal to a . One may say, to a reasonable degree of approximation, that the

peaks occur for $r = 0.9\,a$. Then the ratio of the peak current density to the peak initial current density at the beam edge, may be computed as a function of distance along the drift pipe. This ratio can be expressed as

$$\frac{i_{out}}{i_{in}} = 2\sum \frac{\tau_n a \; J_o(0.9\tau_n a)}{(\tau_n a)^2 + (\beta_e a)^2 \; J_1(\tau_n a)} \left[\cos \frac{\beta_p z}{\sqrt{1+(\frac{\tau_n a}{\beta_e a})^2}} + j e^{j\frac{4\pi}{3}} \sqrt{1+(\frac{\tau_n a}{\beta_e a})^2} \frac{\beta_e}{\beta_p} \sin \frac{\beta_p z}{\sqrt{1+(\frac{\tau_n a}{\beta_e a})^2}} \right] \tag{17.1}$$

The results of this calculation are shown in Fig. 17.5 . These results are also listed in Table 17.1 .

The "I_o" parts of the current density can be found by means of (13.26) which is applied in the form of (13.30). A similar calculation for velocity is also possible using (13.31). The results for various values of drift pipe length are listed in Table 17.2 .

Table 17.3 gives a summary of the radial distributions of alternating velocity. Table 17.4 gives the "I_o" components of current and velocity at various distances along the drift tube.

Using Fig. 17.5, one can determine the relative input powers at the beginning of the drift pipe which would give equal peak current densities at various distances along the drift pipe. If one postulates that saturation sets in when the peak current density reaches the direct current density, then these relative powers will be the relative power inputs required to cause saturation at the end of a drift pipe.

Measurements were taken on the tube described above. Figs. 17.6 and 17.7 show the results of these measurements. The plots indicate the relative power required to cause saturation as a function of the position at which saturation effects are measured. The first one is plotted in terms of distance beyond the attenuator. The second is in terms of relative position, the length of the attenuator being the parameter for the

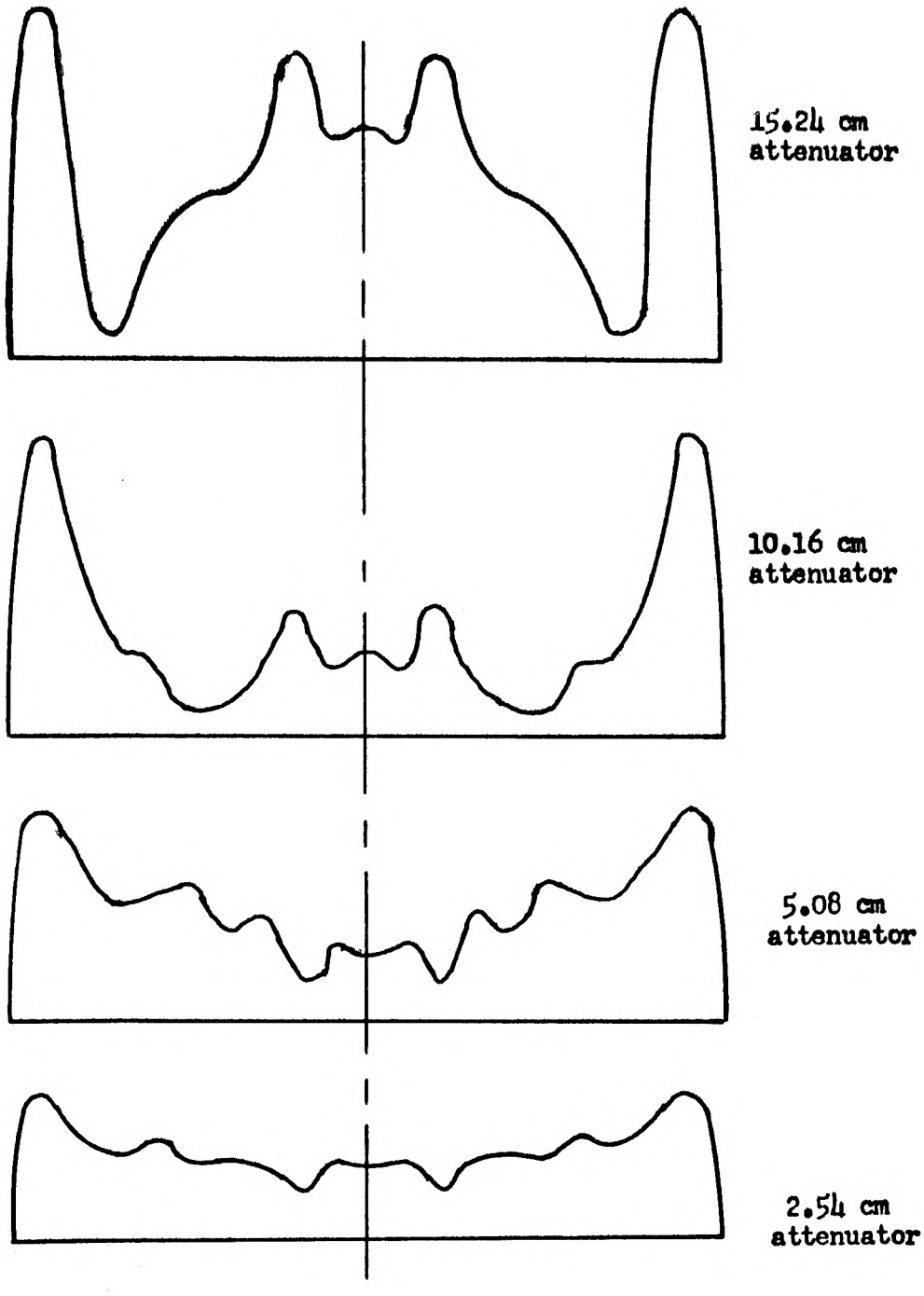

Absolute Current Density Profiles

Fig. 17.1

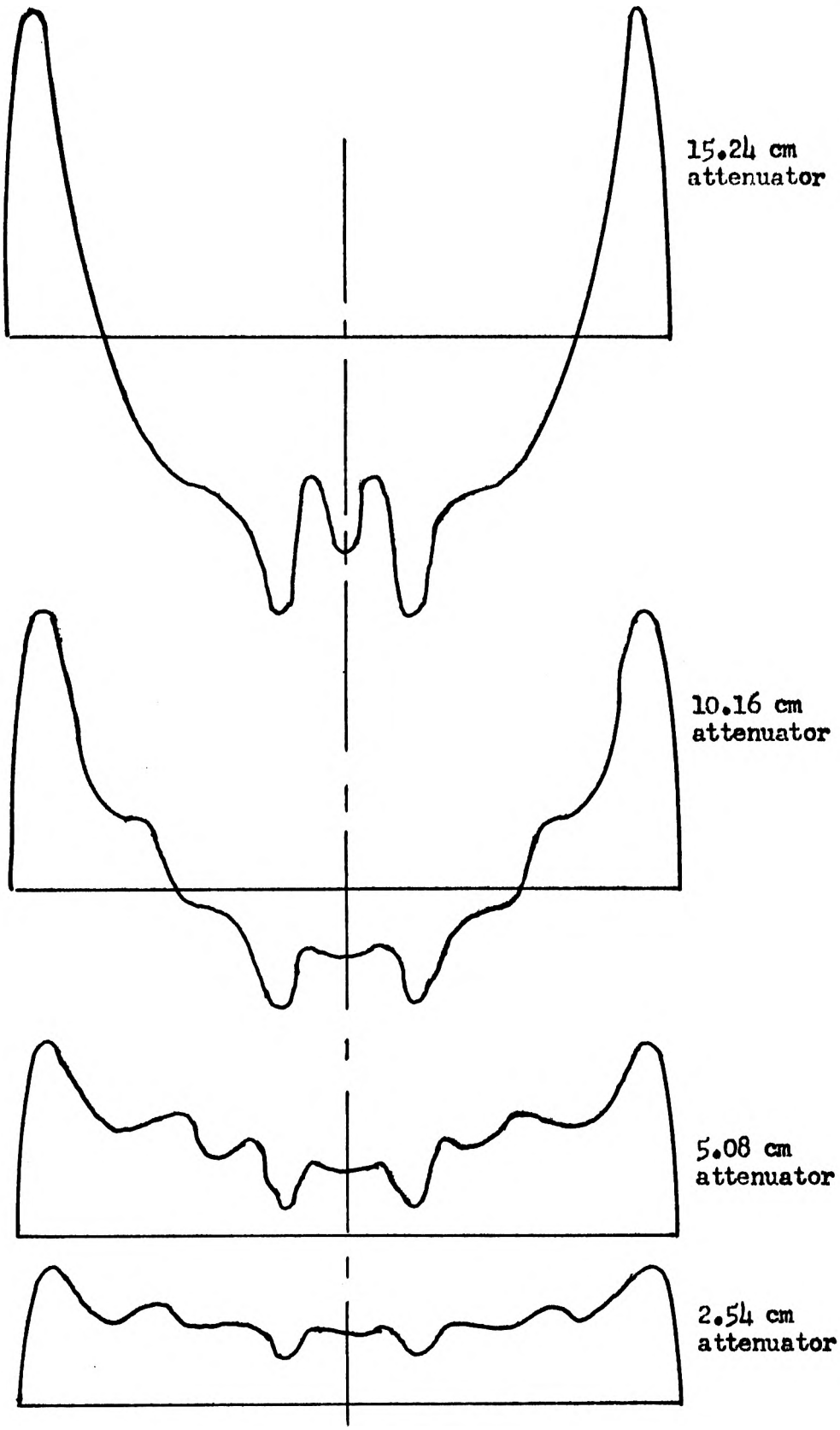

Instantaneous Current Density at Moment
of Peak Density

Fig. 17.2

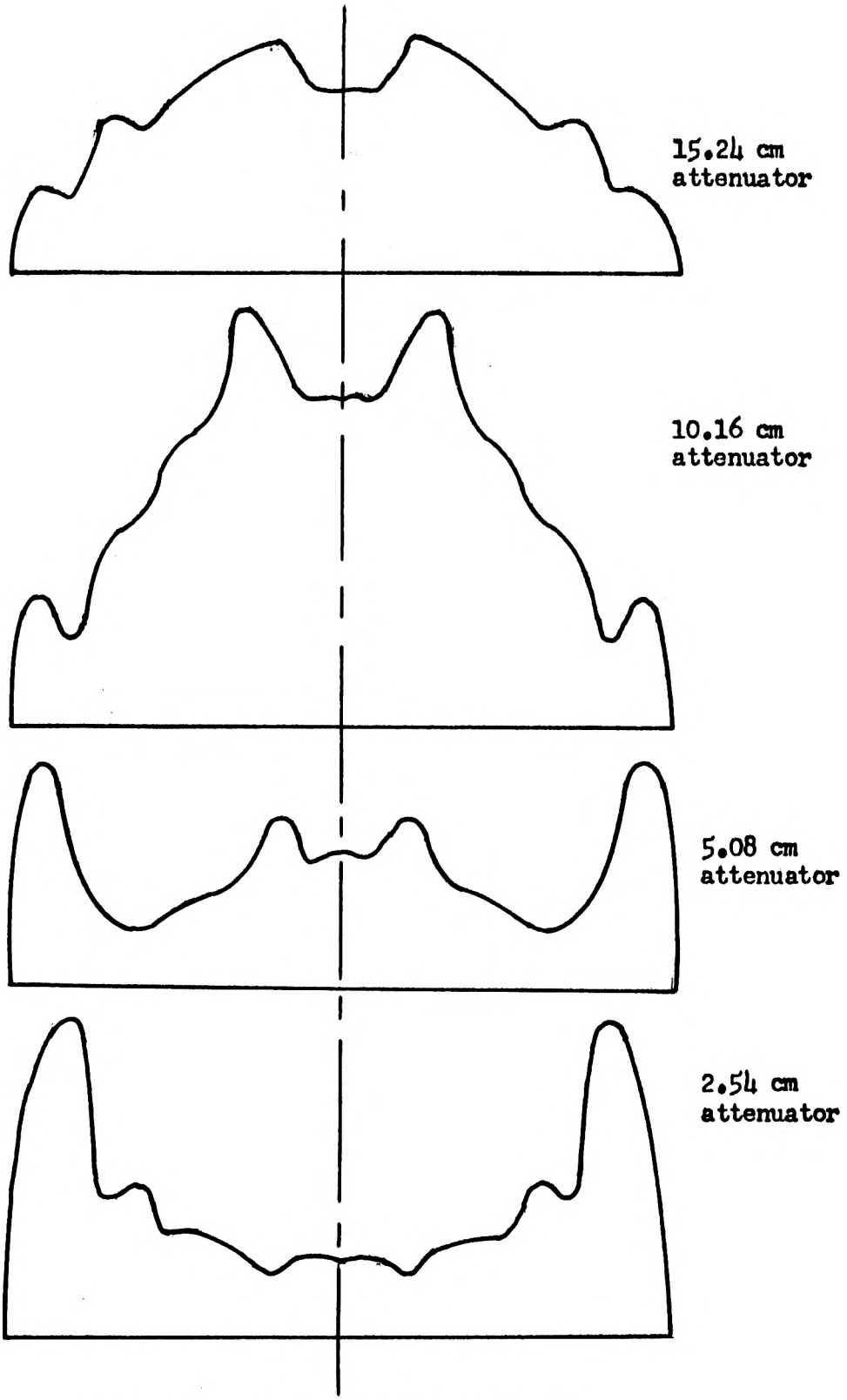

Absolute Magnitude Velocity Profiles

Fig. 17.3

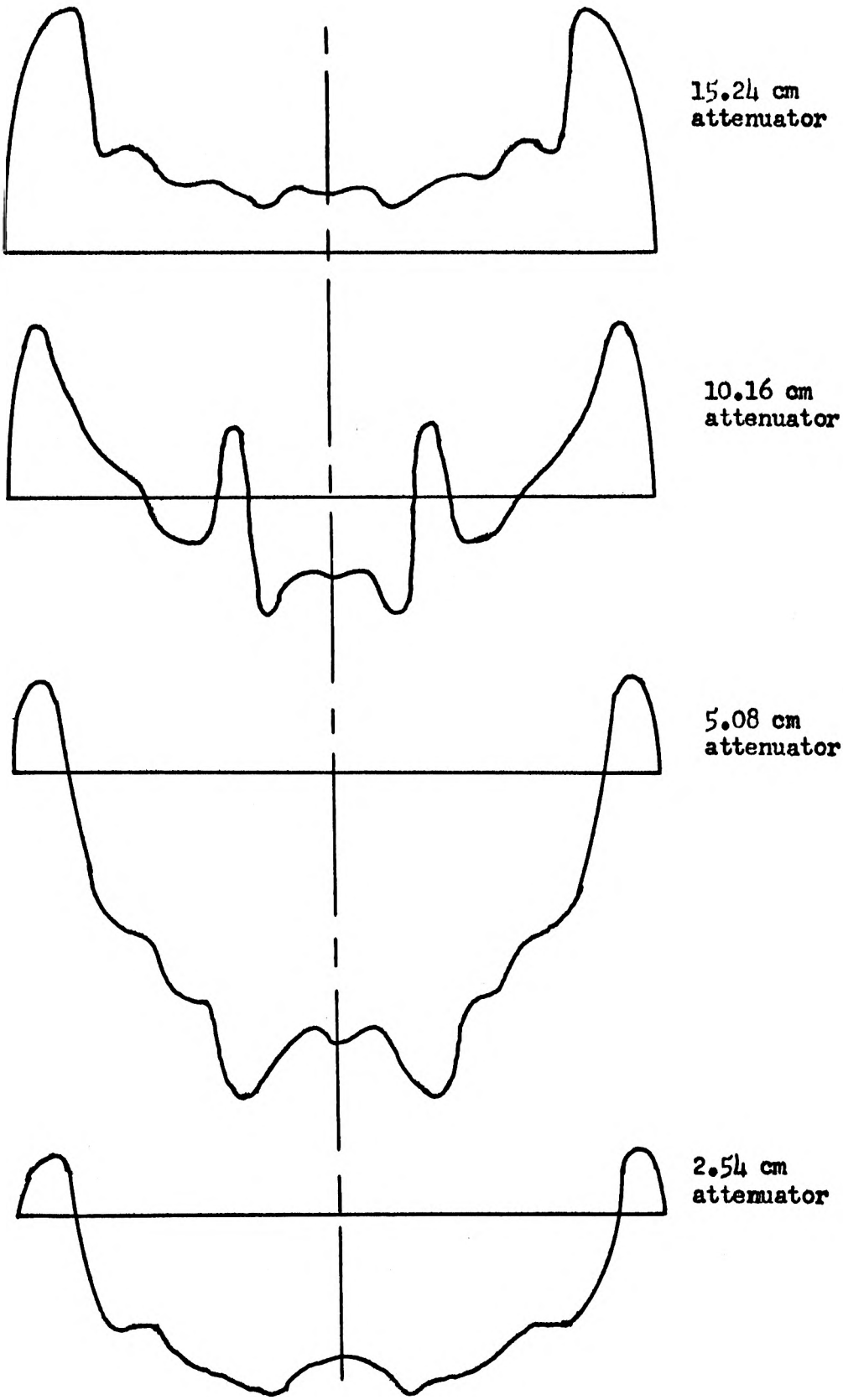

Instantaneous Velocity Profile at Moment of Peak Velocity
Fig. 17.4

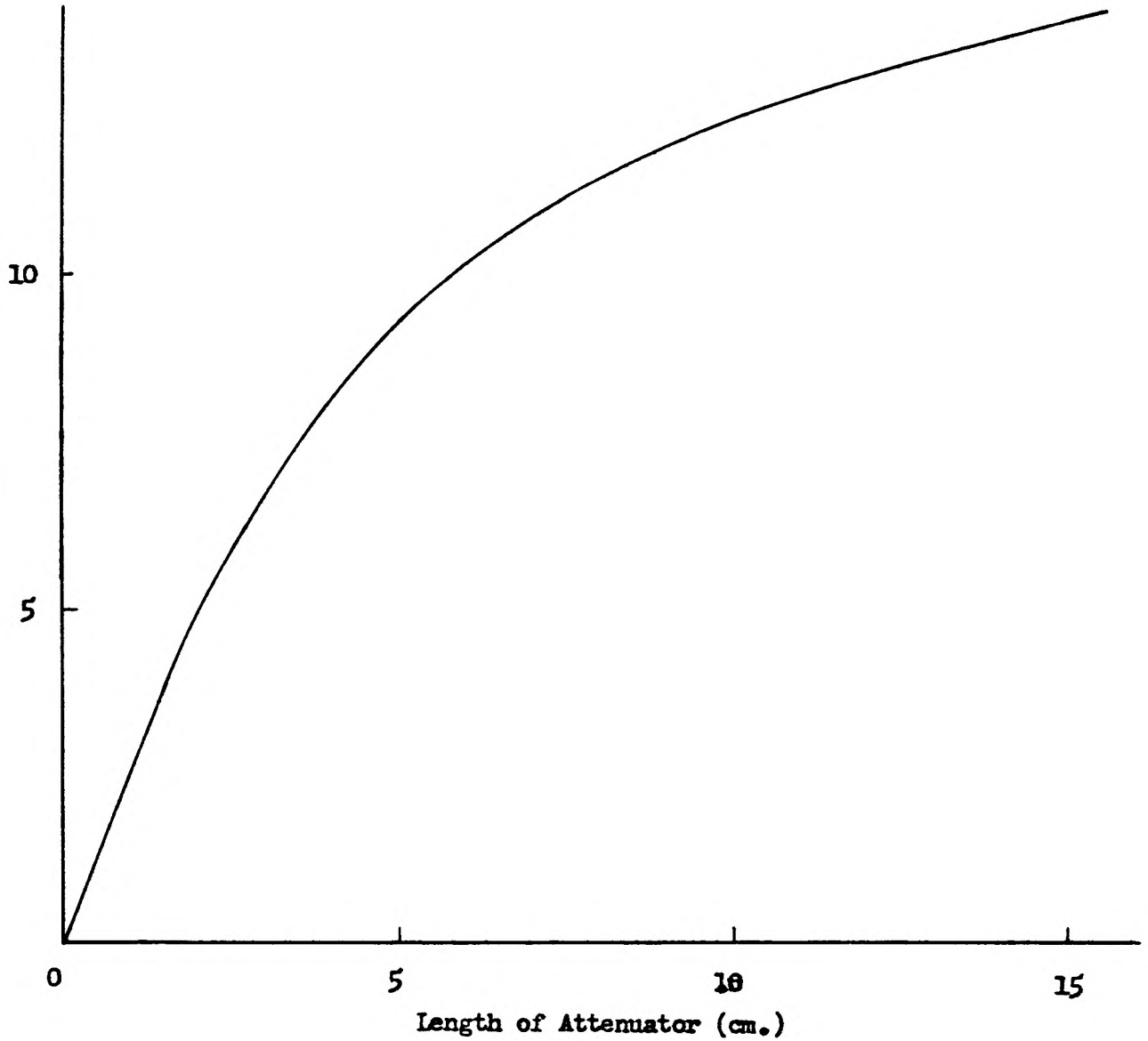

Ratio of Peak Current Density at End of Attenuator to Peak Current Density at Beginning of Attenuator vs. Length of Attenuator

Fig. 17.5

curves. The expected relative differences in power levels required to produce saturation are indicated on the plots. The agreement for the two shortest attenuators with the theoretical value is fair. The experimental power level difference for the two longest attenuators is greater than what was expected. The discrepancy is due to the incompleteness of the theory. It is especially probable that the large length of the attenuators and the impossibility of representing the attenuator by a drift pipe result in considerable amplification under the attenuator. Such a situation would require less power input in order to cause saturation.

Variation of power output as a function of distance along the tube is indicated in Figs. 17.8 and 17.9 for two different attenuator lengths. These plots show the over-all behavior of a traveling-wave tube as a function of drive and attenuator length.

The experimental arrangement is indicated in Fig. 17.10 . The probe consists of a single turn of wire which encircles the tube at a sufficient distance to prevent reflections being set up on the tube. The output of the probe was detected and amplified. The signal source was square wave modulated. Cold measurements were used to obtain power calibrations. The calibration enables one to determine the power level in terms of the voltage at the oscillograph. The tube was mounted in a magnet providing a longitudinal field of about 400 gauss.

In order to get an estimate of the power input required to cause saturation at points beyond the attenuator, some further calculations are required. The "I_o" components of current and velocity are subtracted from the current distributions found at the end of the attenuator. The remaining distribution, the hash, is then assumed to continue along the beam in the form of space charge waves. Saturation is assumed to set in when the peak current density in the current density distribution becomes equal to the direct current density. The results of these calculations appear superimposed upon the curves of Fig. 17.6 in Fig. 17.11 .

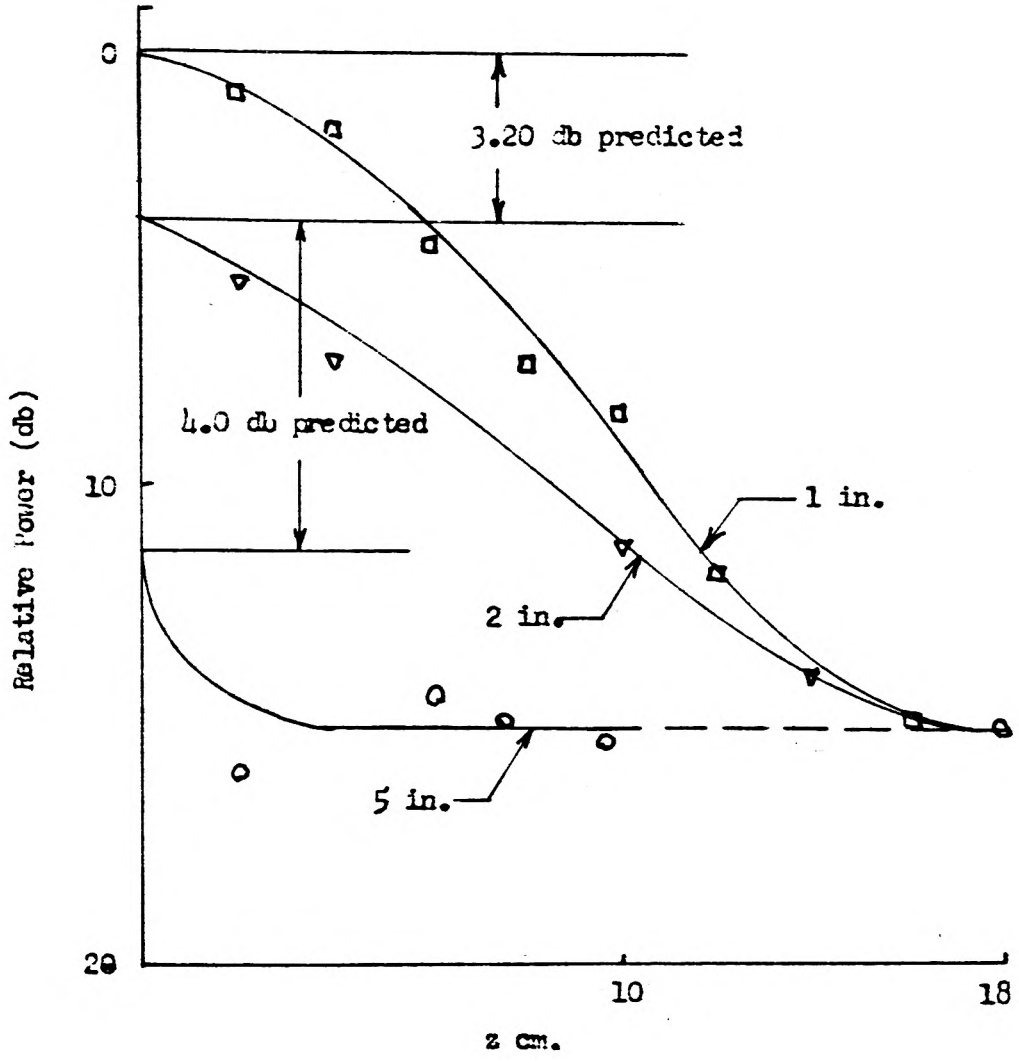

Relative Power Level Required to Saturate vs. Distance from End of Attenuator

Fig. 17.6

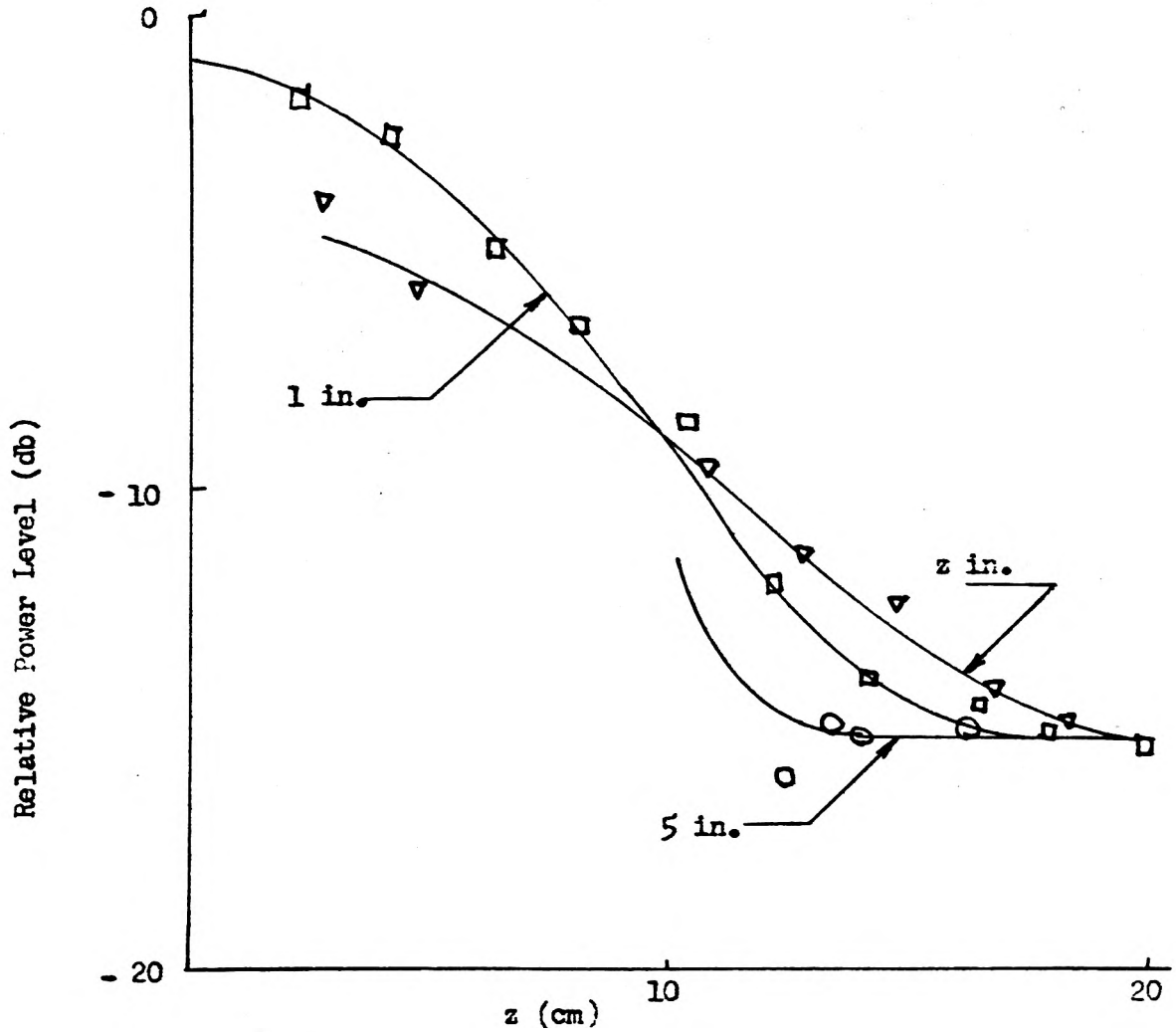

Relative Power Level to Saturate vs. Distance along the Tube.

Fig. 17.7

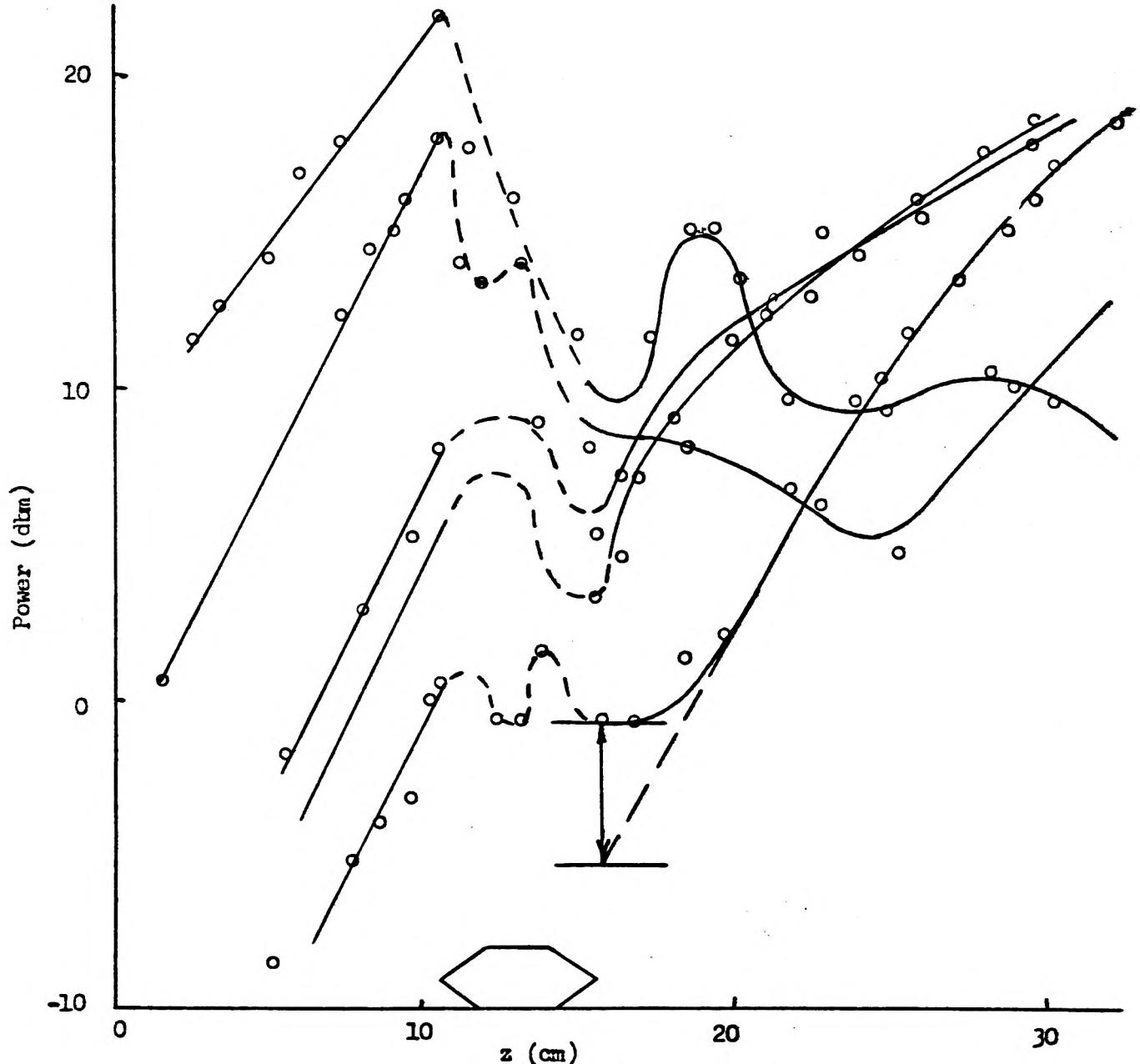

Fig. 17.8 Power on Helix vs. Distance along the Tube for a 2" Attenuator.

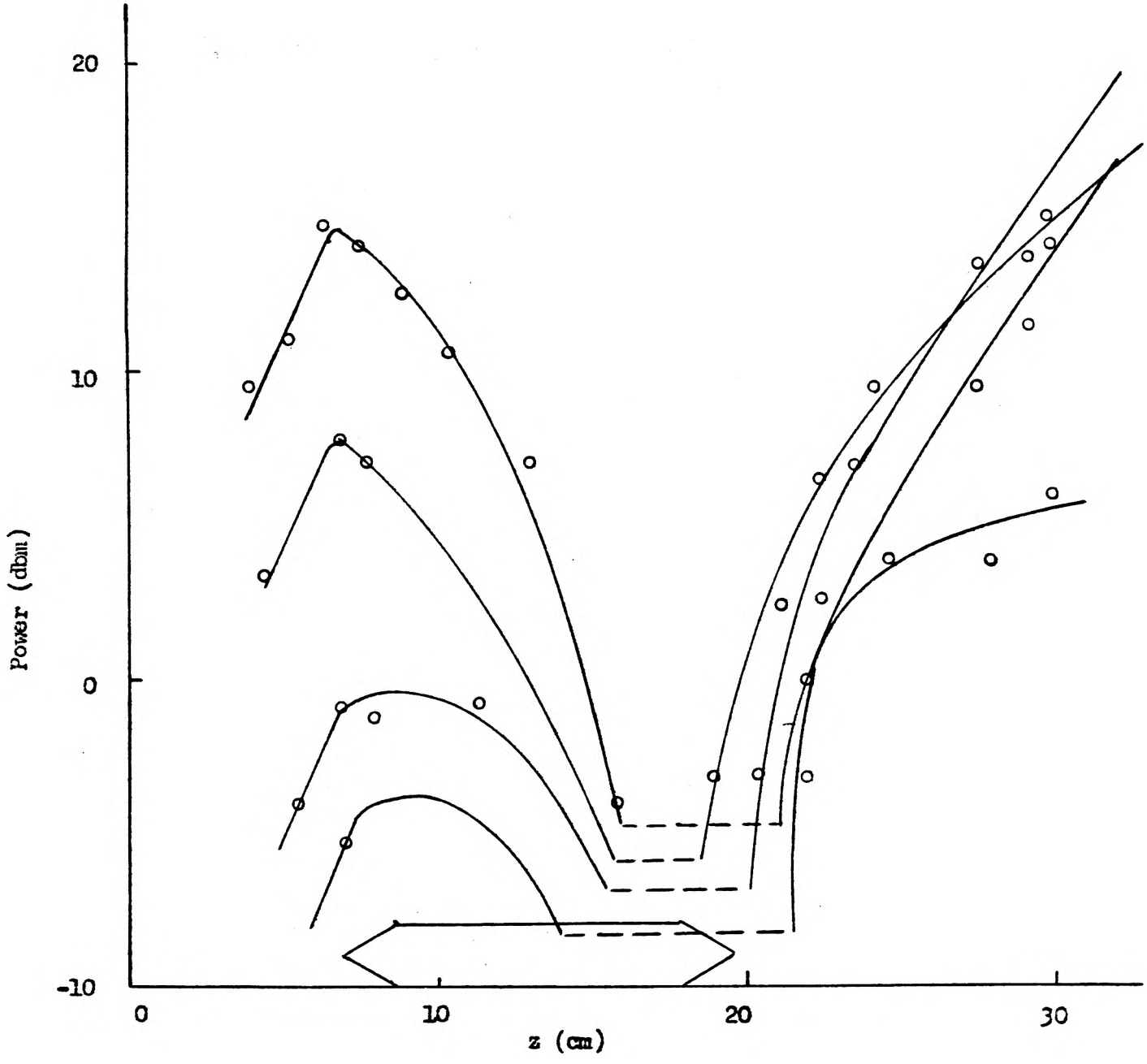

Fig. 17.9 Power on Helix vs. Distance along the Tube for a 5" Attenuator

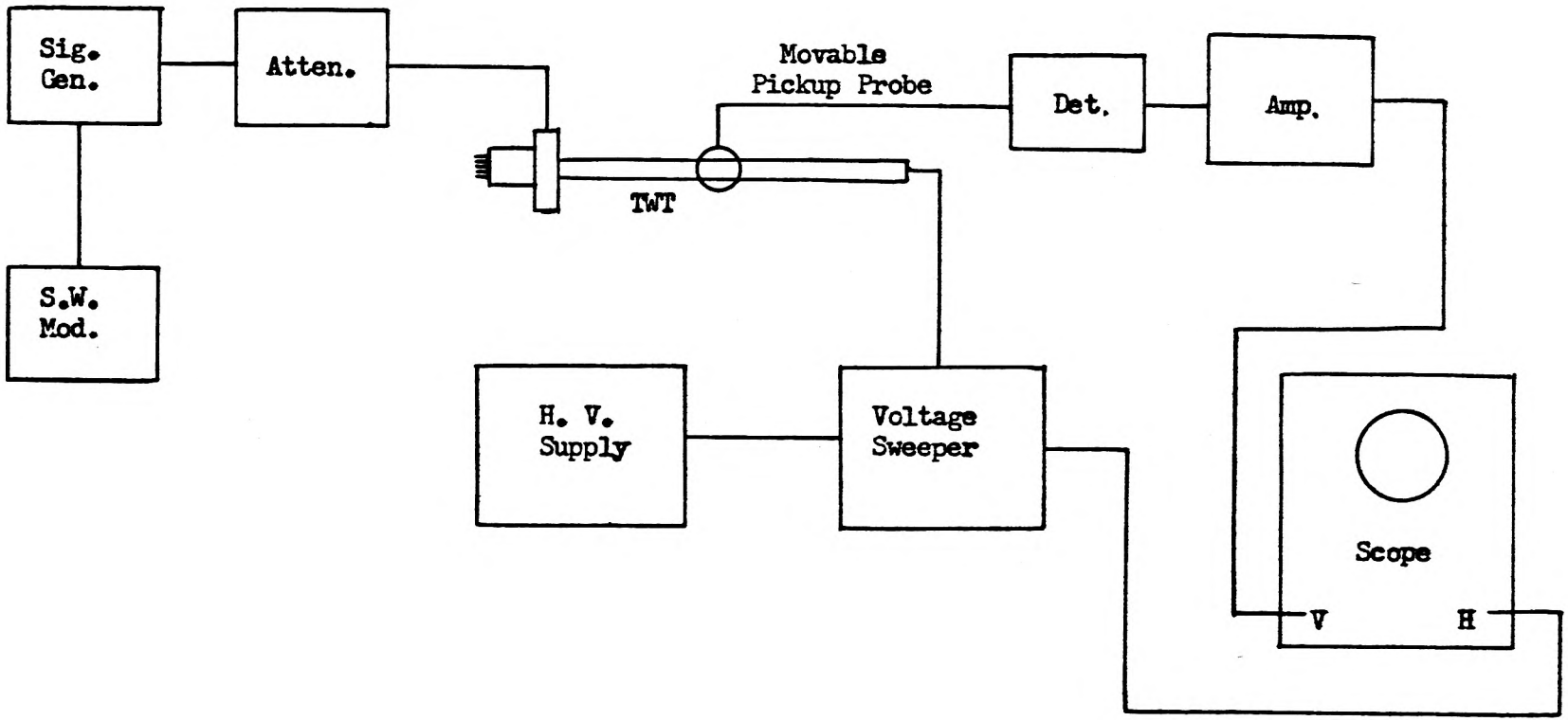

EXPERIMENTAL ARRANGEMENT

Fig. 7.10

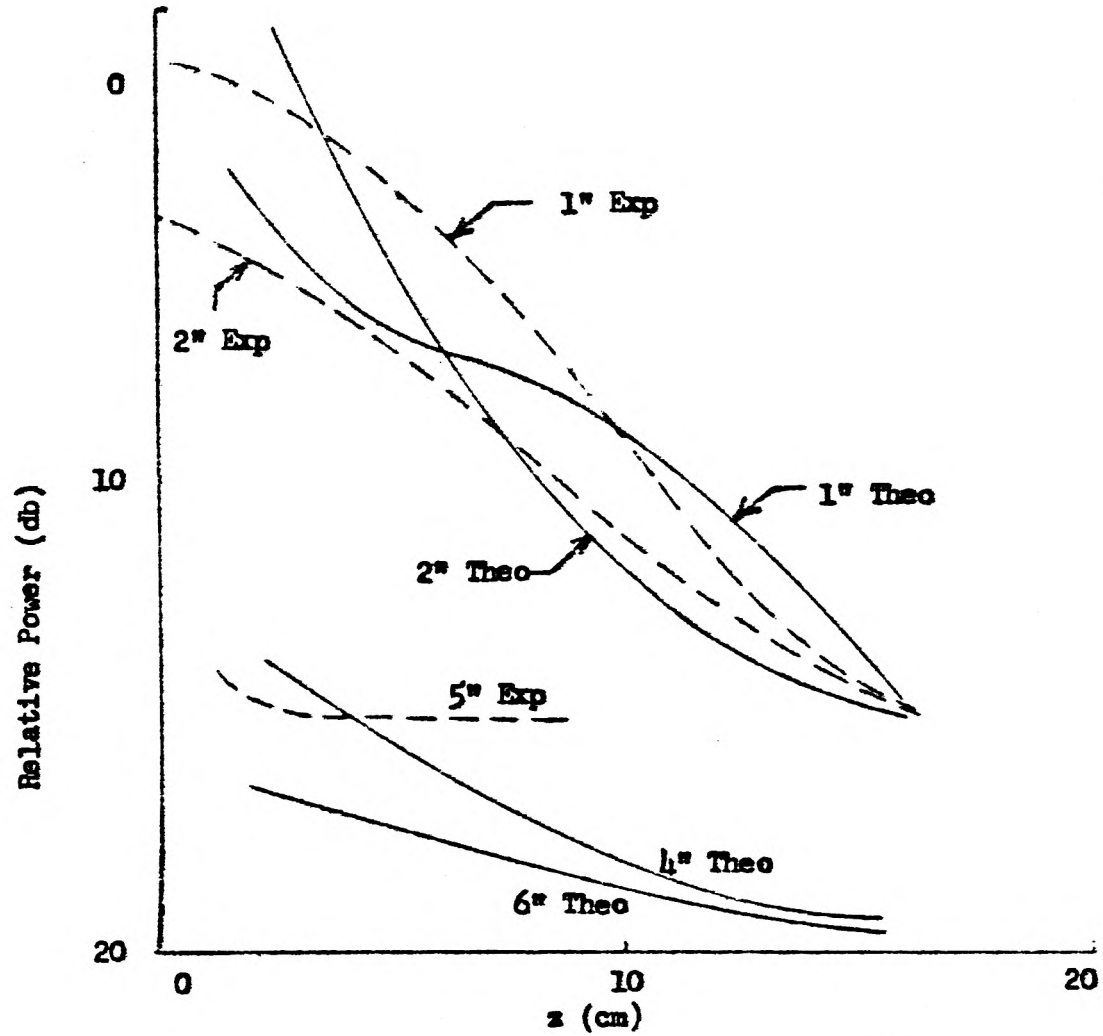

Fig. 17.11 Relative Drive Level at Attenuator Input Necessary to Cause Saturation at Various Distances Beyond End of Attenuator

TABULATION OF RESULTS

$\frac{i}{2 i_o I_o(\beta_e a)}$ at the end of the attenuating section vs. length of attenuator (in cm.) .

Z r/a	0	.2	.4	.6	.8	.9
2.54	.538 -17.05°	.364 -17.4°	.608 -16.7°	.7159 -20.79°	.767 -16.7°	1.013 -15.6°
5.08	.487 -28.5°	.252 -43.7°	.618 -26.0°	.885 -23.7°	1.08 -22.1°	1.46 -21.1°
10.16	.524 176.3°	.898 167.4°	.230 -153.6°	.514 -42.1°	1.05 -10.4°	2.09 -26.0°
15.24	1.633 159.1°	2.14 158.2°	1.167 161.2°	.793 171.9°	.875 -33.4°	2.465 -27.8°

Table 17.1

$\frac{\frac{i}{i_o} \text{ peak out of attenuator}}{\frac{i}{i_o} \text{ peak into attenuator}}$ vs. Attenuator Length

Z cm	$\frac{(i/i_o) \text{ peak out}}{(i/i_o) \text{ peak in}}$	$\frac{(i/i_o) \text{ peak out}}{(i/i_o) \text{ peak in}}$ in db
0	1	0
2.54	2.026	6.12
5.08	2.92	9.32
10.16	4.18	12.44
15.24	4.93	13.88

Table 17.2

Velocity Profiles,

Values plotted are $\frac{v \times 10^2}{2 v_o I_o (\beta_e a)} = \frac{v \times 10^2}{2 \frac{i_o}{\rho_o} I_o(\beta_e a)}$ at the End of an Attenuator vs. Attenuator Length (in cm.)

z \ r/a	0	.2	.4	.6	.8	.9
2.54	-.455 24.2°	-.355 -1.2°	.594 36.8°	-.901 47.9°	1.883 29.8°	-1.635 36.3°
5.08	-.300 -87.4°	1.01 84.3°	-.548 -75.1°	-.335 -10.8°	.694 43.3°	-1.34 55.2°
10.16	2.05 67.1°	2.27 66.3°	1.795 68.7°	1.235 72.7°	-.358 -89.4°	-.798 51.9°
15.24	1.10 57.8°	1.425 49.3°	1.225 45.5°	.865 62.0°	.487 60.4°	-.488 60.8°

Table 17.3

Amplitude of the I_o^{th} Component of a.c. Current Density and a.c. Velocity at the Output of an Attenuator, vs. Attenuator Length (in cm.)

z	A_i	A_v
2.54	1.745	-.02640
5.08	2.130	-.01008
10.16	1.789	.01695
15.24	.830	.01179

$i = 2 i_o I_o (\beta_e a) A_i I_o (\beta_e r)$; $v = 2(i_o/\rho_o) I_o(\beta_e a) A_v I_o(\beta_e r)$

Table 17.4

Section XVIII

CONCLUSION AND SUGGESTIONS FOR FURTHER INVESTIGATION

Saturation in traveling-wave tubes with attenuators occurring at lower levels than saturation in similar tubes operating without attenuators can occur in several ways.

It is believed that the mechanism of most importance in high power causes the current to field ratio to increase by the introduction of attenuation. At present only a limited number of calculations have been performed. It would be very desirable to have the results of calculations covering a greater range of parameters. One could also use models which come closer to the actual configurations of traveling-wave tubes than the ones that have been used for the calculations presented here. For instance, calculations should take into consideration the presence of glass envelopes.

The other mechanism which has been proposed to explain saturation consists of space charge wave bunching of the higher order modes. The calculations which have been performed on the basis of this mechanism have been very crude. It would be of great value to be able to calculate the actual contribution to saturation of these higher order modes. Some criteria have been given earlier which indicates when such contribution would be important. To put the matter on a rigorous basis, the author suggests that Sollfrey's work (R-5) be extended to include the effects of dielectrics and lossy surfaces. Then machine calculation of the inverse transform can be used to determine the behavior of the tube taking into account all the effects of higher order modes as well as

the effects of the changes in propagation constants of the three principal modes introduced by addition of loss. An IBM 701 computer or equivalent will probably be required to run such calculations.

The work described above suffers from being a linear theory. It may be necessary to go to a nonlinear theory in order to get to a thorough understanding of the situation. In the nonlinear computations which have been performed to date, (R-7,8), the calculations have been performed while neglecting several important considerations. They start with purely increasing waves. It is very important to consider saturation when all three waves are taken into account because the introduction of an attenuator excites the other waves. The calculations also are based on the Pierce theory. It has already been shown that the Pierce theory must be modified in the presence of loss. Investigation of the variation of the parameters Q and K with loss needs to be carried out. Furthermore, if it turns out that the higher order modes are significant, it will be necessary to perform nonlinear analyses of finite diameter beams.

It may be necessary to develop new methods of treating the problem which do away with the necessity of using large computing machines. That is, better application of the human brain may solve the problem better than the frontal attack of large computing batteries.

Finally, it is well to ask, "What does this all mean with respect to achieving higher efficiency from traveling-wave tubes?" The answer to such a question is not very satisfactory. It seems that the introduction of attenuation will always give attenuator troubles. It may be possible to compare the behavior of various attenuator designs on paper, but the author believes that even the best attenuator obtained by such a

method will not be very good. Design procedure would be largely empirical--several tentative designs being compared by computation.

In order to get about attenuator saturation effects it will probably be necessary to do something drastic, such as changing helix pitch under the attenuator.

There is much left to be done if one wants to understand the operation of attenuating sections. But, it is believed that the material presented above gives a fairly clear picture of the processes which are occurring. It should be able to serve as a starting point for an attempt to eliminate the bad effects of attenuators.

BIBLIOGRAPHY

Numbered references

1. L. J. Chu and J. D. Jackson, Field Theory of Traveling-Wave Tubes, Proc. IRE 36, 853-863 (1948).

2. J. J. Caldwell, O. L. Hoch, Technical Memorandum from a private source.

3. J. R. Pierce, Traveling-Wave Tubes, D. Van Nostrand, (1950).

4. C. K. Birdsall and J. R. Whinnery, Waves in an Electron Stream with General Admittance Walls, J. Appl. Phys. 24, 315-323 (1953.)

5. William Sollfrey, Effect of Initial Conditions on Traveling Wave Tubes, Report No. TW-15 of the Mathematics Research Group, New York University, Washington Square College of Arts and Science,

6. R. C. Fletcher, Helix Parameters used in Traveling-Wave Tube Theory, Proc. IRE, 38, 413-417 (1950).

7. P. K. Tien, L. R. Walker, and V. M. Wolntis, A Large Signal Theory of Traveling-Wave Amplifiers, Proc. IRE, 43, 260-277 (March 1955).

8. Joseph E. Rowe, A Large-Signal Analysis of the Traveling-Wave Amplifier, Technical Report No. 19, Electron Tube Laboratory, Engineering Research Institute, University of Michigan.

9. E. T. Whittaker and G. N. Watson, Modern Analysis, 381 Fourth Ed. Cambridge (1952).

Additional References

C. C. Cutler and D. J. Brangaccio, Factors Affecting Traveling-Wave Tube Power Capacity, Trans. IRE PGED-3, 9-24, (1953).

J. J. Caldwell, High Power Traveling-Wave Tube Gain and Saturation Characteristics as a Function of Attenuator Configuration and Resistivity, Trans. IRE PGED-4 28-36, (1953).

A. Nordsiek, Theory of the Large Signal Behavior of Traveling-Wave Amplifiers, Proc. IRE 41, 630-637 (1953).

DISTRIBUTION LIST - Nonr 220(13)

TECHNICAL REPORTS

		Copies
Chief of Naval Research Navy Department Washington 25, D. C.	Code 427	2
Director Naval Research Laboratory Washington 25, D. C.	Code 5240 Code 7130 Code 2000 Code 5430	1 1 6 1
Commanding Officer Office of Naval Research Branch Office 1000 Geary Street San Francisco 9, California		1
Commanding Officer Office of Naval Research Branch Office 1030 E. Green Street Pasadena, California		2
Commanding Officer Office of Naval Research Branch Office The John Crerar Library Building 86 East Randolph Street Chicago 1, Illinois		1
Commanding Officer Office of Naval Research Branch Office 346 Broadway New York 13, New York		1
Officer-in-Charge Office of Naval Research Navy 100 Fleet Post Office New York, New York		3
Chief, Bureau of Aeronautics Navy Department Washington 25, D. C.	EL 4	1
Chief, Bureau of Ordnance Navy Department Washington 25, D. C.	Re 4 Re 9	1 1
Chief of Naval Operations Navy Department Washington, D. C.	Op 20X Op 421 Op 55	1 1 1
Director Naval Ordnance Laboratory White Oak, Maryland		1

Director Naval Electronics Laboratory San Diego 52, California		1
U.S. Naval Post Graduate School Monterey, California	Dept.of Electronics and Physics Prof. C.E. Menneken	1
Commander Naval Air Missile Test Center Point Mugu, California	Code 366	1
U. S. Naval Proving Ground Dahlgren, Virginia	W. H. Benson	1
Commander U. S. Naval Air Development Center Johnsville, Pennsylvania		1
Committee on Electronics Research and Development Board Department of Defense Washington 25, D. C.		1
Director National Bureau of Standards Washington 25, D. C.	Division 14.0 CRPL, Librarian	1
Commanding Officer Engineering Research and Development Lab. Ft. Belvoir, Virginia		1
Ballistics Research Laboratories Aberdeen Proving Ground, Md.	D.W.H.Delsasso	2
Chief, Ordnance Development Division National Bureau of Standards Connecticut Ave. and Van Ness St., NW Washington 25, D. C.		2
Commanding Officer Frankford Arsenal Bridesburg, Philadelphia, Pa.	COL Kundul	1
Supply Receiving Section Signal Corps Engineering Laboratories Evans Signal Laboratory Building 42 Belmar, New Jersey	Thermionics Branch	5
Commanding General Air Research and Development Command Post Office Box 1395 Baltimore 3, Maryland	RDRR RDDDE-3 RDDDE-5	1 1 1

Commanding General Wright Air Development Center Wright-Patterson Air Force Base, Ohio	WCLC WCLRC	1 1
Commanding General Air Force Cambridge Research Center 230 Albany Street Cambridge 39, Massachusetts	CRRE	1
Commanding General Rome Air Development Center Griffiss Air Force Base Rome, New York	RCRW	1
Armed Services Technical Information Agency Document Service Center Knott Building Dayton 2, Ohio	DSC-SA	5
Director Air University Library Maxwell Air Force Base, Alabama	CR4582	1
Chief, Western Division Air Research and Development Command Office of Scientific Research Post Office Box 2035 Pasadena, California		1
Microwave Laboratory Stanford University Stanford, California	F.V.L.Pindar	1
Engineering Library Stanford University Stanford, California		1
Massachusetts Institute of Technology Cambridge 39, Massachusetts	Research Laboratory of Electronics	1
Document Office of Government Research Contracts G-16, Littanuer Center Harvard University Cambridge, Massachusetts	M.L.Cox, Librarian	1
Sloane Physics Laboratory Yale University New Haven, Connecticut	R. Beringer	1
Department of Electrical Engineering Yale University New Haven, Connecticut	H. J. Reich	1

Electrical Engineering Department University of Illinois Champaign, Illinois	Electron Tube Section	1
Chairman, Div. of Electrical Engineering University of California Berkeley 4, California		1
Technical Report Collection 303a, Pierce Hall Harvard University Cambridge, 38, Massachusetts		1
Laboratory for Insulation Research Massachusetts Institute of Technology Cambridge 39, Massachusetts	A. von Hippel	1
Engineering Library California Institute of Technology		1
Lincoln Laboratory Massachusetts Institute of Technology Cambridge 39, Massachusetts		1
Signal Corps Resident Engineer Electronic Defense Laboratory Post Office Box 205 Mountain View, California	F. W. Morris Jr.	1
Cornell Aeronautical Laboratory Cornell Research Foundation Buffalo 21, New York		1
Director, Electronics Defense Group Engr. Research Institute University of Michigan Ann Arbor, Michigan		1
Georgia Institute of Technology Atlanta, Georgia	Mrs. J. F. Crosland Librarian	1
Varian Associates 611 Hansen Way Palo Alto, California	Fred D. Wilimek	1
Airborne Instrument Laboratory Mineola, New York	John Dyer	1
Bell Telephone Laboratories Murray Hill Laboratory Murray Hill, New Jersey	Leah E. Smith Librarian J. R. Pierce	1 1
Hughes Aircraft Company Culver City, California	John T. Milek Technical Librarian	1

RCA Laboratories Princeton, New Jersey	E. W. Herold and Harwell Johnson	1
Federal Tele. Laboratories, Inc. 500 Washington Avenue Nutley, New Jersey	W. Derick K. Wing	1 1
General Electric Microwave Laboratory 601 California Avenue Palo Alto, California	Technical Library	1
Columbia Radiation Laboratory 538 W 120th Street New York 27, New York		1
Countermeasures Laboratory Gilfillan Bros, Inc. 1815 Venice Boulevard Los Angeles, California		1
The Rand Corporation 1700 Main Street Santa Monica, California	Margaret Anderson Librarian	1
Research and Development Board Pentagon Building Washington 25, D. C.	Technical Library	1
The Motorola Riverside Research Lab. 8330 Indiana Avenue Riverside, California	Mr. John Byrne	1
Chief, Bureau of Aeronautics Department of the Navy Washington, D. C.	EL 43 EL 45	1 1
Chief, Bureau of Ships Department of the Navy Washington, D. C.	Code 816 820 840	1 1 1
Panel on Electron Tubes 346 Broadway (8th Floor) New York 13, New York		1
Supervisor of Research Laboratory Electrical Engineering Bldg. Purdue University Lafayette, Indiana	H.J.Oorthuys	1
University of Florida Department of Electrical Engineering Gainesville, Florida	W. E. Lear	1

Microwave Research Institute Polytechnic Institute of Brooklyn 55 Johnson Street Brooklyn 1, New York	E. Weber	1
New York Naval Shipyard Material Laboratory Library Brooklyn 1, New York	Code 912B	1
University of Washington Department of Electrical Engineering Seattle, Washington	E.A.Harrison A.V.Eastman	1 1
University of Colorado Department of Electrical Engineering Boulder, Colorado		1
Electrical Engineering Dept. Princeton University Princeton, New Jersey		1
National Union Radio Co. 350 Scotland Road Orange, New Jersey	Dr.A.M.Skellet	1
Sperry Gyroscope Company Great Neck, L.I., New York	J. E. Shepherd	1
W. L. Maxson Corporation 460 West 34th Street New York 1, New York	M. Simpson	1
Raytheon Corporation Waltham, Massachusetts	H.R. Argento	1
Electron Tube Div., Research Lab. General Electric Company The Knolls Schenectady, New York	E.D.McArthur	1
Office of Technical Services Department of Commerce Washington 25, D. C.		1
Extra copies for future requirements		25
Electronics Research Laboratory Stanford University Stanford, California	Librarian	1
Professor W. P. Dyke Linfield College McMinnville, Oregon		1